NON-LINEAR VISCOELASTICITY FOR EPOXY-BASED POLYMERS : THEORETICAL MODELING AND NUMERICAL IMPLEMENTATION

A THESIS SUBMITTED TO
THE GRADUATE SCHOOL OF NATURAL AND APPLIED SCIENCES
OF
MIDDLE EAST TECHNICAL UNIVERSITY

BY

ATEŞ KORAL

IN PARTIAL FULFILLMENT OF THE REQUIREMENTS
FOR
THE DEGREE OF MASTER OF SCIENCE
IN
MECHANICAL ENGINEERING

AUGUST 2019

Approval of the thesis:

NON-LINEAR VISCOELASTICITY FOR EPOXY-BASED POLYMERS : THEORETICAL MODELING AND NUMERICAL IMPLEMENTATION

submitted by **ATEŞ KORAL** in partial fulfillment of the requirements for the degree of **Master of Science in Mechanical Engineering Department, Middle East Technical University** by,

Prof. Dr. Halil Kalıpçılar _____
Dean, Graduate School of **Natural and Applied Sciences**

Prof. Dr. M.A. Sahir Arıkan _____
Head of Department, **Mechanical Engineering**

Assoc. Prof. Dr. Hüsnü Dal _____
Supervisor, **Mechanical Engineering Department, METU**

Prof. Dr. Raif Orhan Yıldırım _____
Co-supervisor, **Mechanical Engineering Department, METU**

Examining Committee Members:

Prof. Dr. Suat Kadıoğlu
Mechanical Engineering Department, METU _____

Assoc. Prof. Dr. Hüsnü Dal
Mechanical Engineering Department, METU _____

Prof. Dr. Raif Orhan Yıldırım
Mechanical Engineering Department, METU _____

Assist. Prof. Dr. Sezer Özerinç
Mechanical Engineering Department, METU _____

Assist. Prof. Dr. Omer Music
Mechanical Engineering Department, TED University _____

Date: 28.08.2019

I hereby declare that all information in this document has been obtained and presented in accordance with academic rules and ethical conduct. I also declare that, as required by these rules and conduct, I have fully cited and referenced all material and results that are not original to this work.

Name, Last Name: Ateş Koral

Signature :

ABSTRACT

NON-LINEAR VISCOELASTICITY FOR EPOXY-BASED POLYMERS : THEORETICAL MODELING AND NUMERICAL IMPLEMENTATION

Koral, Ateş
M.S., Department of Mechanical Engineering
Supervisor : Assoc. Prof. Dr. Hüsnü Dal
Co-Supervisor : Prof. Dr. Raif Orhan Yıldırım

August 2019, 119 pages

The present thesis aims at modeling creep behaviour under hydrostatic and uniaxial loadings of a certain silica filled epoxy compound at various temperatures with numerical implementation of algorithms into finite element method. Time dependent behaviour of polymers has been examined and many approaches have been proposed by researchers. Some of the models are inspired from micro-mechanical structure of polymers. These models generally take relaxation of a single entangled chain in a polymer gel matrix upon loading into account. In this thesis, a finite viscoelasticity model, which takes into account volumetric and isochoric creep/relaxation phenomena, is developed for epoxy-based compounds over glass transition temperature. Deformation gradient is multiplicatively split into elastic and inelastic parts and related with associated stretches of the single chain. In this thesis, the non-linear viscous evolution law proposed by Dal [1] is adopted. As a novel aspect, apart from equilibrium bulk modulus parameter, in order to simulate time dependent volumetric creep behaviour of the epoxy compound, a viscous bulk modulus parameter is included in the proposed free energy function. Hence, volumetric effects in viscoelastic behavior is also taken into consideration without needing to split free energy function into vol-

umetric and isochoric parts. Proposed model properly predicts behaviour of epoxy compound above 110°C in the rubbery state and also in the transition range. It has been demonstrated that the model prediction is quite satisfactory around and above the glass transition temperature, whereas the constitutive behaviour of the epoxy-moulding compounds at temperatures well below the glass transition temperature can not be captured as expected. The model parameters are identified from the experimental results. The algorithmic implementation of the model is carried out in the Eulerian setting in the sense of Dal and Kaliske [2] and the computational performance is demonstrated through representative boundary value problem.

Keywords: viscoelasticity, creep, stress relaxation, inelastic stretch, finite element method, non-linear viscoelasticity, epoxy, polymer, material modelling,continuum mechanics, computational mechanics, volumetric effects, time dependent, free energy function, uniaxial, hydrostatic

ÖZ

EPOKSİ TABANLI POLİMERLER İÇİN DOĞRUSAL OLMAYAN VİSKOELASTİSİTE: TEORİK MODELLEME VE NÜMERİK UYGULAMA

Koral, Ateş
Yüksek Lisans, Makina Mühendisliği Bölümü
Tez Yöneticisi : Doç. Dr. Hüsnü Dal
Ortak Tez Yöneticisi : Prof. Dr. Raif Orhan Yıldırım

Ağustos 2019 , 119 sayfa

Bu tez belirli bir silika dolgulu epoksi bileşiminin çeşitli sıcaklıklarda, hidrostatik ve tek yönlü yüklemeler altındaki sünme davranışını modellemeyi ve türetilen algoritmaların sonlu elemanlar metoduna nümerik olarak uygulanmasını hedeflemektedir. Polimer malzemelerin zamana bağlı davranışı, araştırmacılar tarafından incelenmiş ve birçok model geliştirilmiştir. Bu modellerin bazıları polimerlerin mikro-mekanik yapısından esinlenilmiştir. Söz konusu modeller genellikle polimer jelin içinde dolaşmış şekilde bulunan tek bir zincirin yükleme üzerine yumuşama hareketini göz önünde bulundurur. Bu tezde, epoksi tabanlı bir bileşim için hacimsel ve şekilsel sünme/yumuşama davranışlarını hesaba katan bir viskoelastik model, camsı geçiş bölgesinin üstündeki sıcaklıklar için geliştirilmiştir. Deformasyon gradyan matrisi elastik ve inelastik kısımlara çarpımsal olarak ayrılmış ve bahsedilen tek bir zincirin karşılık gelen gerilme oranlarıyla ilişkilendirilmiştir. Tezde, Dal [1] tarafından öne sürülmüş doğrusal olmayan viskoz gelişim denklemi kullanılmıştır. Tezin özgün bir yönü olarak, denge hacimsel modülünün yanı sıra, viskoz hacimsel modülü önerilen serbest enerji fonksiyonuna zamana bağlı hacimsel sünme davranışını modellemek için dahil edilmiştir. Bu nedenle, malzemenin visckoelastik davranışında hacimsel deformasyon

etkileri de serbest enerji fonksiyonunu hacimsel ve şekilsel deformasyon kısımlarına ayırma gereği duymadan hesaba katılmıştır. Önerilen model epoksi bileşiminin 110°C üstünde olan lastiksi bölgesindeki ve geçiş bölgesindeki davranışını oldukça iyi bir şekilde tahmin etmektedir. Modelin tahmin yeteneğinin geçiş bölgesi etrafında ve üstünde oldukça tatmin edici olduğu gösterilmekle birlikte, camsı geçiş sıcaklığının oldukça altındaki sıcaklıklar için davranışın model tarafından yakalanması beklenildiği gibi değildir. Modelin içerdiği parametreler deney sonuçları ile model sonuçlarının karşılaştırılması ile elde edilmiştir. Modelin algoritmik uygulanması Eulerian konfigürasyonunda, Dal and Kaliske [2] makalesine benzer şekilde gerçekleştirilmiş ve hesaplama performansı sınır değer problemi ile gösterilmiştir.

Anahtar Kelimeler: viskoelastisite, sünme, stres yumuşaması, inelastik uzama, sonlu elemanlar metodu, doğrusal olmayan viskoelastisite, epoksi, polimer, malzeme modelleme, sürekli ortamlar mekaniği, hesaplamalı mekanik, hacimsel etki, zamana bağlı, serbest enerji fonksiyonu, tek yönlü, hidrostatik

To my family

ACKNOWLEDGMENTS

I would like to express my deepest gratitude to my supervisor Assoc. Prof. Dr. Hüsnü Dal and my co-supervisor Prof. Dr. Raif Orhan Yıldırım for their expertise, supervision, help, guidance and kindness from the beginning to the end of this dissertation.
I want to thank my parents, Birnur Koral and Orcan Koral, for their support, concern and tolerance during the preparation period of this thesis. I also want to thank Ceren Şimşek for her support during this period. That was the greatest gift she has given to me.
The creep tests presented in this thesis were performed at University of Maryland and Prof. Dr. Bongtae Han allowed me to use the results of the tests. I would not complete this thesis without their help and support. I want to express my gratitude to Prof. Dr. Bongtae Han from Maryland University for his help.
I want to thank to visiting researcher Dr. Osman Gültekin in METU since he spent his valuable time to read my thesis and gave me feedback and assistance.
Lastly, I'm so grateful for being a part of this project. I would like to express my sincere gratitude to Dr.-Ing. Fabian Welschinger and Assoc. Prof. Dr. Hüsnü Dal for giving me this chance.

TABLE OF CONTENTS

LIST OF TABLES

TABLES

LIST OF FIGURES

FIGURES

LIST OF ABBREVIATIONS

BB	Bergström & Boyce
CTE	Coefficient of Thermal Expansion
FBG	Fiber Bragg Grating
FEA	Finite Element Analysis
FEAP	Finite Element Analysis Program
EMC	Epoxy Molding Compound
LVE	Linear Viscoelastic
NLVE	Non-linear Viscoelastic

CHAPTER 1

INTRODUCTION AND OVERVIEW

1.1 Polymeric materials

Polymer mechanics has been an active research area by virtue of the fact that polymers such as epoxy, natural rubber and other elastomers are widely used in industrial applications. Tires, seals, conveyor belts, damping devices, structural components of automobiles, aircrafts and missiles, packages and casings of electronics, which perform in wide range of temperature environment, are some of the industrial applications where polymers are largely used and the role of the material response is very important in terms of performing their functions properly. Although they are used largely in non-structural commercial products, since weight of high performance composite polymers are low compared to the metals and it is possible to obtain the required mechanic properties, polymers are also taking place of metals in some load bearing applications [4]. Besides, there are some industrial applications where the deflection of the material should be within a certain tolerance range upon loading. It is critical to design these materials in an economic and accurate way. For these reasons, since the beginning of the last century, scientists have been trying to simulate real stress-strain, stress-time, strain-time behaviour of these materials using phenomenological modelling approaches which do not have any physical interpretation or kinetic theories which are related with molecular chain deformations. The mechanical behaviour of a polymer may be complicated, non-linear inelastic in large strain region while it can exhibit linear elastic behaviour in small strain region. In large strain region, it is harder to predict the mechanical behaviour since there are differences in stress-strain response of a polymer due to the differences in chemical composition and loading conditions applied. In addition to the highly non-linear response of the polymeric ma-

terials, modeling inelastic behaviour such as viscoelastic, rate dependent behaviour upon a loading condition is also a challenge.

Internal stress or strain like tensorial variables concepts are widely used to form a viscoelastic model by many researchers. Some examples of the models that contain stress like internal variables are proposed by Govindjee and Simo (1992) [6], Holzapfel and Simo (1996) [7], Lion (1996) [8], Kaliske and Rothert (1997) [9]. Generally, in constitutive modeling, inelastic (or viscoelastic) effects are taken into account via superposition of the viscoelastic response (non-equilibrium) with elastic (equilibrium) response. In other words, elastic and inelastic effects are considered separately and superimposed. This decomposition principle has been proposed by Green and Tobolsky (1946) [10] and applied by Lion (1997) [11], Dal and Kaliske (2009) [2], Lubliner (1985) [12], Reese and Govindjee (1998) [13], Reese (2003) [14], Bergström and Boyce (1998) [15], Haupt and Sedlan (2001) [16] with many other researchers in the concept of nonlinear viscoelasticity. In this manner, deformation gradient is split into elastic and inelastic parts with latter being strain-like tensorial variable. Thus, mechanical response can be subdivided into two different branches as equilibrium and viscoelastic to predict the overall response of a polymer. The first branch is ground elastic stress response of the polymer in equilibrium corresponding to large elastic strains. The second branch is viscoelastic over stress response (non-equilibrium response) related with rate-dependent (or time dependent) effects such as relaxation and creep behaviour. In terms of thermodynamical point of view, strain-like variable concept is more appropriate since a theory similar to plasticity theory can be applied to integrate inelastic strain variable [17].

1.1.1 Ground state elastic response

In the last century, many researchers have investigated elastic response (or equilibrium) of polymers experimentally and theoretically and the results were represented by classical finite hyperelasticity models such as Mooney-Rivlin, generalized Neo-Hookean etc. Some of the researches related to experimental characteristics of polymers are found in Treloar (1944) [18], James and Green (1975) [19]. Elastic response of polymers is also investigated based on micro-mechanical structure of polymers. Molecular chain deformation of polymers upon loading is exploited for instance by

Arruda and Boyce (1993a) [20], Anand (1996) [21] using principles of kinetic theory, statistical mechanics and thermodynamic consistency to obtain theoretical constitutive models. Thus, parameters in micro-structure level are utilized in these models. There are also purely phenomenological models developed without considering molecular chain kinetics for instance by Mooney (1940) [22], Blatz and Ko (1962) [23]. The micro-sphere model of Miehe et al. (2004) [24] and Miehe and Göktepe (2005) [25] are more recent micro-mechanically based non-affine models. In these models, tube-like constraints are used and motion of a single free chain is restricted by the surrounding chains that are assumed to move along the tube with a diameter d and length r. They utilized constraint release effects proposed by Marrucci (1996) [26]. In [24], average network stretch is linked to the macro stretches in discrete orientations by using the principle of $p-root$ averaging method. Also, see the extended tube model of Kaliske and Heinrich (1999) [27]. Strain energy functions developed by these models are generally in terms of principle stretches or invariants. One of the most well-known model has been proposed by Bergström and Boyce (1998)[15]. To model elastic response of rubber-like materials, it considers an elastic spring in an elastic branch parallel to viscous branch and contains a micro-mechanical free energy function corresponding to the elastic spring developed by Arruda and Boyce (1993a) [20]. This model was also implemented by [2] in the context of finite element analysis with a precise description of algorithmic setting of non-linear evolution law. In the content of this thesis, the same free energy function will be used by small modifications and a quadratic volumetric free energy function extension to it in order to take viscous volumetric creep into account.

1.1.2 Viscoelastic over-stress response

Prediction of the viscoelastic behaviour is important in terms of many aspects of mechanics. For example, fracture prediction of viscoelastic materials can be simulated by the usage of suitable viscoelastic model [28]. Viscoelastic behaviour of polymeric materials can be observed in experiments where the material is subjected to relaxation and creep or cyclic loading. In contrast to cyclic behaviour of metals, stress-strain curve of polymeric materials exhibit hysteresis on loading and unloading portions of the material which means that there is an energy dissipation proportional to area under

the curve. Such a curve can be seen in Fig. 1.1.2. To observe viscoplastic response, stress relaxation is allowed at certain intermediate constant strains and the terminal points at the relaxed state are recorded for loading/unloading conditions. As stated in

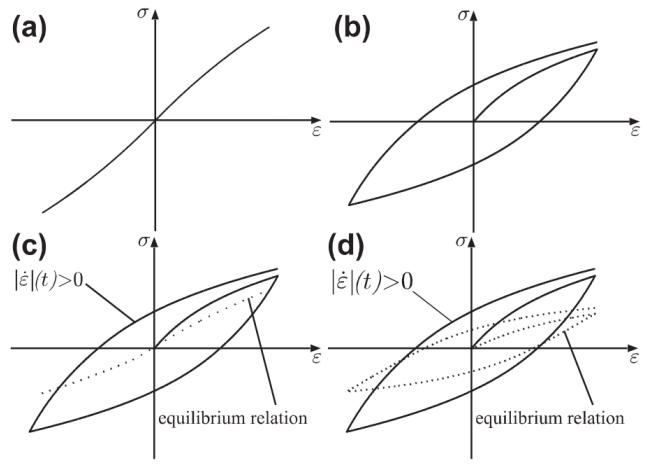

Figure 1.1: Four types of material behaviours taken from Haupt (1993) [3] (a) elasticity, (b) plasticity, (c) viscoelasticity, (d) viscoplasticity

the reports of Bergström and Boyce [15] and Haupt and Sedlan (2001) [16], presence of an equilibrium hysteresis after cyclic loading corresponds to viscoplastic response while equilibrium response without hysteresis corresponds to viscoelastic behaviour of the material tested. Viscoelastic over-stress response of the material is generally represented by a viscous branch containing a spring and a viscous dashpot. Same as ground state elastic part, viscoelasticity can be predicted with purely phenomenological approaches (without physical parameters) such as Lubliner (1985) [12], Lion (1987) [11], Reese and Govindjee (1998) [13] or micro-mechanically motivated approaches such as Johnson et al. (1995) [29], Bergström and Boyce (1998) [15], Miehe and Göktepe (2005) [25]. In the micro-mechanical theories, inelastic strain-like tensorial variable related with the viscous dashpot is a function of time. Evolution of this variable with time is associated with molecular theories, which consider viscous behaviour of polymer segments in cross-linked polymer networks. These molecular approaches can be split into three groups : the bead-spring models, the reptation-type tube models and the transient network model. The first one is developed by Rouse (1953) [30] and Zimm (1956) [31] and is not mentioned here. The second

one (the reptation-type tube models) is proposed by Doi and Edwards (1986) [32]. In this molecular theory, relaxation of a single chain with time is investigated under the scope of relaxation times. In this manner, the concept of a free chain on a cross-linked polymer network with superimposed entanglements under a sudden load is used and the relaxation of the free chain is denoted as a function of time in certain time domains. Bergström and Boyce (1998) [15] derived the evolution of creep rate as function of certain parameters, inelastic chain stretch and stress by using this time function. The third model was proposed by Green and Tobolsky (1946) [10] and was revised by Tanaka and Edwards (1992a,b) in [33], [34]. In this last approach, breakage and reformation of the polymer segments during deformation are considered to obtain a formulation. This approach was used, for example, in Reese (2003) [14] and in others.

1.1.3 Modeling epoxy-based polymers

In this section, literature search regarding behaviour of epoxy-based materials is presented since current thesis is intended to model the mechanical behaviour of a certain epoxy compound. Epoxy is a thermosetting material with high density of cross-links. Epoxy types are used, for instance, in applications such as adhesive bonding, casing of electronics (semi-conductors), new technology asphalt and also in automotive and aerospace industry. The reason for selecting cross-linked epoxy materials for these kind of applications is that they possess high strength, high elastic modulus, good heat and solvent resistances and relatively low price. Similar to rubbers, epoxies also show nonlinear inelastic thermo-mechanical material behaviour with dependence on strain-rate as stated in [35]. This nonlinearity is also distinct in high stress values and temperatures around and above glass transition temperature. Therefore, although linear viscoelastic models and constitutive equations are well understood in the literature, nonlinear viscoelastic models are more efficient in terms of predicting mechanical behaviour of polymeric materials in large strain region. Wide use of these materials in load bearing applications make them important and predicting their long term deformation behaviour is an asset in terms of predicting their warpage, creep-relaxation, residual stress characteristics via implementation of these models into finite element analysis softwares. Most of the researchers in this area con-

ducted experiments to understand various behaviours and they formulated linear and non-linear viscoelastic-viscoplastic models to predict these various behaviours [36]. Some examples of experiments of epoxies under various loading conditions are found in Xinghe and Xia [37], Hu, Yafei and Xia [38], Xia, Zihui and Shen [39], Ferknand and Xia [40], Pandini, Stefano and Pegoretti [41]. In the article [38], an epoxy resin (Epon 826) was studied to investigate the behaviour of this material under multiaxial loading, dependence of hydrostatic pressure and load path on general deformation. From the tests, it is observed that the material shows slight increment in shear stress response corresponding to the same value of applied strain if a hydrostatic load is also applied simultaneously and it (shear and axial strain) also increases with loading rate. However, these effects are not distinct below a certain strain value. Another studied item was the influence of loading path on axial and shear stress response. In this manner, shear strain was first applied to the material. Then, axial strain was applied and shear strain was kept constant at the same strain value (shear-axial test) or vice versa (axial-shear test). According to the experiments, presence of a prior shear stress leads to a lower axial stress value in a shear-axial strain driven test, which means that axial stiffness of the material is lower while vice versa is valid for the other loading path (axial-shear). These tests display the importance of loading history applied to polymeric materials. This is due to the fact that polymer chains are more restricted in the case of multi-axial loading resulting in less viscosity. Besides, it was demonstrated that increasing applied stress value also increases strain recovery rate, magnitude in a stress recovery test and creep compliance value in a creep test. These effects are more distinct after a certain value of applied stress is reached. In the article [37], cyclic deformation tests performed were given. The test were performed for many cyclic loadings under different mean strain values. According to the tests, for higher values of mean strain values, stress-strain curve is more non-linear than that of low mean strain values. Besides, it becomes less non-linear and have a slimmer hysteresis with increasing the number of applied cycles. After a certain number of cycles, hysteresis becomes stable with a lower stiffness for higher mean stress values but this effect is not observable for lower mean stress values. A further observation is that material displays more resistance to creep under uniaxial compressive load compared to tensile load. Similar results to [38] were found in [40]. However, there are further observations. Presence of a tensile hydrostatic pressure increases creep deformation

since there is more volume for molecules to move and this decreases the resistance to the inelastic creep deformation. Presence of a compressive hydrostatic pressure influences in opposite way. Moreover, a superimposed shear stress enhances creep deformation in axial direction.

In article [41], two epoxy resins with different cross-link densities were compared at various temperatures, especially in terms of their Poisson's ratio ν. According to experiments, mechanical properties of the epoxy with less cross-link density varies with temperature greatly while the other epoxy has slight variance in these properties for the temperature range of tests. Therefore, epoxy with high cross-link density is more resistant to viscoelastic flow as expected. In the tests, Poisson's ratio increases with increasing temperature and this means that epoxy resin reaches a nearly incompressible rubbery state with a high Poisson's ratio (close to 0.5) above glass transition temperature. This increment rate in Poisson's ratio is more pronounced around glass transition temperature. Besides, resin with low cross-link density possesses higher Poisson's ratio in the examined temperature range. Increasing strain value applied to epoxy resins enhances Poisson's ratio. Transition from linear to non-linear stress-strain response of the epoxy with high cross-link density is reached at smaller strain values. Around this transition region, Poisson's ratio increment rate is very high compared to that of other epoxy for the same strain value. It is also worth mentioning that, for high values of applied strain, increment in Poisson's ratio with time is more pronounced. Some of the reasonings from these experimental results will be compared with the experimental and numerical results of the silica filled epoxy compound modelled in this thesis. In literature, previously mentioned experiments were used to validate nonlinear viscoelastic constitutive model of Xia and Ellyin [35], Xia and Shen [42] and Xia and Shen [39]. They proposed a nonlinear viscoelastic model in differential form, which uses a branch with a spring and Kelvin elements connected in series. The distinctive property of the model is that it is capable of predicting unloading behaviour of the material in cyclic tests using a switching rule. According to this rule, stiffness of springs located in kelvin elements are a function of an equivalent stress that contains a constant R. This R value is defined as the ratio of the yield stress in compression to yield stress in tension. A shape memory surface is described by a function of maximum equivalent stress during deformation and it updates itself each time stress reaches its maximum value. Stiffness of springs are a function of equiva-

lent stress during loading (on the shape memory surface) while stiffness keeps its last value during unloading (inside of the shape memory domain). By this way, unloading stress-strain curve of the experiments is predicted as concave upward shape properly. In the case of same stiffness values used in loading period, this behaviour is not predicted by any of the viscoelastic models. In [42], Xia and Shen applied the switch rule to 3 well-known viscoelastic models of the same epoxy resin (Epon 826) for cyclic tests : Schapery model (Non-equilibrium thermodynamics approach), Knauss-Emri free volume model (nonlinear free volume approach) and Xia et al. model (a mechanical analogue model in differential form). Upon incorporation of switching rule to the models, their prediction capability improved reasonably although free volume model predictions for unloading were not quite satisfactory. Observations in the previously mentioned experiments of epoxy are also evaluated with the model in the articles [38] and [35]. Creep recovery and compliance tests and effect of stress magnitude on linearity-nonlinearity response in these tests, interaction of shear and normal stress, hydrostatic pressure influence on shear and axial stiffness, shear-axial load path dependence and strain rate dependence were investigated and prediction capabilities of the model were fairly good for all. In cyclic tests, stress relaxation leads to slimmer hysteresis curves with increasing number of cycles and estimated response is in agreement with tests.

In another works for modeling epoxy [43],[44],[45],[5] and in other sources, it is stated that linear viscoelasticity methods are only valid for small strain range while nonlinear viscoelasticity model proposed by Bergström and Boyce [15] has better predictions for all strain regime. Besides, according to the comparisons of LVE and NVLE in [43], LVE is not capable of predicting stress relaxation above a certain strain value (0.001). In the same article, temperature and strain-rate dependence of an epoxy compound were investigated since it is used as encapsulation of semi-conductors in automotive industry and it functions temperatures between -40°C and 250°C, which covers glassy solid and rubbery state of the epoxy. Step-wise strain was applied at various temperatures and strain was kept constant for 120 seconds in every 20 percent of the maximum strain to observe stress dependent intermediate relaxation. In the LVE case, relaxation modulus (creep compliance) is strain independent resulting in worse results while NLVE model gives quite satisfactory results. From these tests, it was observed that stresses were very high even at low strains and low temperatures

below T_g while the material was easily stretched without increasing stress very much at high temperatures. Also, maximum stress relaxation was observed to be around T_g while less amount of stress relaxation was observed at temperatures below T_g. These reasonings were also indicated in [44] and this implies that temperature and strain are two important factors that lead to nonlinearity. Thus, deformation of the epoxy should be handled in the concept of nonlinear models. In the same article and also in [5], linear elastic assumption was used for small strains and this assumption was validated by examining Boltzmann superposition principle (valid in linear regime), successive stress test results and also stress dependence of relaxation modulus.

Jakup and Prisacaru [44] states that BB model is not capable of predicting time dependent large volumetric deformations observed in epoxy compound under hydrostatic load. Free energy function of viscous branch in BB does not include volumetric terms. Therefore, hydrostatic pressure can not be calculated as a function of time. In this contribution, viscous bulk modulus is also included to the free energy function of viscous part and a quadratic volumetric free energy function is proposed to take time dependent volumetric effects into account. In this manner, initial total bulk modulus equal to the sum of equilibrium and viscous bulk modulus values and it converges to equilibrium bulk modulus at the end of the deformation. It is important to emphasize that BB model is actually developed for hyperelastic rubber like materials which are considered to be incompressible in many cases. Consequently, BB model does not take decrease of bulk modulus with time into account. Further tests (three point bending and uniaxial) and comparisons of LVE and NLVE are found in Hong and Gromala [45]. Time-temperature superposition, prony series fitting of bulk modulus and shear modulus parameters, variation of Poisson's ratio with temperature and uniaxial and hydrostatic test results of an epoxy compound can be seen in Lee and Sun [5].

Pap, Kästner and Müller [46] performed displacement controlled step-wise tensile tests and identified viscoplastic behaviour of an epoxy-based adhesive since it displayed equilibrium hysteresis. However, they proposed a nonlinear viscoelastic model with a non-linear elastic stress-strain relation and an overstress. Also, viscosity of the model contains exponential dependence on overstress. This is because the magnitude of overstress affects how fast relaxation behaviour occurs as observed from experiments. In the model of the current thesis, magnitude of overstress is also included

in the evolution equation of viscous strain. Since they were mainly interested in the strain rate dependence of the material, they selected this model. As stated in the article, monotonic relaxation results were adequate but cyclic deformation could not be accurately estimated with the viscoelastic model since there was also plasticity in experiments. Since they observed viscoplastic response, which was deducted from non-equilibrium hysteresis of intermediate stress relaxations tests, they also included a branch with plastic element for equilibrium response and generalized nonlinear elastic behaviour to three dimensional case incorporating bulk and shear modulus and deviatoric and volumetric tensors as stated in[47]. In the model, plastic strain's temporal change is a function of arclength, total strain, a parameter controlling non-linearity of the relation and plastic strain. Material parameters of the equilibrium part were determined by comparing equilibrium stress and the terminal points reached during intermediate relaxation test. The remaining parameters associated with overstress part were determined from monotonic relaxation tests. Results of monotonic tension and relaxation simulations were reasonably in agreement with experiments. Path dependence, interaction of shear and axial stress and cyclic tests were also studied. Results were similar to the ones in [38], [42]. Same tests were compared with a small strain fractional non-linear model proposed by Kästner and Müller [48]. It was found that fractional model gives good results for all type of tests except cyclic loading and unloading tests with intermediate holding times.

There are also other worthwhile works. Ryther, Chad E used the viscoplasticity based on overstress model developed by Krempl and co-workers [49] to simulate PMR-15 material, which is a high-temperature thermosetting polymer, at a certain temperature range, at which the material shows viscoplastic behaviour. They improved the model by making certain parameters involved in the model such as Young Modulus, tangent modulus, viscosity and a function of temperature based on the experimental behaviour of these parameters with temperature. Experimental procedure of the article included relaxation drop, creep with prior strain-rate and temperature dependence. Results of the relaxation tests indicated that stress relaxation drop was greater for higher prior strain values. Initial modulus was also greater for higher prior strain values. At high temperatures, both of them were lower for the same prior-strain rates, which was the

reason of the decrease in the flow stress as stated by the author. It was also observed that increasing temperature or prior strain-rate made creep accumulation greater. The comparisons of the simulations and the experiments were fairly sufficient for both relaxation and creep.

Bardella [50] proposed a phenomenological non-linear viscoelastic model for epoxy resins. The model includes a linear spring connected to a nonlinear Kelvin element in series. For the spring of Kelvin element, phenomenological non-linear Ramber-Osgood relation (based on equivalent stress and some parameters) and, for the dashpot, Eyring theory were employed. Eyring theory includes a molecular transformation relation between equivalent stress and strain rate, which contains an energy barrier term for molecule crosses, absolute temperature, Boltzmann factor, equivalent viscous stress, and action volume of polymer segments. Energy barrier and absolute temperature make the model a thermomechanical one and it can be used to predict temperature dependence. However, dependence of the material parameters on temperature are also required for this purpose. As stated in the article, using this theory and a tensorial stress-strain law for the dashpot, one can determine time dependent response of the dashpot. Creep tests under various stress levels were in good agreement with simulations only for certain stress levels. The other results were not good because of the deviation of stiffness in the epoxy material tested and some technical issue as stated by Bardella. The unloading behaviour of the model during the cyclic test was also simulated properly. Lastly, as stated in [42], combination manner of springs and dashpot also affects capability of simulations.

1.1.4 Aim of thesis

Viscoelastic materials are largely used in industry for different purposes and it is important to predict their life cycles, deformation characteristics and residual stresses on them to design products properly. The stress caused by the mismatch of the coefficient of thermal expansion (CTE) between epoxy based compound EMC and adjacent materials is one of the major causes for premature failure. Numerical methods are critical since they are used largely to decrease time spent in product development process. However, material characterization is a critical stage in product development. The product works under large strain regime with non-linear effects and high temperature

differences. Linear viscoelasticity theories are valid only for small strain regimes and temperatures close to T_g. Therefore, a complete non-linear material theory formed for the special material is required after the characterization of the material is done.
The utilized material can be subjected to high hydrostatic loadings especially after molding process and other types of varying thermo-mechanical loadings during product's life cycle. For this reason, the material exhibits significant volumetric viscosity in addition to shear viscosity.
Thus, the aim of this thesis is to simulate uniaxial and volumetric creep behaviour of an epoxy compound and determining dependence of the response on temperature so that we form a model that can be implemented into commercial finite element softwares to predict three dimensional response of similar materials considering viscous volumetric effects. Experimental characterization of the epoxy compound indicates that there is also significant non-linear volumetric creep behaviour under hydrostatic loading. As indicated earlier in this chapter, viscous volumetric response of epoxy materials are not considered in BB model and in other rubber models since they display nearly incompressible behaviour. However, in this thesis, viscous bulk modulus value is also included and the epoxy material has a variable bulk modulus value between the sum of equilibrium and viscous bulk modulus value at the initial instant, and equilibrium bulk modulus value after deformation which leads to the time dependent volumetric response. Besides, the proposed model is implemented into FEAP (open source Finite Element Analysis Program) and various mechanical material properties and their alteration with temperature are investigated by comparison of the simulations and the experiments.
Another distinctive contribution is the application of a new evolution equation proposed by Dal [1] for the evolution of the viscous deformations. It is developed based on the inelastic and elastic molecular motion of a single chain in a chain forest.
The proposed model is proven to be a very powerful tool for accelerating the development process of electronic control units and power modules by better prediction and evaluation of the limits.

1.1.5 Structure of the work

Chapter 2 outlines viscoelastic behaviour of polymers. Moreover, one-dimensional basic viscoelasticity is introduced and then it is extended to three dimensional methods in the framework of larger strain continuum mechanics. Proposed evolution law of creep rate, rheological model, proposed free energy based on micro-structure is also presented in this chapter. Chapter 3 is devoted to Kirchoff stress and consistent tangent modulus derivations along with the algorithmic structure of the proposed model in Eulerian setting. Uniaxial and volumetric tests conducted by Maryland University are explained in Chapter 4. Besides, comparisons of numerical and experimental results, effects of the parameters on simulation results are presented in Chapter 4. Chapter 5 is devoted to conclusion.

CHAPTER 2

2.1 Characteristics and mechanical properties of polymers

Polymeric materials are used in all type of products. For example, basic structure of biological tissues are similar to structure of synthetic polymers. Chemical engineers or chemists formulates the synthetic polymer in accordance with requirements of a product. Other engineers who design certain engineering components of a product use these polymers in their design due to their particular properties. Polymeric materials are preferred because of their properties such as lack of heat and electrical conductivity, toughness, resistance to corrosion, low cost. They also may be deformed up to a few times of their initial length due to their long chain molecular structure. Stress and strain in most of the polymeric materials shows time-dependent behaviour. Loading and unloading response of the material may be very different since dissipation occurs during the deformation. This chapter covers up these issues regarding polymers.

2.1.1 Types of polymeric materials

Although there are many ways to classify polymers, two general polymer types are thermosets and thermoplastics. Difference between them can be explained by looking at their bond structure which holds molecular chains of polymers together and determines the mechanical properties of polymers. In thermosets, there are primary bonds (or crosslinks) between molecular chains, which are stronger than secondary bonds (Van Der Waals) found in thermoplastics. Due to weak strength of secondary bonds, thermoplastics can be melted or molded while thermosets can not be melted

at least in a general way. Thus, thermosetting polymers are used in products that perform within large temperature ranges. They should also satisfy dimensional requirements and polymer degradation (change in properties such as strength, shape, color) should be avoided during service life duration. Some application examples of these materials are electronic packages (where there is a need for electrical and thermal insulation, high strength, low warpage), adhesives, composites, seals, automobile bumpers, tires. Some of the thermosetting materials used for this purposes are epoxides, aminos, polyesters, etc. Besides, fiber reinforced polymers takes the place of metals in structural applications due to their high modulus and strength.

2.1.2 Mechanical properties of polymeric materials

Polymers show quite different response compared to metals when they are subjected to loads in various conditions. Metals show resistance to the applied load by attractive and repulsive forces in inter-atomic bonds which are related with interaction of electron shells of atoms and these forces vary depending upon the distance between the atoms [4]. Therefore, yield point of metals is reached for low strain values. In contrast to metals, polymers are more complicated with long chain molecules in a polymer gel matrix. Because of their molecular structure, they can be deformed up to large strains which also varies for all polymers. Many researchers [2], [25] explain viscoelastic or time-dependent properties of polymers by using crosslinked strong network and the superimposed entanglements of a free chain as shown in Fig. 2.1. Free chains are sometimes called elastically inactive since they carry less load and

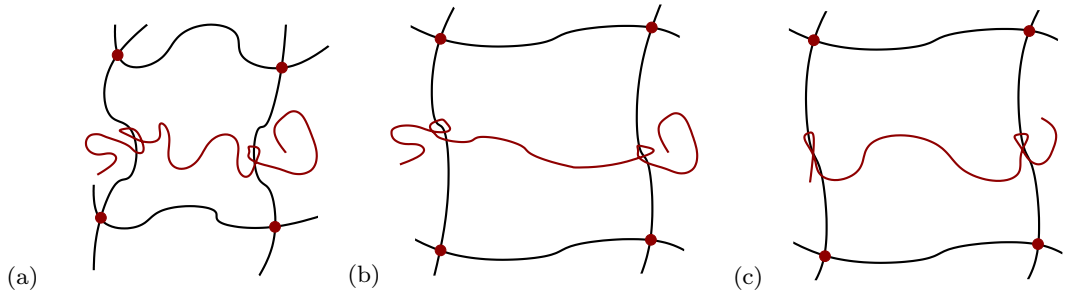

Figure 2.1: Micromechanical representation of superimposed free chains in (a) undeformed, (b) deformed state after sudden loading and (c) deformed and relaxed state.

tend to change their conformation during loading. Same as network, free chains also carry load when a sudden load is applied to the material. These chains entangling around other chains start to loosen if the sudden applied load is held constant for a certain amount of time. Temperature also plays a role in this loosening process since reptational and Brownian motions of a free chain as described by Doi and Edwards [32] are triggered in an easier way at high temperatures leading to variations in stress and strain with time. After this process, the material reaches a more relaxed state with less stress. Bergström and Boyce [15] developed an evolution equation relating stretch and creep rate using governing reptational motion of the free chain as a function of time, which is described by Doi and Edwards [32].

2.1.2.1 Temperature and time dependence of polymers

It is shown by many researchers that the mechanical response of the many polymeric materials are strain-rate and temperature dependent as shown in Fig. 2.2. Strain-

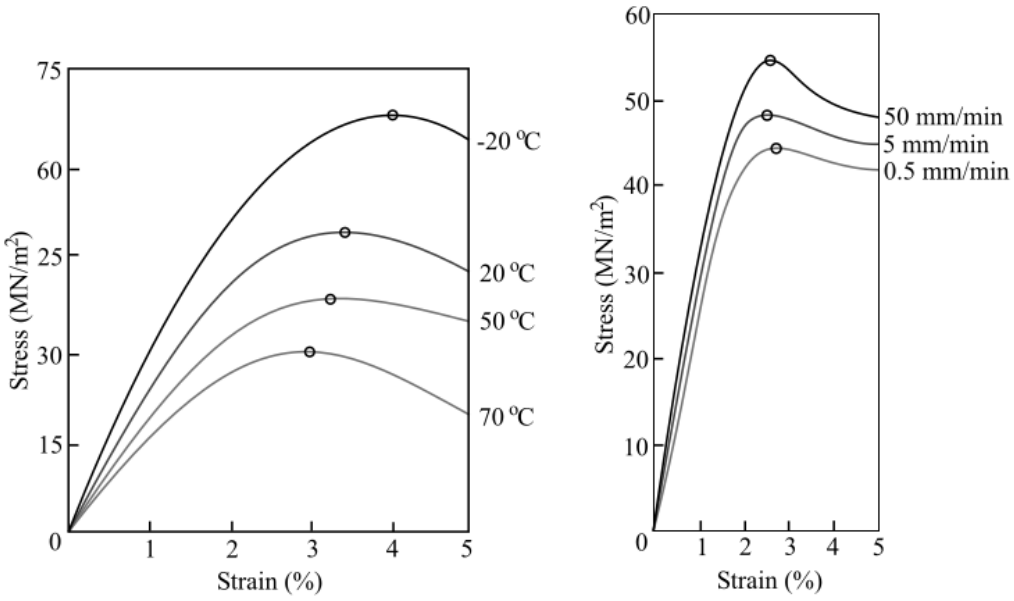

Figure 2.2: Typical temperature (on the left) and strain-rate (on the right) dependent stress-strain response [4].

rate dependence of polymeric materials can basically be explained by the fact that at high strains, chains immediately align themselves in the direction of loading since

there is no time for entanglements to loosen with reptational motion. At low loading rates, there is more time for entanglements to become loose easily leading to lower resistance shown by free chains to the applied load compared to higher loading rates. On the other hand, as temperature increases, fluctuations of polymer chains increase making motion of them easier within the network. As a result, they disentangle from the network in an easier way compared to low temperatures reducing the load carrying capability of the material. It should be also noted that the dependence on temperature and strain rate are more pronounced at large strains. In Fig. 2.3, stress-strain response of a brittle epoxy material is shown. At low temperatures, the epoxy exhibits a glassy behaviour with linearly increasing stress with strain and it ruptures at relatively low stress values. At high temperatures, the epoxy behaves more like a rubber showing high stretch values with nearly constant stress before failure. Obviously, a transition region from rubbery to glassy behaviour exists in all polymeric materials although temperature range of the transition region observed is different for all materials. Therefore, at room temperature, a polymeric material displays glassy behaviour while another polymeric material displays rubbery behaviour. It is engineer's responsibility to select the compatible polymer by taking the working conditions such as temperature, mechanical loadings into account.

2.1.3 Viscoelastic properties of polymers

Rate and temperature dependence or viscoelasticity of polymeric materials are explained in the previous sections departing from their unique molecular structure. Because of this molecular structure, polymers exhibit viscoelastic behaviour and behave as elastic solids or viscous fluids at certain times while they behave as both in some instances. For this reason, they can not be represented by the mathematical laws of elastic solids or fluids purely. Amount of strength and modulus shown by the material generally depends on the micro-structure and ambient temperature although there can be other factors such as corrosion, moisture and other environmental effects. As mentioned previously, network of the polymer is brittle as a glassy solid, shows resistance to fluid like flow (high viscosity) and it has high strength and modulus at lower temperatures. At high temperatures, viscosity of fluid type response decreases and strength and modulus are lower showing rubbery response. These transition from

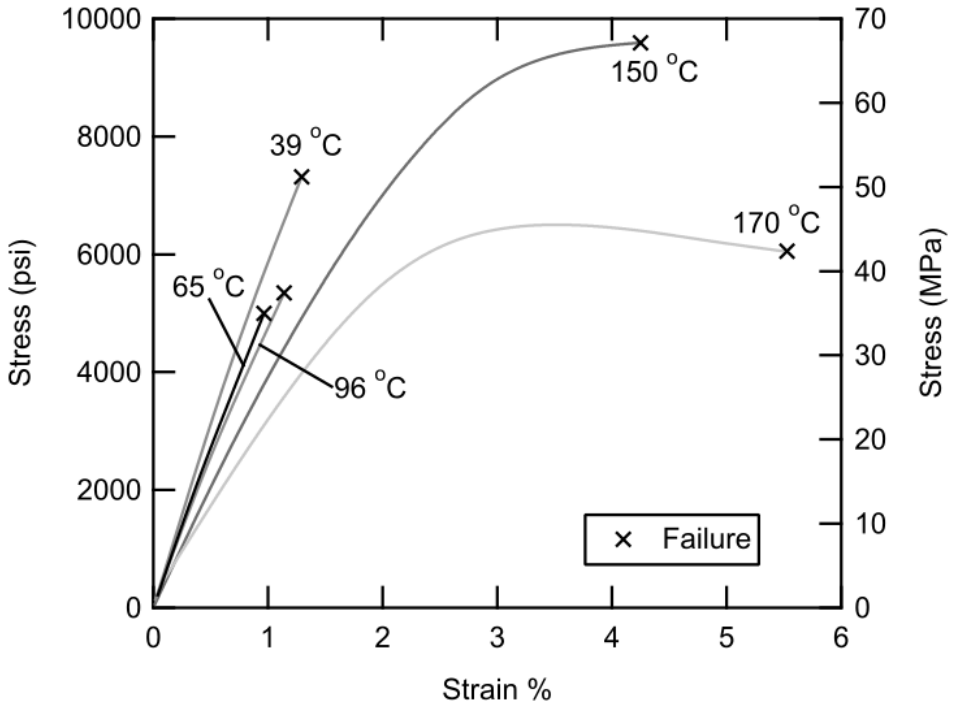

Figure 2.3: Temperature dependent stress-strain response of a typical brittle epoxy [4].

glassy to rubbery state will be explained later in this section. Firstly, relaxation and creep behaviours of polymers will be mentioned.

2.1.3.1 Relaxation and creep

Relaxation and creep behaviours are the most known behaviours used for characterizing time dependent response of polymers. In a relaxation process, as shown in Fig. 2.4, a constant strain ε_0 applied to the material uniaxially and in a quasi-static way (no inertia effects) at $t = t_0$ leading to a sudden stress σ_0, which decreases with time to the equilibrium value σ_∞. This is an ideal case since loading a material instantaneously would not be possible in the real life. Relaxation of stress takes place due to the fact that chains in the polymer change their conformation to a more relaxed state with time. As a result, compared to the deformed state, free chains no more carry load resulting in a lower load carrying capacity of the material at constant strain

value. Another fact is that thermosetting materials converge to a constant stress value while ideal thermoplastic materials converge to zero stress value. The reason for this kind of behaviour is because of the difference in dominant bonds between monomers. In thermosetting materials, there are primary bonds between the monomers, which are also called cross-links. Primary bonds found in thermosets give rise to a more solid behaviour. Accordingly, the material can not flow after some limit time due to the applied force. Density of cross-links in the material determines the magnitude of equilibrium stress. Thermosets with highly cross-linked micro structure display a high equilibrium stress value. Besides, there are filler particles used in the micro-structure for increasing modulus and strength of polymers. In contrast to thermosets, there are weaker secondary bonds (or Van Der Waals) between monomers of thermoplastics. These weak bonds break with time upon loading since monomers slide past each other and this leads to a reduction in viscosity. In other words, thermoplastics behave like a liquid and there is not a limit value for this flow. Liquid-like behaviour is especially dominant for high temperature ranges as the secondary bonds between monomers break easily (melt) unlike primary bonds. A relaxation modulus (t) can be defined for this relaxation process since stress is rate-dependent and strain is constant,

$$E(t) = \frac{\sigma(t)}{\varepsilon_0} \tag{2.1}$$

which is only valid for constant strain values. The other important time dependent

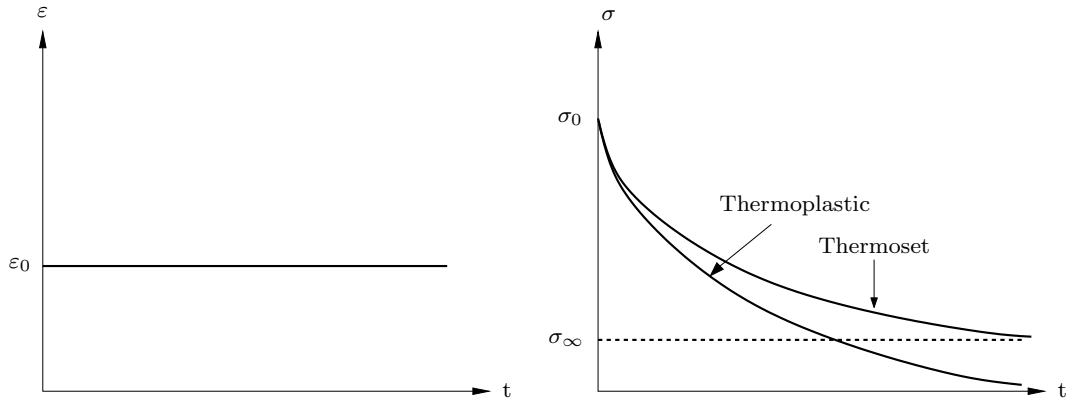

Figure 2.4: Strain input (on the left) and corresponding relaxation behaviour of thermoset and thermoplastic (on the right)

behaviour of polymers is creep behaviour. Creep occurs if a sudden and constant

stress is applied uniaxially (or in another deformation mode) to the material. In a creep test, load should be applied quasi-statically to prevent inertia effects so that there is no prior history since viscoelastic materials are history dependent unlike metals. Under this stress, strain increases with time to a constant value for thermosets as observed from Fig. 2.5. In the case of thermoplastics, there is no limit for the strain value to reach since monomers slide past each other continuously similar to a liquid due to lack of primary bonds (cross-links). Again, creep observed at a certain time is higher for higher temperatures for both thermosets and thermoplastics with secondary bonds. A new quantity called creep compliance $D(t)$ can be defined for

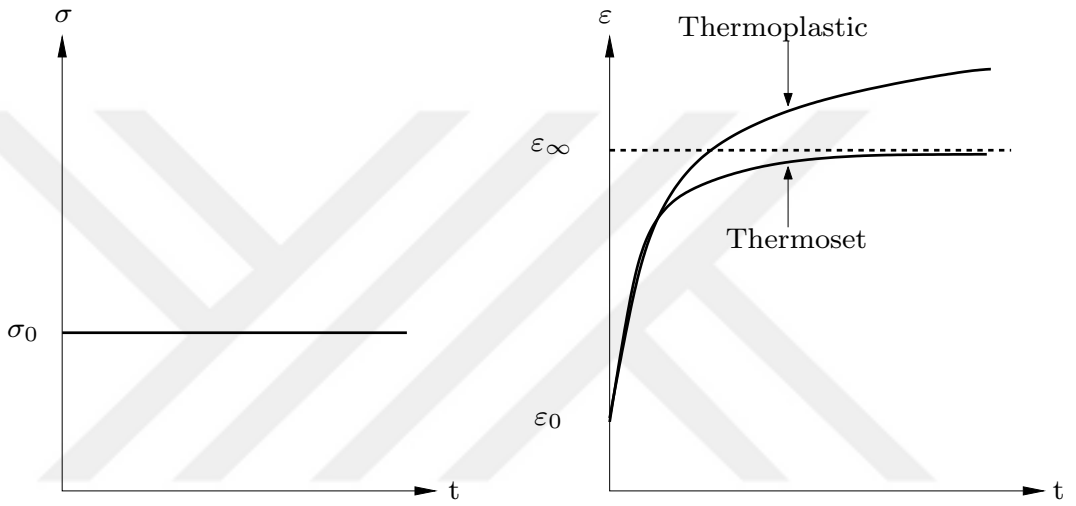

Figure 2.5: Stress input (on the left) and corresponding creep behaviour of thermoset and thermoplastic (on the right)

creep behaviour, which gives information about the sensitivity of strain to the applied constant stress. In this sense, it is like relaxation modulus $E(t)$.

$$D(t) = \frac{\varepsilon(t)}{\sigma_0} \tag{2.2}$$

Of course, it can be extended to non-constant load cases, however, with integral representations.

Another important mechanical property of polymers is creep recovery. If the stress is removed suddenly as shown in Fig. 2.6, strain will decay to zero in a long time. At the first instant, elastic strain decreases rapidly with 90 degree to time axis. Afterwards, viscous part of the strain decays to zero or to a constant strain value (ε_p)

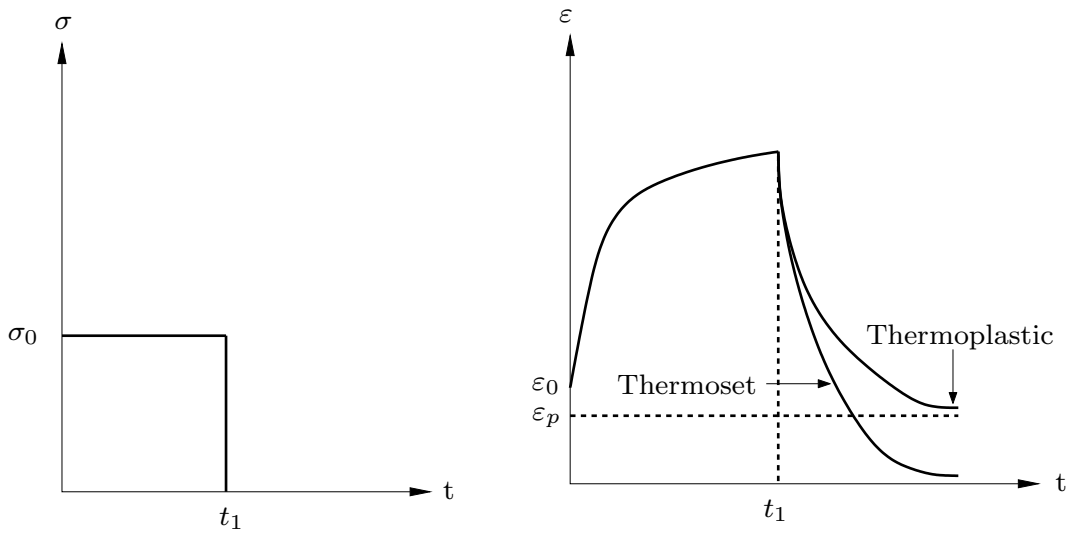

Figure 2.6: Stress input (on the left) and creep recovery behaviour (on the right) of thermoset and thermoplastic

for thermosets or thermoplastics, respectively. Again, a permanent or plastic strain exists in equilibrium of thermoplastics. All in all, initial moduli of thermosets is related with cross-links (primary bonds) and entanglements while equilibrium moduli is related with only crosslinks. Thermoplastics behave more like a fluid in terms of the mechanical response.

2.1.3.2 Isochronus modulus vs temperature

In Fig. 2.7, variation of relaxation modulus at the instant of 10th second $E(t = 10[sec]) = \frac{\sigma(10[sec])}{\varepsilon_0}$ is shown as a function of temperature for amorphous, crystalline and cross-linked polystyrene materials. The figure is separated into 5 regions as glassy, transition, rubbery plateau, rubbery flow and liquid flow, respectively. Flow region is only valid for thermoplastics since thermosets does not exhibit any flow unless temperature is very high. For very high temperatures and long durations, some degradation and fluid time flow along with change in color can be observed in thermosets, as well. The first observation from Fig. 2.7 is that there is a transition region between glassy and rubbery regions where $E(10)$ drops rapidly corresponding to temperature T_g. The transition region can be explained from the free volume vs

temperature in Fig. 2.8. Free volume can be defined as the volume that is not occupied by the main molecular mass of the material while occupied volume is the volume occupied by molecular mass or atoms and quantum shells of atoms. The slope of the V_r vs T curve gives the coefficient of thermal expansion. As we observe from the figure, with increasing temperature, free volume also increases. At some point called glass transition temperature T_g (may be temperature range instead of a point), free volume increases with a steeper line. In other words, there is a discontinuity in the free volume increment at point T_g. The polymer behaves like a glassy solid before the T_g. When temperature is around the range of T_g for that polymer, it shows more pronounced viscoelastic response as we can understand from the rapid drop in relaxation modulus. This is related to the change in free volume around T_g since molecular

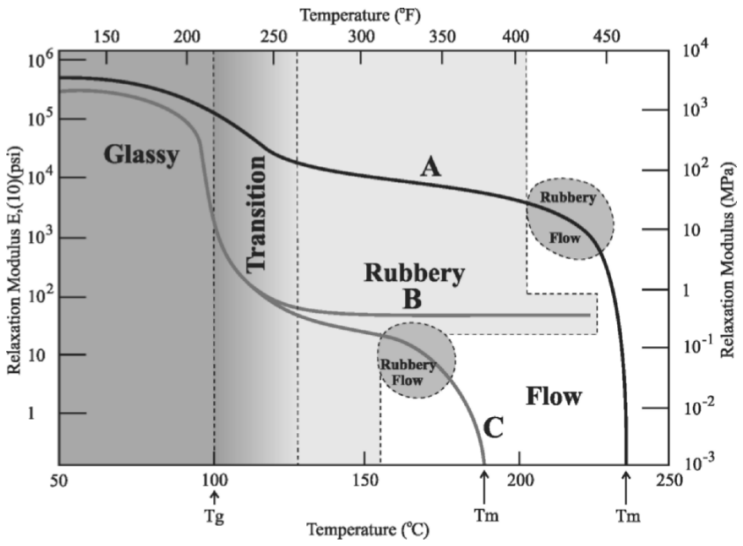

Figure 2.7: E(10 Sec.) for a crystalline polystyrene, A, a lightly cross-linked polystyrene, B, and amorphous polystyrene, C, [4].

chains find more free volume to vibrate freely. Thus, translational and configurational motions of chains take place in an easier way compared to the glassy phase where this molecular motions take place only in some local regions. Frequency and amplitude of motion increase as temperature increases. These motions cause chains to reach a more relaxed state decreasing the stress required for holding the constant strain. Below T_g (in glassy region), these motions and amplitude of vibrations are very small. Therefore, stretching, changing bond angles and change in length of the bonds (primary and

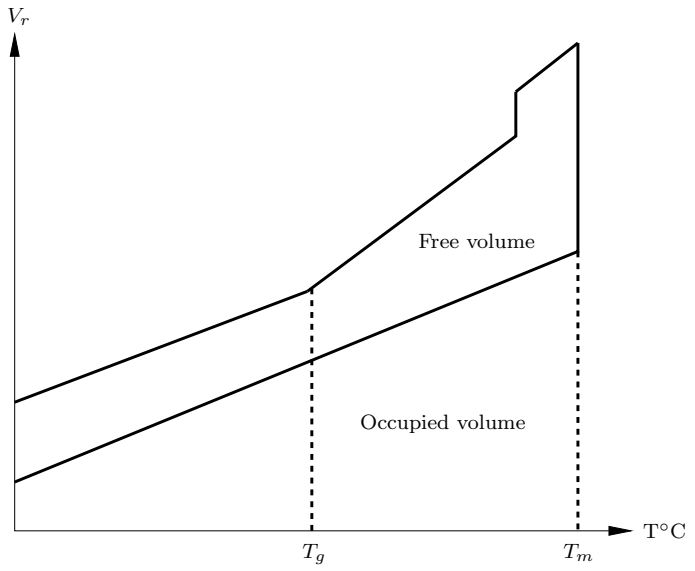

Figure 2.8: Relative volume vs. temperature

secondary bonds for thermosets and only secondary bonds for thermoplastics) under the applied load are the basic reasons for viscoelastic behaviour of glassy region and the behaviour is mostly associated with side polymer groups. Molecular motions of rubbery region are similar to the transition region except for smaller time duration of creep or relaxation. This effect can be observed in Fig. 2.9 from creep response of the test at 170°C with smaller retardation time compared to smaller temperatures. Thus, in rubbery region around 170°C , limit strain value is reached within a few minutes while it may take weeks in glassy region around 155°C. Another important difference between glassy and rubbery (or liquid) range is that permanent deformations due to fluid-like flow may occur in the latter since secondary (sometimes primary) bonds can be ruptured and reformed during deformation. This case is more pronounced for thermoplastics as a result of the denstiy of secondary bonds between chains. Liquid phase can be considered to exist only for thermoplastics. In Fig. 2.8, melting temperature T_m is also shown, at which polymers exhibit a high drop in relaxation modulus.

All polymers have different glass transition temperature range. Therefore, a material may behave like a glassy solid at the temperature, at which another material behaves like a rubber.

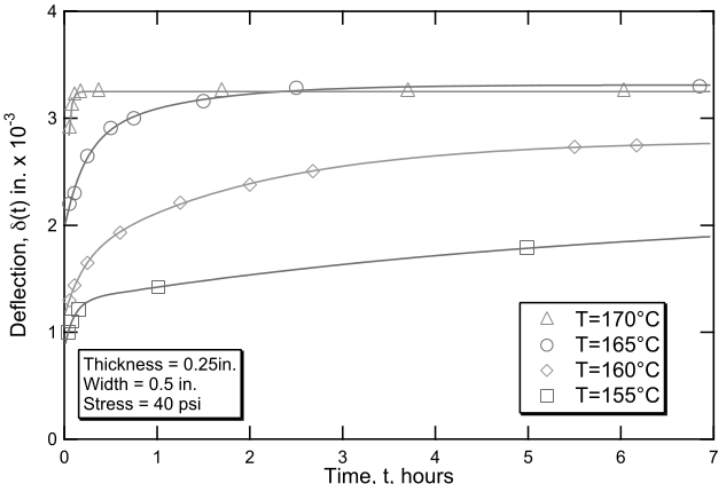

Figure 2.9: Creep of an epoxy at various temperatures [4].

2.1.3.3 Linearity of viscoelastic materials

It is very important to know whether a polymer shows linear or non-linear response under thermo-mechanical loading. Applicability of some rules valid for linear viscoelasticity is evaluated with such knowledge. In contrast to metals, linearity of polymeric materials can not be understood from stress-strain curve since stress (or strain) changes with time and the relation between them is always non-linear in such a curve. Therefore, stress (or strain) independence of creep compliance or relaxation modulus should be checked by testing methods. Creep or stress relaxation tests can be conducted at different values of stress (or strain). One sample is shown in Fig. 2.10. At least three test at different stress values should be done. If the ratio of stress to strain is the same for all three cases at a certain time as shown, the material is said to be linear. Otherwise, it is non-linear.

2.2 Mechanical modelling of one dimensional linear viscoelasticity

2.2.1 Phenomenological models

This section is devoted to the mechanical models created for representing some aspects of viscoelastic materials without considering molecular structure of the mate-

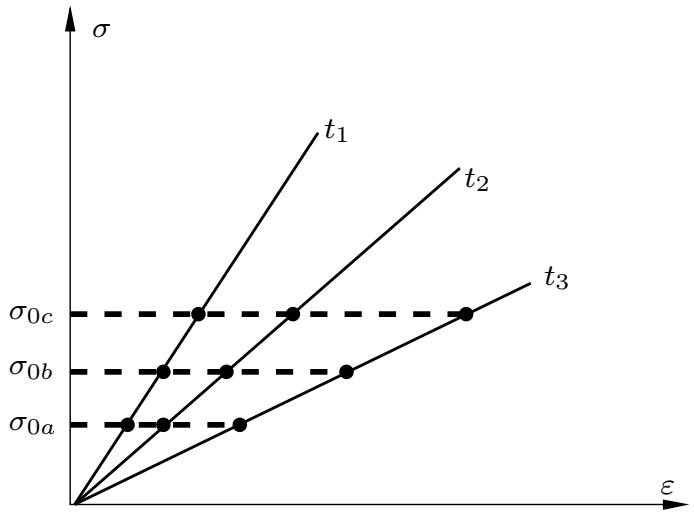

Figure 2.10: Linearity of material indicated by using creep tests with different stress levels

rial. In this manner, some important rate-dependent behaviour of the material such as stress relaxation and creep will be explained. Generally, springs and dashpots are used in the mathematical models of viscoelastic materials. Springs usage is necessary for modeling energy storage (elastic behaviour) and dashpot is necessary for modeling energy dissipating (viscous behaviour) properties of the material. One can assume a linear or nonlinear spring element to represent the behaviour of the material. A linear spring behaves in accordance with Hooke's law stating that stress is proportional to strain with Young Modulus E as $\sigma = E\varepsilon$. Thus, the energy stored in the spring element is $\frac{1}{2}E\varepsilon^2$. On the other hand, stress on a linear dashpot element is proportional to strain rate with viscosity μ since the dashpot behaves in accordance with the Newtonian law of viscosity, $\tau = \mu\dot{\varepsilon}$. By looking Newtonian law, one can realize that the dashpot element becomes stiffer for high strain rates compared to low strain rates. Hence, the dashpot is used to model strain rate dependent materials such as polymers. Spring and dashpot elements can be combined in a variety of combinations to represent real viscous material behaviour. The early basic combinations are Kelvin and Maxwell models.

2.2.2 Kelvin model

Kelvin model is used to describe the creep behaviour of the material. Fig. 2.11 shows the Kelvin solid model, which combines a spring and a dashpot in parallel. Total

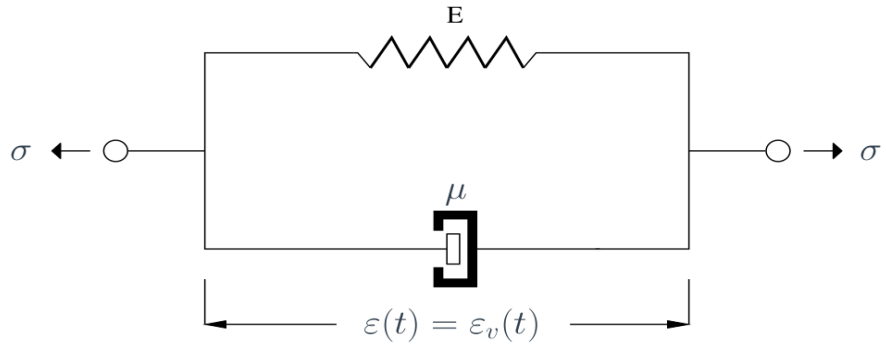

Figure 2.11: Kelvin model

stress is sum of the stresses in two branches and strain is the same for both branches.

$$\sigma(t) = \sigma_e(t) + \sigma_v(t) = E\varepsilon(t) + \mu\frac{\partial\varepsilon(t)}{\partial t} \tag{2.3}$$

$$\varepsilon = \varepsilon_v \tag{2.4}$$

By applying a sudden stress to the solid model and keeping it constant as σ_0 and solving the ODE for the strain $\varepsilon(t)$

$$\begin{aligned} &\varepsilon(t) = \frac{\sigma_0}{E}(1 - \exp(-(\frac{t}{\tau})) \\ &\text{where} \qquad \tau = \frac{\mu}{E} \text{ is relaxation time} \end{aligned} \tag{2.5}$$

This equation and stress on both elements can be plotted for certain values of the parameters as follows, which is creep behaviour of the Kelvin solid model. Creep response with time is due to the expansion of the dashpot under constant load. As shown in Fig. 2.12, stress on the dashpot decreases with time while it increases on the spring. This keeps the load on the total solid model constant for all times.

Kelvin model can not be used to describe stress relaxation behaviour. According to the Newtonian law of viscosity, a sudden strain applied to the model is not possible

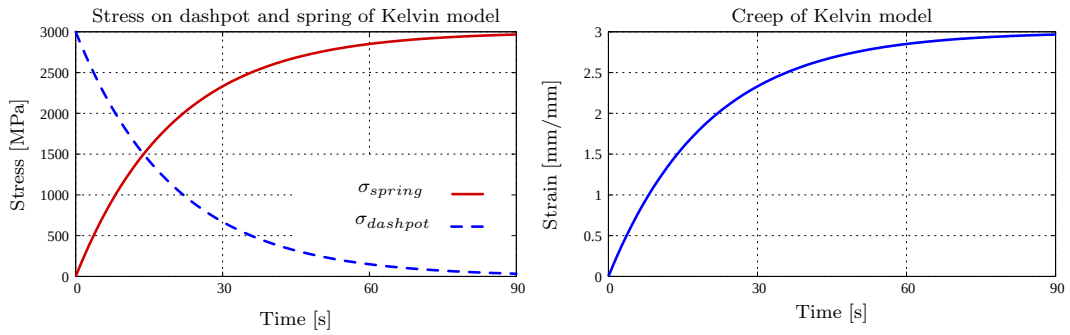

Figure 2.12: Stress on dashpot and spring (on the left) and creep (on the right) on Kelvin model

since it results in infinite stress in the dashpot branch. However, by adding a spring in series to the dashpot, the spring takes the instantaneous strain by storing energy and that prevents infinite stress.

2.2.3 Maxwell model

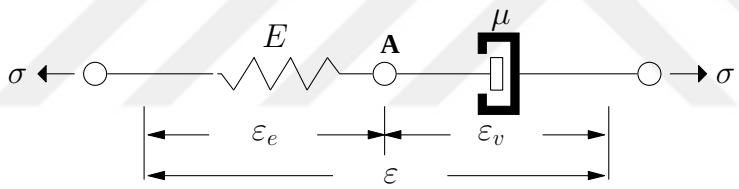

Figure 2.13: Maxwell model

In Maxwell model, the spring and the dashpot are combined in series as demonstrated in Fig. 2.13. In this model, stresses in the spring and the dashpot are same and the total strain is the sum of the strains in the elements.

$$\begin{aligned} &\sigma(t) = \sigma_e(t) = \sigma_v(t) \\ &= \sigma(t) = E(\varepsilon(t) - \varepsilon_v(t)) = \mu \frac{\partial \varepsilon_v(t)}{\partial t} \end{aligned} \tag{2.6}$$

$$\varepsilon = \varepsilon_e + \varepsilon_v \tag{2.7}$$

If a sudden strain ε_0 is applied and kept constant for a certain amount of time, relaxation of the model occurs due to the expansion of the dashpot. Arranging equation

2.6 and taking $\varepsilon(t) = \varepsilon_0$

$$\frac{\partial \varepsilon_v(t)}{\partial t} + \frac{E}{\mu}\varepsilon_v(t) = \frac{E}{\mu}\varepsilon_0 \tag{2.8}$$

Solving the ODE

$$\varepsilon_v(t) = \varepsilon_0(1 - \exp(-(\frac{t}{\tau}))) \tag{2.9}$$

is obtained. It can be used in $\sigma(t) = E(\varepsilon_0 - \varepsilon_v(t))$ to find stress.

$$\sigma(t) = E\varepsilon_0 \exp(-(\frac{t}{\tau})) \tag{2.10}$$

At the time $t = \tau$, which is called relaxation time and used as an indicator of how fast relaxation occurs, it takes a value of $\frac{\sigma_0}{e}$. Stress relaxation behaviour of Maxwell model is shown in Fig. 2.14.

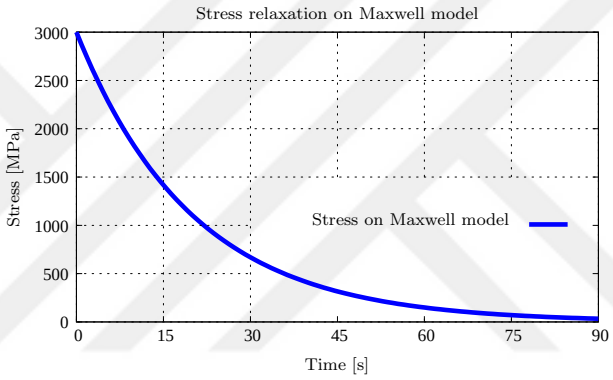

Figure 2.14: Stress relaxation on Maxwell model

2.2.4 Viscoelastic material model

Above described models can not be used to predict the behaviour of a real viscoelastic material since they are given to show the relaxation and creep processes. For instance, Kelvin model does not show any permanent strain after unloading. In the same manner, Maxwell model does not show time-dependent recovery and can not be used to model primary creep behaviour. A more realistic model will be used in the thesis to simulate the viscoelastic materials. Thus, the one dimensional version of the proposed model includes two branches as shown in Fig 2.15. The first branch includes only a spring and associated with the equilibrium response, which is reached

after a certain amount of time has passed while the second branch parallel to the first one includes a dashpot in series with another spring. The second branch is used to simulate viscous behaviour. When a sudden load is applied to the material model,

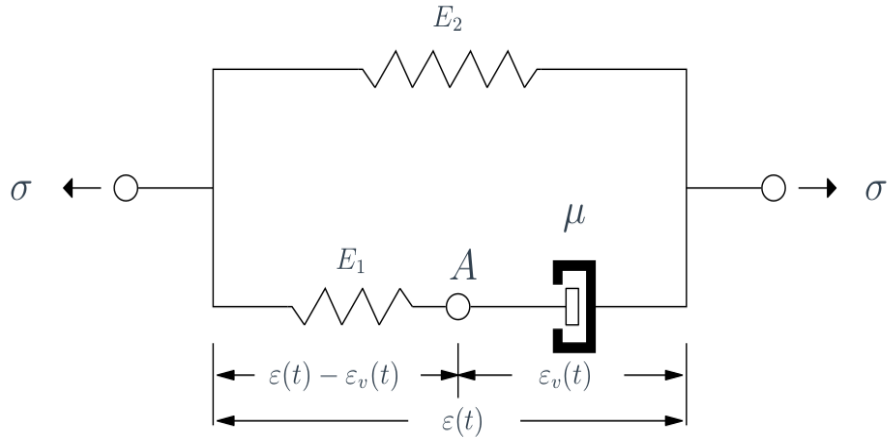

Figure 2.15: Rheological finite viscoelastic model

first branch reacts immediately by storing energy in the spring element. Similarly, the spring in the viscous branch expands in the same way and the dashpot acts as a rigid element since there is no time for it to elongate. After keeping the load constant for a certain amount of time, the dashpot deforms in accordance with Newtonian law of viscosity increasing viscous strain $\varepsilon_v(t)$ and reducing elastic strain. Tension in the spring is no longer available due to the released end of the spring by the dashpot. Hence, strain of spring in the viscous branch decreases and energy stored by that element is released. In other words, the energy of the spring is wasted by the dissipation element, the dashpot. As a result of this process, creep is observed in the model.

Instead, if a sudden strain is applied to the model, dashpot does not immediately react to the sudden strain and it takes time for viscous strain $\varepsilon_v(t)$ to increase up to the level of applied strain, ε_0. However, strain in the first branch immediately reaches the applied strain value by storing energy. Since the total strain in two branches must be the same, the spring in the second branch also reaches the same value. As time passes by, the dashpot becomes less stiff because of decreasing stress carrying capacity of the second spring with expansion of the dashpot and the stress on the second branch decreases. Eventually, viscous strain in the dashpot reaches the value of applied strain with a zero slope ($\sigma_d = \mu \frac{\partial \varepsilon_v}{\partial t} = 0$) and the only stress remaining in the model is the

equilibrium stress in the first branch although the same strain value ε_0 is applied.

2.2.4.1 Creep behaviour of the model

For the creep process, total applied stress σ_0 is the sum of two branches

$$\sigma_0 = E_1(\varepsilon(t) - \varepsilon_v(t)) + E_2\varepsilon(t) \tag{2.11}$$

Also, the spring and the dashpot of the viscous branch are connected in series meaning that the stress on them should be equal.

$$\mu\frac{\partial\varepsilon_v(t)}{\partial t} = E_1(\varepsilon(t) - \varepsilon_v(t)) \tag{2.12}$$

Solving for $\varepsilon(t)$ in the first equation and inserting it into the second equation

$$\begin{aligned}\frac{\partial\varepsilon_v(t)}{\partial t} + \frac{E_1\varepsilon_v(t)}{\mu} &= \frac{E_1}{\mu}(\frac{\sigma_0 + E_1\varepsilon_v(t)}{E_2 + E_1}) \\ = \frac{\partial\varepsilon_v(t)}{\partial t} + \frac{E_1E_2}{(E_1 + E_2)\mu}\varepsilon_v(t) &= \frac{E_1}{\mu}\frac{\sigma_0}{E_2 + E_1}\end{aligned} \tag{2.13}$$

Solution of the above equation can be found easily as $x(t) = \frac{B}{A}(1-\exp(-(At))$ since it is in the form of $\dot{x} + Ax = B$. Hence,

$$\varepsilon_v(t) = \frac{\sigma_0}{E_2}[1 - \exp(-(\frac{E_1E_2}{(E_1 + E_2)\mu})t] \tag{2.14}$$

Solving equation 2.11 for $\varepsilon(t)$ in terms of $\varepsilon_v(t)$

$$\varepsilon(t) = \frac{\sigma_0 + E_1\varepsilon_v(t)}{E_1 + E_2} \tag{2.15}$$

This result is plotted along with $\varepsilon_v(t)$ in Fig. 2.16. Constants of the springs and the dashpot are taken as $E_1 = 1000$ MPa, $E_2 = 3000$ MPa, $\mu = 20000$ MPa.s and applied constant stress is $\sigma_0 = 3000$ MPa. In accordance with the previous comments, the dashpot starts with zero strain while the spring of first branch start with a strain $\frac{\sigma_0}{E_1+E_2}$, which is also equal to the total strain. Then, the dashpot elongates and strain of both branches reaches the equilibrium value. During this process, stress on the first branch spring increases taking the load carried by the second branch spring as a function of time.

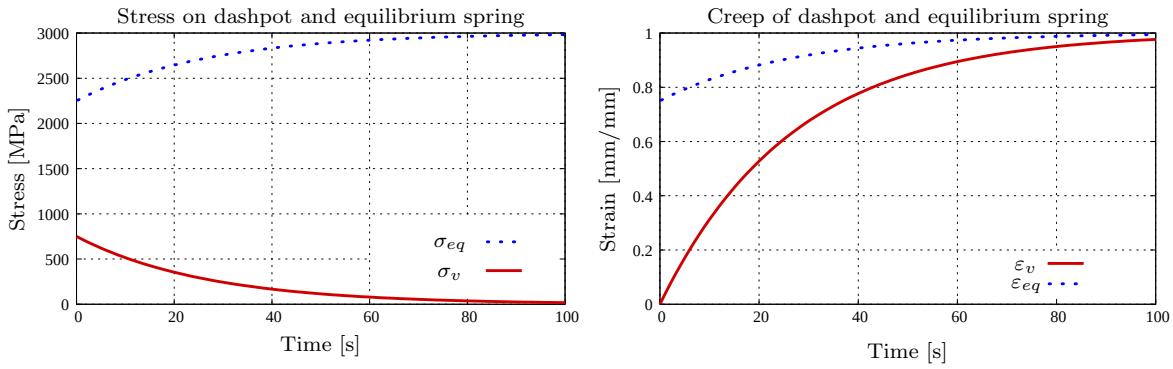

Figure 2.16: Stress on dashpot and equilibrium spring (on the left) and creep of dashpot and equilibrium spring (on the right)

2.2.4.2 Relaxation behaviour of the model

For the relaxation of the model, a sudden constant strain ε_0 is applied. Thus, total stress becomes

$$\sigma(t) = E_1(\varepsilon_0 - \varepsilon_v(t)) + E_2\varepsilon_0 \tag{2.16}$$

Also, stress in the dashpot and the viscous spring is same

$$\begin{aligned} \mu\frac{\partial\varepsilon_v(t)}{\partial t} &= E_1(\varepsilon_0 - \varepsilon_v(t)) \\ \frac{\partial\varepsilon_v(t)}{\partial t} + \frac{E_1}{\mu}\varepsilon_v(t) &= \frac{E_1}{\mu}\varepsilon_0 \end{aligned} \tag{2.17}$$

Solving eq. 2.17 for $\varepsilon_v(t)$, we find

$$\varepsilon_v(t) = \varepsilon_0[1 - \exp(-(\frac{t}{\tau}))] \tag{2.18}$$

Inserting it into the equation 2.16, we find total stress as

$$\sigma(t) = E_1\varepsilon_0 \exp(-(\frac{t}{\tau})) + E_2\varepsilon_0 \tag{2.19}$$

Using the same parameters in the creep part and taking constant strain $\varepsilon_0 = 1$ $[mm/mm]$, we can plot the following relaxation Fig. 2.17. The total stress amount is reduced at the same amount initially carried by viscous branch.

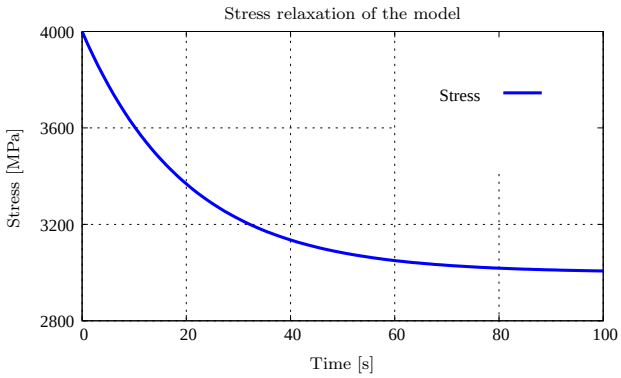

Figure 2.17: Stress relaxation of the model

2.2.5 Prony series representation

As stated earlier, Maxwell and Kelvin models have limited usage in representing real behaviour of most viscoelastic materials. A more realistic model is obtained using prony series approach in which a series of Maxwell model is used along with a equilibrium spring to obtain equilibrium response at infinite time. It is usually not possible to represent the behaviour with only one Maxwell element. Thus, as shown in Fig. 2.18, n Maxwell elements can be used in parallel, which is called Generalized Maxwell model or Prony series representation. Prony series representation is used in representing behaviour of thermoplastics. However, in Fig. 2.18, a spring is added to represent the behaviour of a thermoset with a residual stress at infinity, which is known as Wiechert model. Generally, 5-15 elements are used in Generalized Maxwell model.

Considering the Prony series representation for only 2 branch Maxwell elements, we can define kinetic relations as

$$\sigma = \sigma_1 + \sigma_2 \tag{2.20}$$

$$\varepsilon = \varepsilon_1 = \varepsilon_2 \tag{2.21}$$

Using the previously shown constitutive equations for Maxwell elements

$$\begin{aligned} \sigma_1 + \frac{\mu_1}{E_1}\frac{\partial \sigma_1}{\partial t} &= \mu_1 \frac{\partial \varepsilon_1}{\partial t} \\ \sigma_2 + \frac{\mu_2}{E_2}\frac{\partial \sigma_2}{\partial t} &= \mu_2 \frac{\partial \varepsilon_2}{\partial t} \end{aligned} \tag{2.22}$$

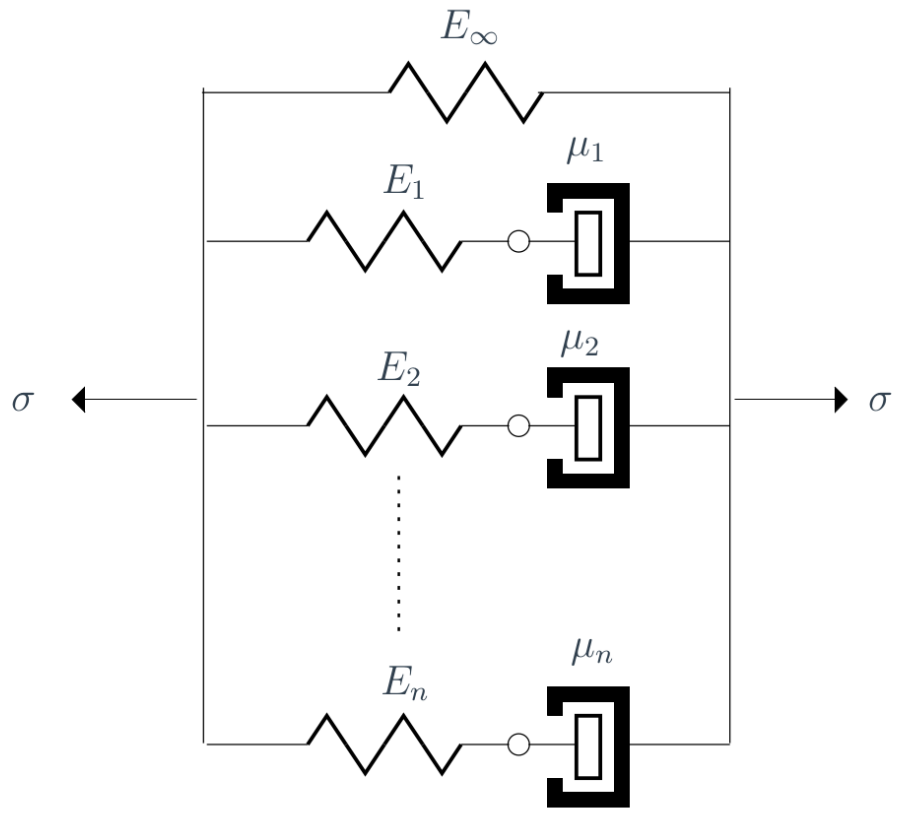

Figure 2.18: Wiechert model

Since strain is same for all branches, solving above equations for stress, substituting into kinetic relations and rearranging, we obtain a partial differential relation containing total stress and strains as

$$\sigma + a_1\dot{\sigma} + a_2\ddot{\sigma} = b_1\dot{\varepsilon} + b_2\ddot{\varepsilon} \tag{2.23}$$

where

$$\begin{aligned} a_1 &= \tau_1 + \tau_2 \qquad a_2 = \tau_1\tau_2 \\ b_1 &= \mu_1 + \mu_2 \qquad b_2 = \mu_1\tau_2 + \tau_1\mu_2 \end{aligned} \tag{2.24}$$

Solution of the single differential equations or the equation 2.23 gives the stress as a function of time for a given strain input. First order differential equations have the

following form for a constant strain ε_0 input

$$\begin{aligned}\sigma_1(t) &= \varepsilon_0 E_1 \exp(\frac{-t}{\tau_1}) \\ \sigma_2(t) &= \varepsilon_0 E_2 \exp(\frac{-t}{\tau_2})\end{aligned} \tag{2.25}$$

For a n element Maxwell model, first order equations takes the form

$$\sigma_i + \tau_i \frac{\partial \sigma_i}{\partial t} = \mu_i \frac{\partial \varepsilon_i(t)}{\partial t} \tag{2.26}$$

Since the total stress is the sum of the all stresses in all branches, we obtain the total stress and relaxation modulus as

$$\sigma(t) = \varepsilon_0 [E_\infty + \sum_{i=1}^{n} E_i \exp(\frac{-t}{\tau_i})] \tag{2.27}$$

$$E(t) = [E_\infty + \sum_{i=1}^{n} E_i \exp(\frac{-t}{\tau_i})] \tag{2.28}$$

At $t = \infty$, relaxation modulus takes the value of E_∞ meaning that only the equilibrium spring contributes to stiffness of the material. The Prony series representation is useful in the case of simulating behaviour of real viscoelastic materials since the parameters entering the equation is easy to interpret by relating them to the springs and the dahspots. Each branch is represented by an exponential, which models the time-dependent behaviour within 1 decade of time. Each spring represents elastic response while each dashpot represents viscous response.

Solving the nth order differential equation or n number of first order differential equation for stress is decided based on the particular loading history. In the case of complicated strain driven loadings, it may be more advantageous to solve nth order differential equation using numerical approaches. Also, if the stress is applied, it is easier to solve higher order differential equation since $\sigma_i(t)$ values are not known in ODE.

2.3 Finite viscoelasticity with volumetric effects

Adopting the same approach as in the previous chapter, three dimensional viscoelastic model can be depicted. Fig. 2.19 describes the rheological model, which differs from one dimensional model in that it contains stretches instead of one dimensional

strains and tensors are used to represent three dimensional deformations. Besides, volume change of the deformed body is also taken into account using determinant of deformation tensor $J = \det \boldsymbol{F}$ in free energy function.

Rheological model contains two branches. Second branch is viscous (or non-

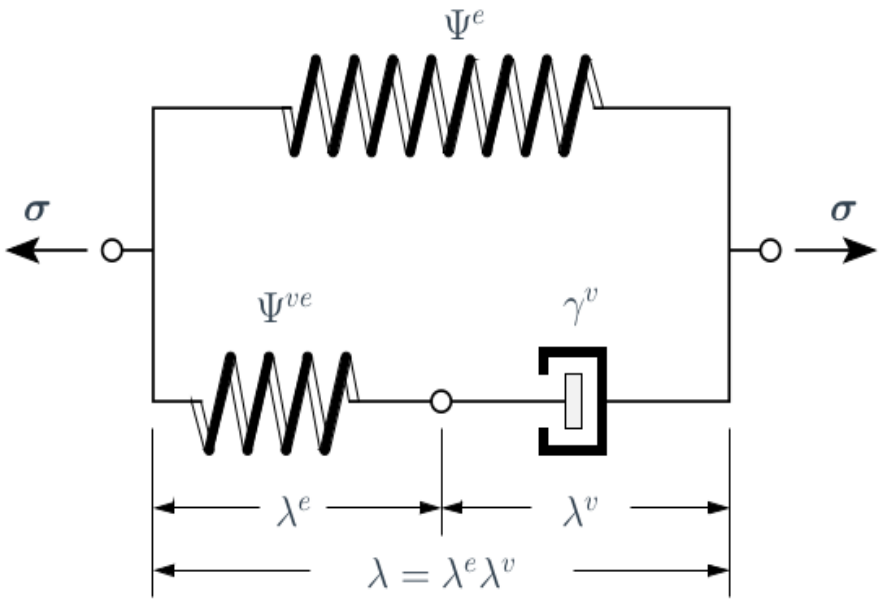

Figure 2.19: Rheological finite viscoelastic model

equilibrium) branch while the first branch is elastic (or equilibrium) branch. Again, the dashpot is used as a dissipative element while springs are used to store energy (free energy) during deformation. Total free energy (stored energy) of the system is summation of the free energies associated with the springs of these two branches. Hence, one can split the total free energy into equilibrium Ψ^e and viscous Ψ^{ve} parts as follows

$$\Psi = \Psi^e(\boldsymbol{F}) + \Psi^{ve}(\boldsymbol{F}^e) \tag{2.29}$$

where $\boldsymbol{F} = \frac{\partial \boldsymbol{x}}{\partial \boldsymbol{X}}$ is the deformation gradient and it basically transforms a particular point P from reference configuration position $\boldsymbol{X}$ to the current configuration position $\boldsymbol{x}$. It can also be written in spectral decomposition in terms of eigenvalues λ_a and eigenvectors $\boldsymbol{n}_A$ (in current configuration) and $\boldsymbol{N}_a$ (in reference configuration).

$$\boldsymbol{F} = \sum_{a=1}^{3} \lambda_a (\boldsymbol{n}_a \otimes \boldsymbol{N}_a) \tag{2.30}$$

λ_a can be one of the three eigenvalues λ_1, λ_2 and λ_3. It is common to decompose $\boldsymbol{F} = \boldsymbol{F}^e\boldsymbol{F}^v$ in a multiplicative way, where $\boldsymbol{F}^e$ represents elastic deformation and $\boldsymbol{F}^v$ represents viscous deformation in the viscous branch. We should also define left Cauchy-Green strain tensor $\boldsymbol{b} = \boldsymbol{F}\boldsymbol{F}^T$ in spectral decomposition as

$$\boldsymbol{b} = \sum_{a=1}^{3} \lambda_a^2 (\boldsymbol{n}_a \otimes \boldsymbol{n}_a) \tag{2.31}$$

from which we can define first invariant using trace of $\boldsymbol{b}$ as

$$\mathrm{tr}(\boldsymbol{b}) = \lambda_a^2 = \lambda_1^2 + \lambda_2^2 + \lambda_3^2 = I_1 \tag{2.32}$$

In following chapters, focusing on molecular level 8-chain model, the relation $\sqrt{\frac{I_1}{3}} = \lambda$ between first invariant and chain stretch λ in the rheological model of Fig. 2.19 will be derived, which was developed by Arruda and Boyce [20]. Network stretch λ can be also decomposed in a multiplicative way as $\lambda = \lambda^e\lambda^v$. Thus, total stretch in viscous branch is equal to the first branch stretch from rheological model and it is composed of elastic stretch λ^e in the spring and viscous stretch λ^v in the dashpot. Since elastic part contains only the equilibrium spring and it elongates in the amount of total stretch λ (ratio of final to initial length), we can associate the equilibrium contribution of free energy with I_1. However, viscous contribution of free energy depends on elastic first invariant $I_1^e = \mathrm{tr}(\boldsymbol{F}^e\boldsymbol{F}^{e^T}) = \mathrm{tr}(\boldsymbol{b}_e)$ since viscoelastic stretch is related with elastic stretch as

$$\lambda^v = \frac{\lambda}{\lambda^e} = \sqrt{\frac{I_1}{I_1^e}} \tag{2.33}$$

Volume change from infinite small volume dV in reference configuration to current volume dv during a deformation process is mapped using $J = \det \boldsymbol{F}$ as previously stated.

$$dv = JdV \tag{2.34}$$

The Jacobian related with volumetric effects can be also split into two parts as elastic and viscous Jacobians.

$$J^e = \det(\boldsymbol{F}^e) \qquad J^v = \det(\boldsymbol{F}^v) \qquad J = J^eJ^v \tag{2.35}$$

Within the concept of many articles, volumetric effects are not taken into account for modeling viscoelastic behaviour of polymeric materials since it is assumed that

viscoelasticity is mostly related with isochoric (constant volume) deformation. However, in this thesis, it will be taken into consideration. Hence, based on the above mentioned statements, we come up with the following generalized specific form of the free energy function

$$\Psi = \Psi^{e}(J, I_1) + \Psi^{ve}(J^{e}, I_1^{e}) \tag{2.36}$$

In the following chapters, free energy functions for equilibrium and viscous contributions will be given. By taking the derivative of the free energy function, stress contribution of both branches can be obtained, which will be derived in chapter 3.

2.4 The new evolution law

A new evolution law will be used in this thesis to integrate Kernel relation, which was derived by Reese and Govindjee [13]. The new evolution law was proposed by Dal in [1]. A single free chain in the polymer matrix is shown in Fig. 2.20. Both ends of the single chain entangled around obstacles. In the single chain, there are N number

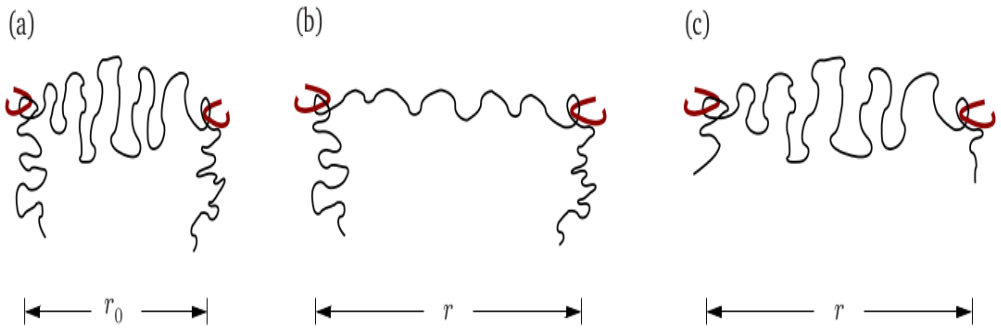

Figure 2.20: Stretch and relaxation of a single chain entangled around an obstacle: (a) undeformed state, (b) deformed state after rapid stretch, (c) deformed and fully relaxed state [1].

of rigid links or segments with each of them having a length of l. Upon straining, these rigid links demonstrate rigid body motion. From random walk consideration mentioned at [20], the initial length of chain is estimated as

$$r_0 = \sqrt{N_0} l \tag{2.37}$$

which is also shown at part (a) of Fig. 2.20. Similarly, at the fully strained state, all of the rigid links is aligned back to back. Hence, at this state, end to end distance of the free chain can be estimated as

$$r = Nl \tag{2.38}$$

Besides, upon a sudden loading, these rigid links take a more ordered conformation, which causes the entropy of the chain to decrease and free energy to increase. At this state, the single chain obtains its maximum stretch value λ_{max}, which is the ratio of final length to initial length.

$$\lambda_{max} = \frac{r}{r_0} = \frac{Nl}{\sqrt{N}l} = \sqrt{N} \tag{2.39}$$

Additionally, we can normalize the stretch ratio λ compared to the maximum stretch ratio as

$$\lambda_r = \frac{\lambda}{\lambda_{max}} = \frac{\lambda}{\sqrt{N}} \tag{2.40}$$

which is called relative stretch. It takes values between 0 corresponding to undeformed configuration and 1 corresponding to fully deformed configuration. Thus, ranges of the stretches are $\lambda_r = [0, 1]$ and $\lambda = [0, \lambda_{max}]$. Keeping the load constant for a while causes the free ends of the chain to loosen by moving due to reptational and Brownian motion combinations during which elastic stretch decreases and viscous stretch increases. Consequently, distance between free ends takes the most favorable or stable value $r = \sqrt{N_\infty}l$ due to loosening of entanglements at the final state with a pure viscous stretch. This state is shown in part (c) of Fig. 2.20. N_∞ here denotes segment number at deformed and fully relaxed state. It can be related to initial segment number N_0 and stretch λ

$$N_\infty = \lambda^2 N_0 \qquad \text{where} \qquad \lambda = \frac{r}{r_0} \tag{2.41}$$

Furthermore, an intermediate state between the states at part (b) and part (c) of Fig. 2.20 can be defined. The intermediate state is reached when the load is removed and is called most preferable state of the chain with distance between free ends being $\bar{r}(t) = \sqrt{N(t)}l$. Hence, upon removel of load, elastic deformation $\lambda_e(t) = \frac{r}{\bar{r}(t)}$ disappears and r reaches to the most preferable length $\bar{r}(t)$. Therefore, we can decompose the total stretch into elastic and inelastic components in a multiplicative way as follows

$$\lambda = \frac{r}{r_0} = \frac{r}{\bar{r}(t)}\frac{\bar{r}(t)}{r_0} = \lambda_e(t)\lambda_v(t) \tag{2.42}$$

We should deduce from this equation that at the initial state $(t = 0)$ and $\bar{r}(0) = r_0$ meaning that deformation is purely elastic $\lambda = \lambda_e$ while at the fully stretched and relaxed state $(t = \infty)$ and $\bar{r}(t = t_\infty) = r$ meaning that deformation is purely inelastic $\lambda = \lambda_v$.

To derive the evolution equation, we firstly write segment number of free chain at a random time in the rate form as

$$\dot{N(t)} = \frac{1}{\tau}[N_\infty - N(t)] \tag{2.43}$$

where τ is relaxation time as mentioned in [1]. Equation 2.43 is a simple first order differential equation, which has the following analytical solution

$$N(t) = (N_\infty - N_0)[1 - \exp(\frac{-t}{\tau})] + N_0 \tag{2.44}$$

Taking time derivative of λ_v and using 2.37, 2.42

$$\dot{\lambda_v} = \frac{\partial \frac{\bar{r}(t)}{r_0}}{\partial t} = \frac{1}{2\sqrt{N(t)N_0}}\dot{N(t)} \tag{2.45}$$

Using 2.43 in $\dot{\lambda_v}$ leads to

$$\lambda_v = \frac{1}{2\tau}\frac{1}{\sqrt{N_0}}[\frac{N_\infty}{\sqrt{N(t)}} - \sqrt{N(t)}] \tag{2.46}$$

Following relations are necessary to simplify above equation

$$\lambda_e = \frac{\sqrt{N_\infty}}{\sqrt{N(t)}} \qquad \text{and} \qquad \lambda = \frac{\sqrt{N_\infty}}{\sqrt{N_0}} \tag{2.47}$$

Hence,

$$\dot{\lambda_v} = \frac{1}{2\tau}\lambda[\lambda_e - \frac{1}{\lambda_e}] = \frac{1}{2\tau}\lambda_v[\lambda_e^2 - 1] \tag{2.48}$$

If we divide with λ_v and replace $\frac{1}{2\tau}$ with creep constant $\dot{\gamma_0}$, we get

$$\frac{\dot{\lambda_v}}{\lambda_v} = \dot{\gamma_0}[\lambda_e^2 - 1] \tag{2.49}$$

This equation shows that creep is faster for smaller relaxation times as expected. Besides, initially elastic strain is high, which results in a high creep rate. Creep rate is zero when elastic stretch reaches its equilibrium value 1. Creep process of viscoelastic materials depends also on energy activation, which motivates us to add a multiplicative power term $(\frac{\tau_v}{\hat{\tau}})^m$. This is also observed in experiments in which the

higher applied stress or strain, the higher creep rate or stress relaxation rate. Thus, we finally end up with the following creep rate function

$$\dot{\gamma} = \dot{\gamma_0}[\lambda_n^{e^2} - 1](\frac{\tau_v}{\hat{\tau}})^m \tag{2.50}$$

where $\hat{\tau}$ is added to make the expression unitless. It should be noticed that effects of both hydrostatic pressure and deviatoric stress are considered in the equivalent viscous stress τ_v term of the energy activation term. Therefore, both of these components affects the creep rate in contrast to conventional viscoelasticity models including only deviatoric stress. Note that stretch of the single chain λ_e is replaced with network stretch of 8-chain model, $\lambda_n^{e^2}$.

2.5 Free energy function

In this section, free energy function $\Psi(J, I_1)$ for finite viscoelasticity with the volumetric effects will be proposed for equilibrium and viscous branches. We will use quadratic version of previously defined Generalized neo-Hookean model for the volumetric free energy function. Then, we will extend this free energy function with three dimensional 8-Chain model proposed by Arruda and Boyce [20].

2.5.1 Generalized neo-Hookean model

In order to derive free energy function for compressible finite viscoelasticity, we start with the generalized quadratic compresible neo-Hookean model, of which free energy function for equilibrium part in terms of J, and first invariant I_1 is as follows

$$\Psi^e(J, I_1) = \frac{\lambda^e}{4}[(\ln(J))^2] + \frac{\mu^e}{2}(I_1 - 2\ln(J) - 3) \tag{2.51}$$

where λ and μ are lame parameter and shear modulus, respectively. They are related to the bulk modulus with the relation $\kappa = \lambda + \frac{2\mu}{3}$. Bulk modulus κ is used as a measure of resistance of the body against volume change. In incompressible rubber assumption, it is taken large enough to enforce incompressibility of rubber-like materials. However, this is not the case of this thesis since we are dealing with compressible finite viscoelasticity for epoxy based materials. The Kirchhoff stress derived from

this free energy function is

$$\boldsymbol{\tau}^e = [(\frac{\lambda^e}{2}(\ln(J)) - \mu^e]\boldsymbol{g}^{-1} + \mu^e\boldsymbol{b} = \hat{p}^e\boldsymbol{g}^{-1} + \mu^e\boldsymbol{b} \tag{2.52}$$

The Cauchy stress is

$$\boldsymbol{\sigma}^e = \frac{1}{J}[\frac{\lambda^e}{2}(\ln(J)) - \mu^e]\boldsymbol{g}^{-1} + \frac{1}{J}\mu^e\boldsymbol{b} = \frac{1}{J}\hat{p}^e\boldsymbol{g}^{-1} + \frac{1}{J}\mu^e\boldsymbol{b} \tag{2.53}$$

The neo-Hookean free energy function and Kirchhoff stress are zero in the ground state (undeformed configuration), in which $\boldsymbol{b} = \boldsymbol{I}$, $J = 1$, $I_1 = tr(\boldsymbol{C}) = 3$, which are called ground conditions. In the above equation $\hat{p}^e$ is the hydrostatic pressure or negative pressure associated with dilatational (volume expansion or contraction) elastic response. In other words, a change in the volume of the body during deformation is resisted by the associated hydrostatic pressure no matter whether the deformation tends to increase or decrease the volume of the body. Thus, when volume ratio $\det(\boldsymbol{F}) = J = \frac{V}{V_0}$ increases or decreases infinitely, hydrostatic pressure must also take infinite values to resist volume change. In Fig. 2.21, pressure term of equations 2.52 and 2.53 are plotted. Although at small deformations around $J = 1$ pressure acts as expected, at large deformations around $J = 3$, pressure does not increase towards infinity. In other words, plot does not obey monotonic growth condition of pressure term. This is due to linear logarithmic term in volumetric part of the free energy function. Hence, by adding a quadratic term $(J-1)^2$ to the volumetric free energy part, we can guarantee that the hydrostatic pressure is linear and increases with volume change J.

$$\Psi^e(J, I_1) = \frac{\lambda^e}{4}[(\ln(J))^2 + (J-1)^2] + \frac{\mu^e}{2}(I_1 - 2\ln(J) - 3) \tag{2.54}$$

The pressure term $\hat{p}^e$ derived from this free energy function obeys the monotonic growth condition ($\hat{p}^e \to \infty$ as $J \to \infty$ and $\hat{p}^e \to -\infty$ as $J \to -\infty$) as observed in Fig. 2.22.

2.5.2 8-chain model

The neo-Hookean model is an idealization, which assumes that there are finite segment numbers N^e in a single chain. Arruda and Boyce [20] using the macromoleculer network structure of the rubber-like materials proposed three dimensional 8-chain

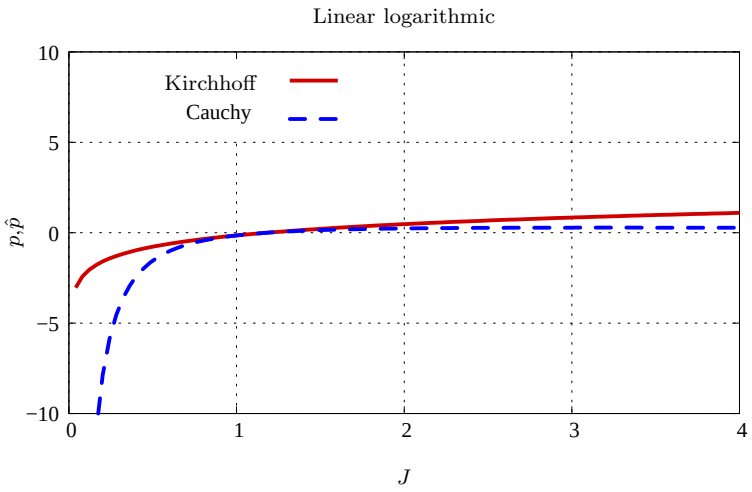

Figure 2.21: Logarithmic and linear free energy function ($\mathcal{K} = 1$)

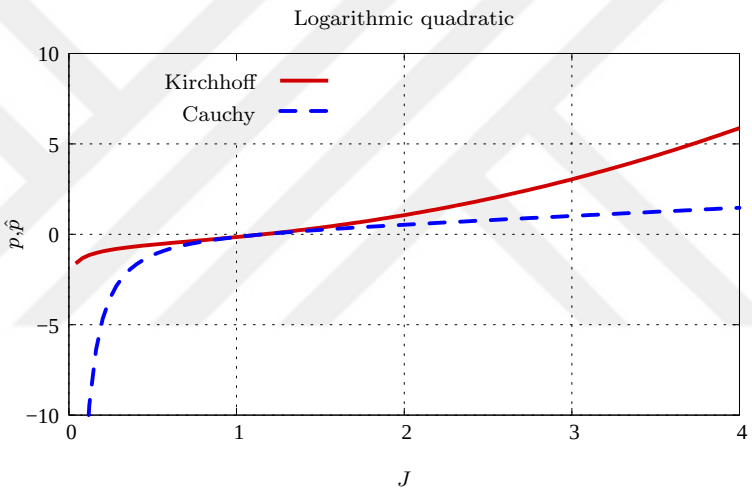

Figure 2.22: Logarithmic and quadratic free energy function ($\mathcal{K} = 1$)

model, which is one of the best models having the capability of capturing network deformation and requiring only two parameters. It is better in terms of effectiveness to predict the behaviour of the rubber-like materials than earlier proposed models such as three chain model of James and Guth [51].

8-chain model considers eight chain orientations in three dimensional space of a cube as shown in Fig. 2.23 in the undeformed and deformed configurations. Each chain is linked to the center of the cube with distance between free ends being r_0 initially.

The edges of the cube remain aligned with the principal stretch directions of right

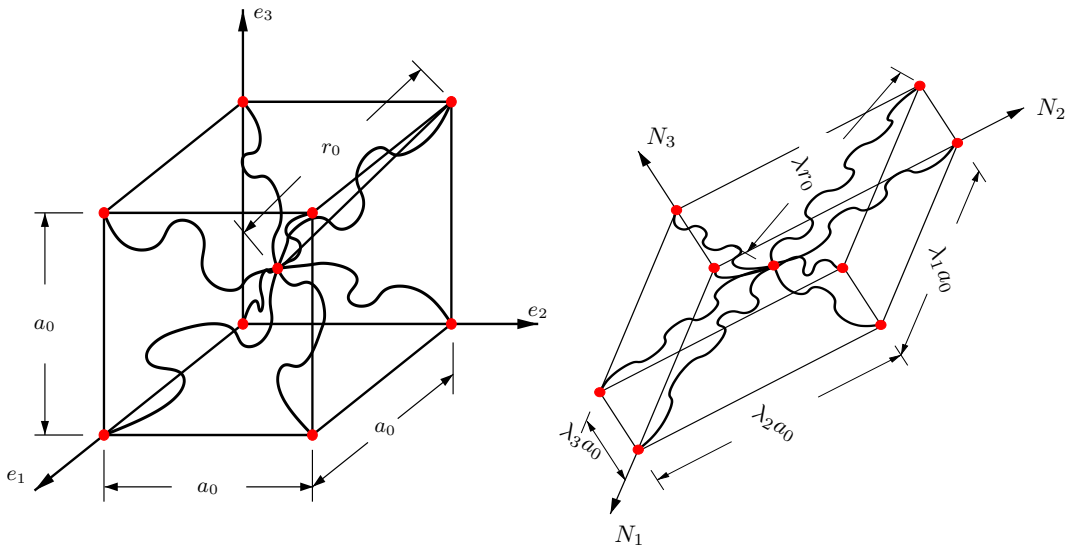

Figure 2.23: 8-chain model representation of rubber network in the undeformed (on the left) and deformed (on the right) configuration [2]

Cauchy-Green tensor $\boldsymbol{C}$ during deformation. Directions on which stretches act rotate with deformation, which proves usefulness of the model. In other words, a principal stretch frame exist in any deformation. Hence, chains in the reference frame will stretch proportional to principal stretch values (square root of eigenvalues of $\boldsymbol{C}$), λ_1, λ_2, λ_3 and edge lengths take values $\lambda_1 a_0$, $\lambda_2 a_0$, $\lambda_3 a_0$ after deformation. Also, after deformation edges of the deformed cube will be aligned with eigenvector space of right Cauchy-Green tensor $\boldsymbol{C}$ as shown in the Fig. 2.23

From the geometry of the cube, we obtain

$$(2ro)^2 = (a_0\sqrt{2})^2 + a_0^2 \tag{2.55}$$

$$a_0 = \frac{2}{\sqrt{3}} r_0 \tag{2.56}$$

After deformation, since edges will expand proportional to square root of principal stretch values and first invariant $I_1 = \lambda_1^2 + \lambda_2^2 + \lambda_3^2$, we can define a vector extending through any of the single chains from center to the corner as follows,

$$\begin{aligned} \boldsymbol{c} &= \frac{a_0}{2}\lambda_1 \boldsymbol{i} + \frac{a_0}{2}\lambda_2 \boldsymbol{j} + \frac{a_0}{2}\lambda_3 \boldsymbol{k} \qquad \text{with a length of} \\ r &= \frac{a_0}{2}\sqrt{(\lambda_1^2 + \lambda_2^2 + \lambda_3^2)} = \frac{a_0}{2}\sqrt{I_1} \end{aligned} \tag{2.57}$$

Using equations 2.56, 2.57 and knowing that stretch is the ratio of final r to initial r_0 distance between the ends of the chain, we obtain chain stretch λ as

$$\lambda = \frac{r}{r_0} = \frac{\frac{a_0}{2}\sqrt{I_1}}{\frac{\sqrt{3}}{2}a_0} = \sqrt{\frac{I_1}{3}} \tag{2.58}$$

and from equation 2.40 relative stretch λ_r as

$$\lambda_r = \sqrt{\frac{I_1}{3N^e}} \tag{2.59}$$

in terms of first invariant $I_1 = \mathrm{tr}\,\boldsymbol{C}$, which is the trace of right Cauchy-Green tensor. Micro-macro transition is obtained by relating the stretch λ of the single chain relaxing in the polymer matrix to the tensor $\mathrm{tr}\,\boldsymbol{C}$ of the continuum.

Accordingly, Arruda and Boyce [20] proposed the following model as a function of the previously defined stretches λ and λ_r. We will exchange $\frac{\mu^e}{2}I_1$ term of neo-Hookean model with the following free energy function proposed by Arruda and Boyce,

$$\Psi(\lambda_r) = \mu N[\lambda_r \mathcal{L}^{-1}(\lambda_r) + \ln \frac{\mathcal{L}^{-1}(\lambda_r)}{\sinh \mathcal{L}^{-1}(\lambda_r)}] \tag{2.60}$$

Hence, based on the viscoelastic split equation 2.29, elastic part of extension of the quadratic version of the volumetric 8-chain model can be represented with the free energy function using 2.54 and 2.60

$$\begin{aligned}\Psi^e(J, I_1) &= \frac{\lambda^e}{4}[(\ln(J))^2 + (J-1)^2] - \frac{\mu^e}{3}\frac{3N^e - 1}{N^e - 1}(\ln J) \\ &+\mu^e N^e[\lambda_r \mathcal{L}^{-1}(\lambda_r) + \ln \frac{\mathcal{L}^{-1}(\lambda_r)}{\sinh \mathcal{L}^{-1}(\lambda_r)}]\end{aligned} \tag{2.61}$$

It should be noted that the terms that include J is used in volumetric part of 2.61. μ^e shear modulus is replaced with $\tilde{\mu^e} = \frac{\mu^e}{3}\frac{3N^e-1}{N^e-1}$. One should note that when segment number of chain N^e converges to infinity, $\tilde{\mu^e}$ converges to μ^e and the neo-Hookean model is recovered. Thus, this model is a generalized version of the neo-Hookean model. In the free energy function, inverse Langevin function $\mathcal{L}^{-1}(\lambda_r)$ can be approximated from the Padé approximation as

$$\mathcal{L}^{-1}(\lambda_r) \approx \lambda_r \frac{3 - \lambda_r^2}{1 - \lambda_r^2} \tag{2.62}$$

proposed by Cohen [52]. Padé approximation is known to give exact results at $\lambda_r = 0$ and worst result around $\lambda_r = 0.8$.

Following the same approach and using viscous parameters, previously defined scalars and tensors of viscous branch, the viscous part of the free energy function can be written as

$$\Psi^{ve}(J^e, I_1^e) = \frac{\lambda^v}{4}[(\ln(J^e))^2 + (J^e - 1)^2] - \frac{\mu^v}{3}\frac{3N^v - 1}{N^v - 1}(\ln J^e) \\ +\mu^v N^v[\lambda_r^e \mathcal{L}^{-1}(\lambda_r^e) + \ln \frac{\mathcal{L}^{-1}(\lambda_r^e)}{\sinh \mathcal{L}^{-1}(\lambda_r^e)}] \tag{2.63}$$

CHAPTER 3

ALGORITHMIC SETTING FOR THE CONSITUTIVE MODEL

3.1 Kirchhoff stresses

3.1.1 Elastic and viscoelastic Kirchhoff stress expressions

The equilibrium response of the material is represented by a branch including a spring and viscous (inelastic) response is represented by a parallel branch including a spring and a dashpot in series. The total Kirchhoff stress is summation of the stresses in these branches. Thus, the Kirchhoff stress can be decomposed into equilibrium and viscoelastic parts.

$$\begin{aligned} &\boldsymbol{\tau} = \boldsymbol{\tau}^e + \boldsymbol{\tau}^\nu \qquad \text{where} \\ &\boldsymbol{\tau}^e = 2\partial_{\boldsymbol{g}}\Psi^e(J, I_1) \qquad \text{and} \quad \boldsymbol{\tau}^v = 2\partial_{\boldsymbol{g}}\Psi^{ve}(J^e, I_1^e) \qquad \text{or} \\ &\boldsymbol{\tau}^e = 2\boldsymbol{b}\partial_{\boldsymbol{b}}\Psi^e(J, I_1) \qquad \text{and} \quad \boldsymbol{\tau}^v = 2\boldsymbol{b}_e\partial_{\boldsymbol{b}_e}\Psi^{ve}(J^e, I_1^e) \end{aligned} \tag{3.1}$$

Elastic contribution of the Kirchhoff stress is found by taking derivative of elastic part of Helmholtz free energy function with respect to metric tensor $\boldsymbol{g}$, $\partial_{\boldsymbol{g}}\Psi^e(J, I_1)$. To evaluate this derivative, one needs $\partial_{\lambda_r}\Psi^e(J, I_1)$. For the sake of simplicity, we will first take derivative of the third term in the equation 2.61 with respect to $\boldsymbol{g}$. Thereafter, other two terms assosicated with $U(J)$ will be taken into consideration in order to derive remaning part of the elastic Kirchhoff stress. Using $\mathcal{L}^{-1}(\lambda_r) = \beta$

$$\begin{aligned} &\frac{\partial[\mu^e N^e(\lambda_r \mathcal{L}^{-1}(\lambda_r) + ln\frac{\mathcal{L}^{-1}(\lambda_r)}{\sinh \mathcal{L}^{-1}(\lambda_r)})]}{\partial \lambda_r} \\ &= \mu^e N^e(\beta + \lambda_r\beta' + \tfrac{\sinh\beta}{\beta}[\tfrac{1}{\sinh\beta} - \tfrac{\beta\cosh\beta}{\sinh\beta^2}]\beta') \\ &= \mu^e N^e(\beta + \lambda_r\beta' + [\frac{1}{\beta} - \coth\beta]\beta') \end{aligned} \tag{3.2}$$

Using the relations $-\mathcal{L}(\beta) = [\frac{1}{\beta} - \coth(\beta)]$ and $-\mathcal{L}(\mathcal{L}^{-1}(\lambda_r)) = -\lambda_r$, this expression can be further simplified into

$$\begin{aligned} &\frac{\partial[\mu^e N^e(\lambda_r \mathcal{L}^{-1}(\lambda_r) + ln\frac{\mathcal{L}^{-1}(\lambda_r)}{\sinh \mathcal{L}^{-1}(\lambda_r)})]}{\partial \lambda_r} = \mu^e N^e(\beta + \lambda_r \beta' - \lambda_r \beta') \\ &= \mu^e N^e \beta \end{aligned} \tag{3.3}$$

Using chain rule, (2.58), (2.59) and the following derivatives

$$\frac{\partial \lambda_r}{\partial \lambda} = \frac{1}{\sqrt{N^e}} \tag{3.4}$$

$$\frac{\partial \lambda}{\partial I_1} = \frac{1}{6}(\frac{I_1}{3})^{-1/2} = \frac{1}{6\lambda} = \frac{1}{6\lambda_r \sqrt{N^e}} \tag{3.5}$$

$$\frac{\partial I_1}{\partial \boldsymbol{g}} = \frac{\partial tr(\boldsymbol{b})}{\partial \boldsymbol{g}} = \frac{\partial(\boldsymbol{b} : \boldsymbol{g})}{\partial \boldsymbol{g}} = \boldsymbol{b} : \mathbb{I} = \boldsymbol{b} \tag{3.6}$$

first part of the elastic Kirchhoff stress can be obtained as follows

$$\begin{aligned} &2\frac{\partial \Psi(\lambda_r)}{\partial \lambda_r}\frac{\partial \lambda_r}{\partial \lambda}\frac{\partial \lambda}{\partial I_1}\frac{\partial I_1}{\partial \boldsymbol{b}} = \frac{\mu^e}{3}\frac{\mathcal{L}^{-1}(\beta)}{\lambda_r}\boldsymbol{b} = \hat{\mu}^e \boldsymbol{b} \quad \text{with} \\ &\hat{\mu}^e = \frac{\mu}{3}\frac{3-\lambda_r^2}{1-\lambda_r^2} \end{aligned} \tag{3.7}$$

Volumetric part of the elastic component can be found by taking derivative of elastic part of volumetric free energy function and using chain rule

$$2\partial_{\boldsymbol{g}} U(J) = 2\frac{\partial U(J)}{\partial J}\frac{\partial J}{\partial \boldsymbol{g}} = \hat{p^e}\boldsymbol{g}^{-1} \tag{3.8}$$

where the following identities are used.

$$\frac{\partial J}{\partial \boldsymbol{g}} = \frac{J}{2}\boldsymbol{g}^{-1} \tag{3.9}$$

$$\frac{\partial U(J)}{\partial J} = \frac{\lambda}{2}[ln(J)\frac{1}{J} + (J-1)] - \tilde{\mu}^e \frac{1}{J} \tag{3.10}$$

$$\hat{p^e} = J\frac{\partial U(J)}{\partial J} = \frac{\lambda^e}{2}(ln(J) + J(J-1)) - \tilde{\mu}^e \tag{3.11}$$

In this equation, scalar quantity $J\frac{\partial \Psi^e}{\partial J} = \hat{p^e}$ denotes elastic hydrostatic (negative) pressure. Finally, total elastic Kirchhoff stress is obtained by summing these two derived stress parts.

$$\boldsymbol{\tau}^e = \hat{p^e}\boldsymbol{g}^{-1} + \hat{\mu}^e \boldsymbol{b} = [\frac{\lambda^e}{2}(ln(J) + J(J-1)) - \tilde{\mu}^e]\boldsymbol{g}^{-1} + \hat{\mu}^e \boldsymbol{b} \tag{3.12}$$

Adopting the same approach with viscoelastic parameters $\hat{p^v}$, $\hat{\mu^v}$, viscoelastic (inelastic) Kirchhoff stress can be obtained as follows

$$\boldsymbol{\tau}^v = \hat{p^v}\boldsymbol{g}^{-1} + \hat{\mu^v}\boldsymbol{b}^e = [\frac{\lambda^v}{2}(ln(J^e) + J^e(J^e-1)) - \tilde{\mu}^v]\boldsymbol{g}^{-1} + \hat{\mu^v}\boldsymbol{b}^e \tag{3.13}$$

Viscoelastic Kirchhoff stress contains $\boldsymbol{b}^e$ and J^e instead of $\boldsymbol{b}$ and J respectively due to the reasons mentioned in chapter 2.

3.2 Eulerian moduli expressions

3.2.1 Elastic moduli expression

Eulerian moduli of volumetric part for equilibrium (elastic) response can be defined as

$$\mathbb{C}_{vol} = 4\frac{\partial^2 U(J)}{\partial \boldsymbol{g}^2} = 2\frac{\partial(\hat{p^e}\boldsymbol{g}^{-1})}{\partial \boldsymbol{g}} \tag{3.14}$$

Using the chain rule, $\mathbb{C}_{vol}$ can be derived as

$$\mathbb{C}_{vol} = 2[\frac{\partial \hat{p^e}}{\partial \boldsymbol{g}} \otimes \boldsymbol{g}^{-1} + \hat{p^e}\frac{\partial \boldsymbol{g}^{-1}}{\partial \boldsymbol{g}}] = (\hat{p^e} + \hat{s^e})\boldsymbol{g}^{-1} \otimes \boldsymbol{g}^{-1} - 2\hat{p^e}\mathbb{I} \tag{3.15}$$

where the fourth order tensor is defined as

$$\mathbb{I}^{abcd}_{\boldsymbol{g}^{-1}} := [\delta^{ac}\delta^{bd} + \delta^{ad}\delta^{bc}]/2 \tag{3.16}$$

Note that the following derivation for $\frac{\partial \hat{p^e}}{\partial \boldsymbol{g}}$ is used in equation 3.15

$$\begin{aligned} &\frac{\partial \hat{p^e}}{\partial \boldsymbol{g}} = \frac{\partial(J\frac{\partial U(J)}{\partial J})}{\partial J}\frac{\partial J}{\partial \boldsymbol{g}} = [\frac{\partial U(J)}{\partial J} + J\frac{\partial U^2(J)}{\partial J^2}]\frac{J}{2}\boldsymbol{g}^{-1} = \frac{1}{2}(\hat{p^e} + \hat{s^e})\boldsymbol{g}^{-1} \\ &\text{where } \hat{s^e} = J^2\frac{\partial U^2(J)}{\partial J^2} \end{aligned} \tag{3.17}$$

Substitution of equation 3.17 into equation left part of 3.15, we can find $\mathbb{C}_{vol}$. To find the total equilibrium response, one needs also an additional eulerian moduli expression associated with remaining Kirchhoff stress term $\mu^e\boldsymbol{b}$, which can be derived by taking derivative of $2\mu^e\boldsymbol{b}$ with respect to $\boldsymbol{g}$.

$$2\frac{\partial(\mu^e\boldsymbol{b})}{\partial \boldsymbol{g}} \tag{3.18}$$

To find equation 3.18, we must use chain rule and equation 3.7.

$$2\frac{\partial(\hat{\mu}^e\boldsymbol{b})}{\partial\boldsymbol{g}} = 2\frac{\partial(\frac{\mu^e}{3}\frac{3-\lambda_r^2}{1-\lambda_r^2}\boldsymbol{b})}{\partial\boldsymbol{g}} = 2\frac{\partial(\frac{\mu^e}{3}\frac{3-\lambda_r^2}{1-\lambda_r^2})}{\partial\lambda_r}\frac{\partial\lambda_r}{\partial I_1}\frac{\partial I_1}{\partial\boldsymbol{g}}\otimes\boldsymbol{b} + 2(\frac{\mu^e}{3}\frac{3-\lambda_r^2}{1-\lambda_r^2})\frac{\partial\boldsymbol{b}}{\partial\boldsymbol{g}} \tag{3.19}$$

The following derivations and equation 3.6 are required in order to simplify this form.

$$\frac{\partial\lambda_r}{\partial I_1} = \frac{\partial\lambda}{\partial\lambda_r}\frac{\partial\lambda_r}{\partial I_1} = \frac{1}{6\lambda_r N^e} \tag{3.20}$$

where we have used equations 3.4 and 3.5.

$$\frac{\partial\boldsymbol{b}}{\partial\boldsymbol{g}} = \frac{\partial(\boldsymbol{F}\boldsymbol{G}^{-1}\boldsymbol{F}^T)}{\partial\boldsymbol{g}} = 0 \tag{3.21}$$

By substituting 3.6, 3.20, 3.21 into 3.19 and taking derivative with respect to λ_r, 3.19 simplifies into

$$2\frac{\partial(\frac{\mu^e}{3}\frac{3-\lambda_r^2}{1-\lambda_r^2})}{\partial\lambda_r}\frac{\partial\lambda_r}{\partial I_1}\frac{\partial I_1}{\partial\boldsymbol{g}}\otimes\boldsymbol{b} = 2\frac{\mu^e}{3}\frac{4\lambda_r}{(1-\lambda_r^2)^2}\frac{1}{6\lambda_r N^e}\boldsymbol{b}\otimes\boldsymbol{b} \tag{3.22}$$

Hence, one can find the final form after simplifications as follows

$$2\frac{\partial(\hat{\mu}^e\boldsymbol{b})}{\partial\boldsymbol{g}} = \frac{4}{9}\frac{\mu^e}{N^e}\frac{1}{(1-\lambda_r^2)^2}\boldsymbol{b}\otimes\boldsymbol{b} \tag{3.23}$$

Total eularian equilibrium moduli is summation of volumetric modulus and $2\frac{\partial(\hat{\mu}^e\boldsymbol{b})}{\partial\boldsymbol{g}}$, which represents stress sensivity of elastic branch with respect to elastic strain.

$$\mathbb{C}^e = (\hat{p^e} + \hat{s^e})\boldsymbol{g}^{-1}\otimes\boldsymbol{g}^{-1} - 2\hat{p^e}\mathbb{I} + \frac{4}{9}\frac{\mu^e}{N^e}\frac{1}{(1-\lambda_r^2)^2}\boldsymbol{b}\otimes\boldsymbol{b} \tag{3.24}$$

3.2.2 Integration of the new evolution equation

Before proceeding to algorithmic moduli for the viscous part, we need the current value of elastic left Cauchy-Green deformation tensor $\boldsymbol{b}_e$ at time $t = t_{n+1}$ since it is related to non-equilibrium deformation. $\boldsymbol{b}_e$ is also required for computing the value of viscous Kirchhoff stress contribution, equation 3.13. Therefore, we need to use nonlinear Kernel relation in equation, which is derived in [13]. Result of solution is also dependent on the proposed evolution law.

$$-\frac{1}{2}\boldsymbol{\pounds_\nu}\boldsymbol{b}_e\cdot\boldsymbol{b}_e^{-1} = \tilde{\boldsymbol{d}}_i \tag{3.25}$$

Since inelastic rate of deformation tensor, $\tilde{\boldsymbol{d}}_i$, is also proportional to the effective creep rate, $\dot{\gamma}$, in the direction of Kirchhoff stress, we can also find the following relation.

$$-\frac{1}{2}\boldsymbol{\pounds}_{\boldsymbol{\nu}}\boldsymbol{b}_e \cdot \boldsymbol{b}_e^{-1} = \dot{\gamma}\boldsymbol{N} = \tilde{\boldsymbol{d}}_i \tag{3.26}$$

where stress flow is defined as

$$\boldsymbol{N} = \frac{\boldsymbol{\tau}^v}{\|\boldsymbol{\tau}^v\|} \tag{3.27}$$

We should first determine $\dot{\boldsymbol{b}}_e$. Rate of $\boldsymbol{b}_e = \boldsymbol{F}_e\boldsymbol{F}_e^T$ can be derived as

$$\dot{\boldsymbol{b}}_e = \dot{\boldsymbol{F}}_e\boldsymbol{F}_e^T + \boldsymbol{F}_e\dot{\boldsymbol{F}}_e^T \tag{3.28}$$

By substituting $\dot{\boldsymbol{F}}_e = \dot{\overline{\boldsymbol{F}\boldsymbol{F}_i^{-1}}} = \dot{\boldsymbol{F}}\boldsymbol{F}_i^{-1} + \boldsymbol{F}\dot{\boldsymbol{F}}_i^{-1}$ and $\dot{\boldsymbol{F}}_e^T = \dot{\boldsymbol{F}}_i^{-T}\boldsymbol{F}^T + \boldsymbol{F}_i^{-T}\dot{\boldsymbol{F}}^T$ into equation 3.28 and using $\boldsymbol{F} = \boldsymbol{F}_e\boldsymbol{F}_i$, $\boldsymbol{l}_i = \dot{\boldsymbol{F}}_i\boldsymbol{F}_i^{-1}$, $\boldsymbol{l}_i^{-T} = \dot{\boldsymbol{F}}_i^{-T}\boldsymbol{F}_i^T$ relations

$$\begin{aligned}
\dot{\boldsymbol{b}}_e &= (\dot{\boldsymbol{F}}\boldsymbol{F}_i^{-1} + \boldsymbol{F}\dot{\boldsymbol{F}}_i^{-1})\boldsymbol{F}_e^T + \boldsymbol{F}_e(\dot{\boldsymbol{F}}_i^{-T}\boldsymbol{F}^T + \boldsymbol{F}_i^{-T}\dot{\boldsymbol{F}}^T) \\
&= \dot{\boldsymbol{F}}\boldsymbol{F}^{-1}\boldsymbol{F}_e\boldsymbol{F}_i\boldsymbol{F}_i^{-1}\boldsymbol{F}_e^T + \boldsymbol{F}_e\boldsymbol{l}_i^{-1}\boldsymbol{F}_e^T + \boldsymbol{F}_e\boldsymbol{l}_i^{-T}\boldsymbol{F}_e^T + \boldsymbol{F}_e\boldsymbol{F}_i^{-T}\boldsymbol{F}^T\boldsymbol{F}^{-T}\dot{\boldsymbol{F}}^T \\
&= \boldsymbol{l}\boldsymbol{b}_e + \boldsymbol{b}_e\boldsymbol{l}^T + \boldsymbol{F}_e(\boldsymbol{l}_i^{-1} + \boldsymbol{l}_i^{-T})\boldsymbol{F}_e^T
\end{aligned} \tag{3.29}$$

Second part of this equation can be further simplified using $\boldsymbol{l}_i^{-1} = \boldsymbol{F}_i\dot{\boldsymbol{F}}_i^{-1}$, $\boldsymbol{l}_i^{-T} = \dot{\boldsymbol{F}}_i^{-T}\boldsymbol{F}_i^T$ relations in equation 3.29

$$\begin{aligned}
&\boldsymbol{F}_e(\boldsymbol{l}_i^{-1} + \boldsymbol{l}_i^{-T})\boldsymbol{F}_e^T = \boldsymbol{F}_e\boldsymbol{F}_i(\dot{\boldsymbol{F}}_i^{-1}\boldsymbol{F}_i^{-T} + \boldsymbol{F}_i^{-1}\dot{\boldsymbol{F}}_i^{-T})\boldsymbol{F}_i^T\boldsymbol{F}_e^T \\
&= \boldsymbol{F}(\dot{\overline{\boldsymbol{F}_i^{-1}\boldsymbol{F}_i^{-T}}})\boldsymbol{F}^T = \boldsymbol{F}(\dot{\overline{\boldsymbol{C}_i^{-1}}})\boldsymbol{F}^T
\end{aligned} \tag{3.30}$$

Using equation 3.30 in equation 3.29, we finally end up with

$$\dot{\boldsymbol{b}}_e = \underbrace{\boldsymbol{l}\boldsymbol{b}_e + \boldsymbol{b}_e\boldsymbol{l}^T}_{E} + \underbrace{\boldsymbol{F}(\dot{\overline{\boldsymbol{C}_i^{-1}}})\boldsymbol{F}^T}_{I} \quad \text{or} \quad \dot{\boldsymbol{b}}_e = \underbrace{\boldsymbol{l}\boldsymbol{b}_e + \boldsymbol{b}_e\boldsymbol{l}^T}_{E} + \underbrace{\boldsymbol{\pounds}_{\boldsymbol{\nu}}\boldsymbol{b}_e}_{I} \tag{3.31}$$

First term of the equation 3.31 denoted with E is called elastic predictor and the second term denoted with I is called inelastic corrector. In analogy to elastoplasticity, such a split of the $\boldsymbol{b}_e$ is used since it is easy to integrate the evolution law in this form by sequentially freezing one of the terms E and I in each trial step. For a time increment $t_{n+1} - t_n$ during the deformation, current value of $\boldsymbol{b}_e$ can be calculated approximately using Newton-Raphson iteration and taking advantage of above-mentioned operator split method. In this sense, during elastic trial step, the inelastic term $\dot{\overline{\boldsymbol{C}_i^{-1}}}$ is zero, which implies that there is no change in inelastic stretch λ_i or in

$\boldsymbol{C}_i^{-1}$. Therefore, inverse of trial inelastic right Cauchy-Green tensor $(\boldsymbol{C}_i^{-1})_{tr}$ is equal to its previous value at $t = t_n$.

$$(\boldsymbol{C}_i^{-1})_{tr} = (\boldsymbol{C}_i^{-1})_{t_n} \quad \rightarrow \quad \boldsymbol{b}_e{}^{tr} = \boldsymbol{F}(\boldsymbol{C}_i^{-1})_{t_n}\boldsymbol{F}^T. \tag{3.32}$$

In the same manner, in the inelastic corrector step, $\boldsymbol{l} := \nabla \boldsymbol{v}$ is equal to zero simplifying equation 3.31 into $\dot{\boldsymbol{b}}_e = \boldsymbol{\pounds}_{\boldsymbol{v}}\boldsymbol{b}_e$. This simpler form can be integrated using the so-called exponential mapping method as folows.
Using equation 3.26 and $\dot{\boldsymbol{b}}_e = \boldsymbol{\pounds}_{\boldsymbol{v}}\boldsymbol{b}_e$, we obtain

$$\dot{\boldsymbol{b}}_e = \boldsymbol{\pounds}_{\boldsymbol{v}}\boldsymbol{b}_e = [-2\dot{\gamma}\boldsymbol{N}]\boldsymbol{b}_e{}^{tr} \tag{3.33}$$

We can integrate this expression utilizing the so-called exponential mapping in the time domain $[t_n, t_{n+1}]$

$$\boldsymbol{b}_e = \exp\left[-2\int_{t_n}^{t_{n+1}} \dot{\gamma}\mathbf{N}dt\right]\boldsymbol{b}_e{}^{tr} \tag{3.34}$$

Approximating this equation, we obtain

$$\boldsymbol{b}_e \approx \exp\left[-2\dot{\gamma}\mathbf{N}\Delta t\right]\boldsymbol{b}_e{}^{tr}\ . \tag{3.35}$$

Since material is assumed to be isotropic, $\boldsymbol{\tau}^e$ and thereby $\boldsymbol{N}$ are in the same eigenspace with $\boldsymbol{b}_e$ and with $\boldsymbol{b}_e{}^{tr}$. Hence, they can be written in the principal stretch directions by exploiting spectral decomposition property of symmetric tensors $\boldsymbol{b}_e = \lambda_a^{e\,2}\boldsymbol{n}_a \otimes \boldsymbol{n}_a$, $\boldsymbol{b}_e{}^{tr} = \lambda_a^{e\,tr\,2}\boldsymbol{n}_a \otimes \boldsymbol{n}_a$ and $\boldsymbol{\tau}^v = \tau_a \boldsymbol{n}_a \otimes \boldsymbol{n}_a$.

$$\lambda_a^{e2} \approx \exp[-2\Delta t\dot{\gamma}\frac{\tau_a}{\|\boldsymbol{\tau}^v\|}]\lambda_a^{e\,tr\,2}\ . \tag{3.36}$$

Taking logarithm of both sides to eliminate exponential, dividing by 2 both sides, defining $\|\boldsymbol{\tau}^v\| = \sqrt{\boldsymbol{\tau}^v : \boldsymbol{\tau}^v} = \sqrt{2}\tau_v$ and defining principal logarithmic stretches as $\ln(\lambda_a^e) = \varepsilon_a$, $\ln(\lambda_a^{e\,tr}) = \varepsilon_a^{tr}$

$$\varepsilon_a \approx -\frac{\Delta t\dot{\gamma}}{\sqrt{2}\tau_v}\tau_a + \varepsilon_a^{tr} \tag{3.37}$$

By noting that τ_a and $\dot{\gamma}$ also depends on principal stretches λ_a, one can immediately realizes that 3.37 is a nonlinear equation. By taking the terms at the right side to the left side, one can obtain a nonlinear resiual expression r_a, which should be solved using a iterative algorithm such as Newton-Raphson.

$$r_a = \varepsilon_a + \frac{\Delta t\dot{\gamma}}{\sqrt{2}\tau_v}\tau_a - \varepsilon_a^{tr} = 0 \tag{3.38}$$

After solving equation 3.38 for $\Delta\varepsilon_a$ using a iterative method, we can update ε_a and all the other terms including it for the current time step.

In the context of Newton Raphson iteration, we firstly linearize the residual expression as follows

$$\mathrm{Lin}\, r_a = r_a|_{\varepsilon^k} + \left.\frac{\partial r_a}{\partial \varepsilon_b}\right|_{\varepsilon=\varepsilon^k} \Delta\varepsilon_b^k = 0 \tag{3.39}$$

After finding the $\Delta\varepsilon_b^k$ value that satisfies equation 3.39, ε_b^k is updated and value of r_a is recalculated and checked whether it is below the tolerance or not. If it is not below tolerance, iteration number is increased and equation 3.39 is forced to become a value close to zero at the new ε_b^k value (at iteration $k+1$) in order to find new $\Delta\varepsilon_b^k$. This loop continues until r_a value is within a tolerance around zero determined by the user.

To solve equation 3.39 for $\Delta\varepsilon_b^k$, it is written in the following form

$$\Delta\varepsilon_b^k = -(\frac{\partial r_a}{\partial \varepsilon_b})^{-1} r_a = -\mathcal{K}_{ab}^{-1} r_a \tag{3.40}$$

Slope of the residual equation $\mathcal{K}_{ab}$ can be derived from equation 3.38 using $\frac{\partial \varepsilon_a}{\partial \varepsilon_b} = \delta_{ab}$ and $\frac{\partial \varepsilon_a^{tr}}{\partial \varepsilon_b} = 0$ as follows

$$\mathcal{K}_{ab} = \frac{\partial r_a}{\partial \varepsilon_b} = \delta_{ab} + \frac{\Delta t}{\sqrt{2}} \frac{\partial(\frac{\dot\gamma}{\tau_v})}{\partial \varepsilon_b} \tau_a + \frac{\Delta t}{\sqrt{2}} \frac{\dot\gamma}{\tau_v} \frac{\partial \tau_a}{\partial \varepsilon_b} \tag{3.41}$$

Using equation 2.50, second term of equation 3.41 can be expanded as

$$\frac{\Delta t}{\sqrt{2}} \frac{\partial(\frac{\dot\gamma}{\tau_v})}{\partial \varepsilon_b} \tau_a = \frac{\Delta t}{\sqrt{2}} \tau_a \dot\gamma_0 [(\lambda^2-1)^c \frac{\partial \tau_v^{(m-1)}}{\partial \varepsilon_b} + \tau_v^{(m-1)} \frac{\partial(\lambda^2-1)^c)}{\partial \varepsilon_b}] \tag{3.42}$$

where the first term of equation 3.42 can be expanded using the following derivations

$$\begin{aligned} &\frac{\partial \tau_v}{\partial \varepsilon_b} = \frac{\partial \frac{\|\boldsymbol{\tau}^v\|}{\sqrt{2}}}{\partial \varepsilon_b} = \frac{1}{\sqrt{2}} \frac{\tau_c}{\|\boldsymbol{\tau}^v\|} \frac{\partial \tau_c}{\partial \varepsilon_b} = \frac{1}{\sqrt{2}} \frac{\tau_c}{\|\boldsymbol{\tau}^v\|} \mathcal{T}_{cb} = \frac{1}{2\tau_v} (\sum_{c=1}^{3} \tau_c \mathcal{T}_{cb}) \\ &\text{where} \qquad \frac{\partial \|\boldsymbol{\tau}^v\|}{\partial \boldsymbol{\tau}^v} = \frac{\partial \sqrt{\boldsymbol{\tau}^v : \boldsymbol{\tau}^v}}{\partial \boldsymbol{\tau}_v} = \frac{1}{2} \frac{1}{\|\boldsymbol{\tau}^v\|} 2(\mathbb{I} : \boldsymbol{\tau}^v) \\ &\text{or in indicial notation} \qquad \frac{\partial \|\boldsymbol{\tau}^v\|}{\partial \boldsymbol{\tau}^v} = \frac{\tau_c}{\|\boldsymbol{\tau}^v\|} \end{aligned} \tag{3.43}$$

In the above equation, there is a summation over c from 1 to 3. Then, the first term of equation 3.42 simplifies into

$$\begin{aligned} &\frac{\Delta t}{\sqrt{2}} \tau_a \dot\gamma_0 (\lambda^2-1)^c \frac{\partial \tau_v^{(m-1)}}{\partial \varepsilon_b} = \frac{\Delta t}{\sqrt{2}} \tau_a \dot\gamma_0 (\lambda^2-1)^c \frac{\partial \tau_v^{(m-1)}}{\partial \tau_v} \frac{\partial \tau_v}{\partial \varepsilon_b} \\ &= (\frac{\Delta t}{2\sqrt{2}} (m-1) \dot\gamma_0 (\lambda^2-1)^c \tau_v^{(m-3)}) \tau_a (\sum_{c=1}^{3} \tau_c \mathcal{T}_{cb}) = \beta_1 \tau_a \mathcal{D} \end{aligned} \tag{3.44}$$

Using the following relation

$$\frac{\partial\lambda}{\partial\lambda_a} = \frac{\partial(\frac{\lambda_1^2+\lambda_2^2+\lambda_3^2}{3})^{\frac{1}{2}}}{\partial\lambda_a} = \frac{2\lambda_a}{3}\frac{1}{2\lambda} = \frac{\lambda_a}{3\lambda} \tag{3.45}$$

second term of equation 3.42 can be simplified as

$$\begin{aligned}
&\frac{\Delta t}{\sqrt{2}}\tau_a\dot{\gamma}_0\tau_v^{(m-1)}\frac{\partial(\lambda^2-1)^c}{\partial\lambda} = \frac{\Delta t}{\sqrt{2}}\dot{\gamma}_0\tau_v^{(m-1)}\tau_a[c(\lambda^2-1)^{(c-1)}2\lambda\frac{\partial\lambda}{\partial\varepsilon_b}] \\
&= \frac{\Delta t}{\sqrt{2}}\dot{\gamma}_0\tau_v^{(m-1)}\tau_a[c(\lambda^2-1)^{(c-1)}2\lambda\frac{\partial\lambda}{\partial\lambda_a}\frac{\partial\lambda_a}{\partial\ln(\lambda_a)}\frac{\partial\ln(\lambda_a)}{\partial\ln(\lambda_b)}\frac{\partial\ln(\lambda_b)}{\partial\varepsilon_b}] \\
&= \frac{\Delta t}{\sqrt{2}}\dot{\gamma}_0\tau_v^{(m-1)}\tau_a[c(\lambda^2-1)^{(c-1)}2\lambda\frac{\lambda_a}{3\lambda}\lambda_a\delta_{ab}1] \\
&= (\frac{2}{3}\frac{\Delta t}{\sqrt{2}}\dot{\gamma}_0\tau_v^{(m-1)}c(\lambda^2-1)^{(c-1)})\tau_a\lambda_b^2 = \beta_2\tau_a\lambda_b^2
\end{aligned} \tag{3.46}$$

Third term of equation 3.41 can be simplified as $\beta_3\mathcal{T}_{ab}$. Thus, using the equations 3.44 and 3.46in equation 3.41 we can define $\mathcal{K}_{ab}$ as

$$\mathcal{K}_{ab} = \delta_{ab} + \beta_1\tau_a\mathcal{D} + \beta_2\tau_a\lambda_b^2 + \beta_3\mathcal{T}_{ab} \tag{3.47}$$

Lastly, we need to derive $\mathcal{T}_{ab}$ before using $\mathcal{K}_{ab}$ in NR-iteration algoritm.

$$\begin{aligned}
\mathcal{T}_{ab} &= \frac{\partial\tau_a}{\partial\varepsilon_b} = \frac{\partial(\frac{\mu_v}{3}\frac{3-\lambda_r^2}{1-\lambda_r^2}\lambda_a^2)}{\partial\varepsilon_b} \\
&= \frac{\mu_v}{3}[\frac{\partial(\frac{3-\lambda_r^2}{1-\lambda_r^2})}{\partial\varepsilon_b}\lambda_a^2 + \frac{\partial\lambda_a^2}{\partial\varepsilon_b}\frac{3-\lambda_r^2}{1-\lambda_r^2}]
\end{aligned} \tag{3.48}$$

where using the previously derived expressions, the first term of equation 3.48 simplifies into

$$\begin{aligned}
&\frac{\mu_v}{3}\lambda_a^2\frac{\partial(\frac{3-\lambda_r^2}{1-\lambda_r^2})}{\partial\varepsilon_b} = \frac{\mu_v}{3}\lambda_a^2[\frac{\partial(\frac{3-\lambda_r^2}{1-\lambda_r^2})}{\partial\lambda_r}\frac{\partial\lambda_r}{\partial\lambda}\frac{\partial\lambda}{\partial\lambda_a}\frac{\partial\lambda_a}{\partial ln(\lambda_a)}\frac{\partial ln(\lambda_a)}{\partial ln(\lambda_b)}\frac{\partial\ln(\lambda_b)}{\partial\varepsilon_b}] \\
&= \frac{\mu_v}{3}\lambda_a^2[\frac{4\lambda_r}{(1-\lambda_r^2)^2}\frac{1}{\sqrt{N_v}}\frac{\lambda_a}{3\lambda_r\sqrt{N_v}}\lambda_a\delta_{ab}] = \frac{4}{9}\frac{\mu_v}{N_v}\frac{1}{(1-\lambda_r^2)^2}\lambda_a^2\lambda_b^2
\end{aligned} \tag{3.49}$$

and the second term is obtained as

$$\begin{aligned}
&\frac{\mu_v}{3}\frac{3-\lambda_r^2}{1-\lambda_r^2}\frac{\partial\lambda_a^2}{\partial\varepsilon_b} = \frac{\mu_v}{3}\frac{3-\lambda_r^2}{1-\lambda_r^2}[\frac{\partial\lambda_a^2}{\partial\lambda_a}\frac{\partial\lambda_a}{\partial\lambda_b}\frac{\partial\lambda_b}{\partial\ln(\lambda_b)}\frac{\partial\ln(\lambda_b)}{\partial\varepsilon_b}] \\
&= \frac{\mu_v}{3}\frac{3-\lambda_r^2}{1-\lambda_r^2}[2\lambda_a\delta_{ab}\lambda_b] = \frac{2}{3}\mu_v\frac{(3-\lambda_r^2)}{(1-\lambda_r^2)}\lambda_a^2
\end{aligned} \tag{3.50}$$

Substituting above expressions into 3.48, we finally obtain $\mathcal{T}_{ab}$ as follows, which is used in calculating equation 3.47.

$$\mathcal{T}_{ab} = \frac{4}{9}\frac{\mu_v}{N_v}\frac{1}{(1-\lambda_r^2)^2}\lambda_a^2\lambda_b^2 + \frac{2}{3}\mu_v\frac{(3-\lambda_r^2)}{(1-\lambda_r^2)}\lambda_a^2 \tag{3.51}$$

The steps of the local Newton iteration are summarized in table 3.1.

Table 3.1: Steps of local Newton iteration

1.	Set initial values	$k = 0,\ \varepsilon_a^k = \varepsilon_a^{tr}$
DO		
2.	Residual equation	$r_a := \varepsilon_a + \frac{\Delta t}{\sqrt{2}}\frac{\dot{\gamma}}{\tau_v}\operatorname{dev}\tau_a - \varepsilon_a^{tr} = 0$
3.	Linearization	$\operatorname{Lin} r_a = r_a\big\vert_{\varepsilon^k} + \left.\frac{\partial r_a}{\partial \varepsilon_b}\right\vert_{\varepsilon=\varepsilon^k}\Delta\varepsilon_b^k = 0$
4.	Compute	$\mathcal{K}_{ab} := \left.\frac{\partial r_a}{\partial \varepsilon_b}\right\vert_{\varepsilon=\varepsilon^k}$
5.	Solve	$\Delta\varepsilon_a^k = -\mathcal{K}_{ab}^{-1} r_a$
6.	Update	$\varepsilon_a^{k+1} \leftarrow \varepsilon_a^k + \Delta\varepsilon_a^k$
		$k \leftarrow k+1$
WHILE		$TOL \leq \|r_a\|$

After the update of logarithmic stretch, one can update elastic stretch $\lambda_a^e = \exp(\varepsilon_a^e)$, which is used in updating $\boldsymbol{b}_e = \lambda_a^{e^2}\boldsymbol{n}_a \otimes \boldsymbol{n}_a$ and $\boldsymbol{C}_i^{-1} = \boldsymbol{F}^{-1}\boldsymbol{b}_e\boldsymbol{F}^{-T}$.

3.2.3 Algorithmic moduli for the viscous part

Derivations of previous section are needed for deriving algorithmic moduli for viscous part, which will be derived in this section. Firstly, the spectral decomposition of the trial elastic deformation tensor is

$$\boldsymbol{F}_e^{tr} = \sum_{a=1}^{3}\lambda_a^{e\,tr}\boldsymbol{n}_a \otimes \boldsymbol{N}^a \tag{3.52}$$

Kirchhoff stress and second Piola-Kirchhoff stress is related to $\boldsymbol{F}_e^{tr}$ as follows

$$\tilde{\boldsymbol{S}} = \boldsymbol{F}_e^{tr^{-1}} \boldsymbol{\tau}^v \boldsymbol{F}_e^{tr^{-T}} \tag{3.53}$$

where Kirchhoff stress and second Piola-Kirchhoff stress are defined as

$$\boldsymbol{\tau}^v = \sum_{a=1}^{3} \tau_a \boldsymbol{n}_a \otimes \boldsymbol{n}_a \tag{3.54}$$

$$\tilde{\boldsymbol{S}} = \sum_{a=1}^{3} s_a \boldsymbol{N}_a \otimes \boldsymbol{N}_a \tag{3.55}$$

Using the relation in equation 3.53, we get the following relation between indicial coefficients τ_a and s_a.

$$s_a = \frac{\tau_a}{\lambda_a^{etr^2}} \tag{3.56}$$

We can derive $\mathbb{C}_{algo}^v$ from the stress increment $\Delta\tilde{\boldsymbol{S}}$ due to the increment in trial right Cauhcy-Green tensor $\boldsymbol{C}_e^{tr}$. Incremental rate equation can be defined as

$$\begin{aligned} 2\Delta\tilde{\boldsymbol{S}} &= \mathbb{C}_{algo}^v : \Delta\boldsymbol{C}_e^{tr} \\ \text{where} \qquad \mathbb{C}_{algo}^v &= 2\partial_{\boldsymbol{C}_e^{tr}} \tilde{\boldsymbol{S}} \end{aligned} \tag{3.57}$$

Using 3.56 in 3.55 and examining, we can deduce that $\mathbb{C}_{algo}^v$ is a two term expression. First term is due to derivative of coefficient of $\tilde{\boldsymbol{S}}$, while the second term is due to derivative of dyadic multiplication with respect to $\boldsymbol{C}_e^{tr}$. Thus, using the multiplicative rule

$$\begin{aligned} \mathbb{C}_v^{algo} &= 2\partial_{\boldsymbol{C}_e^{tr}} s_a (\boldsymbol{N}_a \otimes \boldsymbol{N}_a) + 2 s_a \partial_{\boldsymbol{C}_e^{tr}} (\boldsymbol{N}_a \otimes \boldsymbol{N}_a) \\ \mathbb{C}_v^{algo} &= 2\frac{\partial(\frac{\tau_a}{\lambda_a^{etr^2}})}{\partial \boldsymbol{C}_e^{tr}} \boldsymbol{N}_a \otimes \boldsymbol{N}_a + 2(\frac{\tau_a}{\lambda_a^{etr^2}}) \partial_{\boldsymbol{C}_e^{tr}} (\boldsymbol{N}_a \otimes \boldsymbol{N}_a) \end{aligned} \tag{3.58}$$

The first term of equation 3.58 can be expanded by using chain rule.

$$\begin{aligned} &2\frac{\partial(\frac{\tau_a}{\lambda_a^{etr^2}})}{\partial \boldsymbol{C}_e^{tr}} \boldsymbol{N}_a \otimes \boldsymbol{N}_a = 2\frac{\partial(\frac{\tau_a}{\lambda_a^{etr^2}})}{\partial \lambda_b^{etr^2}} \boldsymbol{N}_a \otimes \boldsymbol{N}_a \otimes \frac{\partial \lambda_b^{etr^2}}{\partial \boldsymbol{C}_e^{tr}} \qquad \text{where} \\ &2\frac{\partial(\frac{\tau_a}{\lambda_a^{etr^2}})}{\partial \lambda_b^{etr^2}} = 2[\frac{1}{\lambda_a^{etr^2}} \frac{\partial \tau_a}{\partial \varepsilon_b^{tr}} \frac{\partial \varepsilon_b^{tr}}{\partial \ln(\lambda_b^{etr})} \frac{\partial \ln(\lambda_b^{etr})}{\partial \lambda_b^{etr}} \frac{\partial \lambda_b^{etr}}{\partial \lambda_b^{etr^2}} + \tau_a (\frac{\partial(\frac{1}{\lambda_a^{etr^2}})}{\partial \lambda_b^{etr}}) \frac{\partial \lambda_b^{etr}}{\partial \lambda_a^{etr}} \frac{\partial \lambda_a^{etr}}{\partial \lambda_a^{etr^2}}] \\ &= 2[\frac{1}{\lambda_a^{etr^2}} c_{ab} \frac{1}{\lambda_b^{etr}} \frac{1}{2\lambda_b^{etr}} + \tau_a \frac{-2}{\lambda_a^{etr^3}} \delta_{ab} \delta_{ba} \frac{1}{2\lambda_a^{etr}}] \\ &= \frac{c_{ab} - 2\tau_a \delta_{ab}}{\lambda_a^{etr^2} \lambda_b^{etr^2}} \end{aligned} \tag{3.59}$$

and since $\boldsymbol{C}_e^{tr} = \lambda_b^{etr^2} \boldsymbol{N}_b \otimes \boldsymbol{N}_b$

$$\partial_{\boldsymbol{C}_e^{tr}} \lambda_b^{etr^2} = \boldsymbol{N}_b \otimes \boldsymbol{N}_b \tag{3.60}$$

Then, the first term of $\mathbb{C}_v^{algo}$ is found by substituting 3.59 and 3.60 into first term of 3.58. Since there is a summation over a and b, we also add previously omitted summation symbol.

$$\sum_{a=1}^{3}\sum_{b=1}^{3}[\frac{c_{ab} - 2\tau_a\delta_{ab}}{\lambda_a^{etr^2}\lambda_b^{etr^2}}]\boldsymbol{N}_a \otimes \boldsymbol{N}_a \otimes \boldsymbol{N}_b \otimes \boldsymbol{N}_b \tag{3.61}$$

or if define fourth order tensor

$$\begin{gathered} \boldsymbol{M}_a = \boldsymbol{N}_a \otimes \boldsymbol{N}_a \qquad \text{and} \qquad \boldsymbol{M}_b = \boldsymbol{N}_b \otimes \boldsymbol{N}_b \\ \text{or in indicial notation} \\ M_a^{IJ} = N_a^I N_a^J \qquad \text{and} \qquad M_b^{KL} = N_b^K N_b^L \end{gathered} \tag{3.62}$$

M_a^{IJ} has 27 elements since a, I and J take values between 1 and 3. Similarly $M_a^{IJ}M_b^{KL}$ has 729 elements. They can be easily calculated and stored using a programming language. Hence, it is possible to express 3.61 as

$$\sum_{a=1}^{3}\sum_{b=1}^{3}[\frac{c_{ab} - 2\tau_a\delta_{ab}}{\lambda_a^{etr^2}\lambda_b^{etr^2}}]M_a^{IJ}M_b^{KL} \tag{3.63}$$

As observed from equation 3.61, we should also derive c_{ab}. Since it is defined as $\frac{\partial \tau_a}{\partial \varepsilon_b^{tr}}$ if we take a intermediate derivative with respect to ε_c as follows

$$c_{ab} = \frac{\partial \tau_a}{\partial \varepsilon_b^{tr}} = \frac{\partial \tau_a}{\partial \varepsilon_c}\frac{\partial \varepsilon_c}{\partial \varepsilon_b^{tr}} = \mathcal{T}_{ac}\frac{\partial \varepsilon_c}{\partial \varepsilon_b^{tr}} \tag{3.64}$$

where we used the definition of $\mathcal{T}_{ac}$, which is equation 3.51. Now, in order to derive $\frac{\partial \varepsilon_c}{\partial \varepsilon_b^{tr}}$, we can take the total derivative of residual expression r_a with respect to ε_b^{tr} and equate it to zero since r_a is zero. Using the intermediate partial derivative with respect to ε_c, we obtain the total derivative as

$$\begin{aligned} \frac{dr_a}{d\varepsilon_b^{tr}} &= \frac{\partial r_a}{\partial \varepsilon_b^{tr}} + \frac{\partial r_a}{\partial \varepsilon_c}\frac{\partial \varepsilon_c}{\partial \varepsilon_b^{tr}} = 0 \\ &= -\delta_{ab} + \mathcal{K}_{ac}\frac{\partial \varepsilon_c}{\partial \varepsilon_b^{tr}} = 0 \\ &= \frac{\partial \varepsilon_c}{\partial \varepsilon_b^{tr}} = \mathcal{K}_{ac}^{-1}\delta_{ab} \\ &= \frac{\partial \varepsilon_c}{\partial \varepsilon_b^{tr}} = \mathcal{K}_{cb}^{-1} \end{aligned} \tag{3.65}$$

Hence, inserting the equation 3.65 into the definition of c_{ab} 3.64, we finally end up with

$$c_{ab} = \mathcal{T}_{ac}\mathcal{K}_{cb}^{-1} \tag{3.66}$$

which is used in the first part of $\mathbb{C}_v^{algo}$. For deriving second term of $\mathbb{C}_v^{algo}$, we should adopt the first part of equation 3.57. Hence, using spectral decomposition expression of $\boldsymbol{S}$ and multiplicative rule of infinite-small increment

$$2\Delta\tilde{\boldsymbol{S}} = 2\Delta[(s_a\boldsymbol{N}_a \otimes \boldsymbol{N}_a)] = 2\Delta s_a(\boldsymbol{N}_a \otimes \boldsymbol{N}_a) + 2s_a(\Delta\boldsymbol{N}_a \otimes \boldsymbol{N}_a + \boldsymbol{N}_a \otimes \Delta\boldsymbol{N}_a) \tag{3.67}$$

where the first term of above equation has been already found. Therefore, our interest is on the second term. To simplify this form, we should use skew-symmetric spin tensor expression $\Delta\boldsymbol{N}_a = \sum_{b=1}^{3} \Omega_{ab}\boldsymbol{N}_b$. Substituting this expression into second term of 3.67

$$2s_a(\Omega_{ab}\boldsymbol{N}_b \otimes \boldsymbol{N}_a + \boldsymbol{N}_a \otimes \Omega_{ab}\boldsymbol{N}_b) \tag{3.68}$$

By exchanging a and b in the first part of the above equation and using the property $\Omega_{ab} = -\Omega_{ba}$ for skew-symmetric tensors, it simplifies into

$$2(s_a - s_b)\Omega_{ab}(\boldsymbol{N}_a \otimes \boldsymbol{N}_b) \tag{3.69}$$

Similarly, we can express the second part of $\Delta\boldsymbol{C}_e^{tr}$, using spectral decomposition

$$(\lambda_a^{etr^2} - \lambda_b^{etr^2})\Omega_{ab}(\boldsymbol{N}_a \otimes \boldsymbol{N}_b) \tag{3.70}$$

Since $(\lambda_a^{etr^2} - \lambda_b^{etr^2})\Omega_{ab}$ denotes off-diagonal elements $C_{e_{ab}}^{tr}$ of $\boldsymbol{C}_e^{tr}$, we can express Ω_{ab} alternatively as

$$\Omega_{ab} = \frac{C_{e_{ab}}^{tr}}{(\lambda_a^{etr^2} - \lambda_b^{etr^2})} \tag{3.71}$$

Since $\Delta\boldsymbol{C}_e^{tr} = C_{e_{aa}}^{tr}(\boldsymbol{N}_a \otimes \boldsymbol{N}_a) + C_{e_{ab}}^{tr}(\boldsymbol{N}_a \otimes \boldsymbol{N}_b)$, $C_{e_{ab}}^{tr}$ can be expressed as

$$C_{e_{ab}}^{tr} = \frac{(\boldsymbol{N}_a \otimes \boldsymbol{N}_b + \boldsymbol{N}_b \otimes \boldsymbol{N}_a)}{2} : \Delta\boldsymbol{C}_e^{tr} \tag{3.72}$$

Inserting above equation into equation 3.71,

$$\Omega_{ab} = \frac{(\boldsymbol{N}_a \otimes \boldsymbol{N}_b + \boldsymbol{N}_b \otimes \boldsymbol{N}_a)}{2(\lambda_a^{etr^2} - \lambda_b^{etr^2})} : \Delta\boldsymbol{C}_e^{tr} \tag{3.73}$$

Now, substituting equation 3.73 into equation 3.69, and noting that there is summation over a and b,

$$\begin{aligned} &2(s_a - s_b)\Omega_{ab}(\boldsymbol{N}_a \otimes \boldsymbol{N}_b) \\ &= \sum_{a\neq b}^{3}\sum_{b=1}^{3} \frac{s_a - s_b}{(\lambda_a^{etr^2} - \lambda_b^{etr^2})}(\boldsymbol{N}_a \otimes \boldsymbol{N}_b \otimes \boldsymbol{N}_a \otimes \boldsymbol{N}_b + \boldsymbol{N}_b \otimes \boldsymbol{N}_a \otimes \boldsymbol{N}_a \otimes \boldsymbol{N}_b) : \Delta \boldsymbol{C}_e^{tr} \end{aligned} \tag{3.74}$$

where in the summation, $a \neq b$ is added due to the fact that expression is derived from the skew-symmetric tensor Ω_{ab}, of which diagonal elements are zero. Since it is easier to implement, this expression can be written in indicial notation as follows

$$\begin{aligned} &\sum_{a\neq b}^{3}\sum_{b=1}^{3} \frac{s_a - s_b}{(\lambda_a^{etr^2} - \lambda_b^{etr^2})}(N_a^I N_b^J N_a^K N_b^L + N_b^I N_a^J N_a^K N_b^L) \\ &= \sum_{a\neq b}^{3}\sum_{b=1}^{3} \frac{s_a - s_b}{(\lambda_a^{etr^2} - \lambda_b^{etr^2})}(M_a^{IK} M_b^{JL} + M_a^{JK} M_b^{IL}) \\ &= \sum_{a\neq b}^{3}\sum_{b=1}^{3} \frac{s_a - s_b}{(\lambda_a^{etr^2} - \lambda_b^{etr^2})}(\mathbb{G}_{ab}) \end{aligned} \tag{3.75}$$

Hence, we finally come up with the expression of $\mathbb{C}_v^{algo}$ by summing equations 3.63 and 3.75

$$\mathbb{C}_v^{algo} = \sum_{a=1}^{3}\sum_{b=1}^{3}[\frac{c_{ab} - 2\tau_a\delta_{ab}}{\lambda_a^{etr^2}\lambda_b^{etr^2}}]M_a^{IJ}M_b^{KL} + \sum_{a\neq b}^{3}\sum_{b=1}^{3} \frac{s_a - s_b}{(\lambda_a^{etr^2} - \lambda_b^{etr^2})}\frac{(\mathbb{G}_{ab} + \mathbb{G}_{ba})}{2} \tag{3.76}$$

Here, we have used $\frac{(\mathbb{G}_{ab}+\mathbb{G}_{ba})}{2}$ instead of $\mathbb{G}_{ab}$ in order to make sure that the tensor is symmetric. However, expression 3.76 is still in the fictitious intermediate configuration. By executing the push-forward operation via $\boldsymbol{F}_e^{tr}$, the algorithmic moduli expression in the current configuration is obtained as

$$\mathbb{C}_{algo}^{v}{}^{ijkl} = F_{e\ I}^{tr\,i}\, F_{e\ J}^{tr\,j}\, F_{e\ K}^{tr\,k}\, F_{e\ L}^{tr\,l}\, \mathbb{C}_{algo}^{v}{}^{IJKL} \tag{3.77}$$

Terms τ_a, c_{ab}, $\lambda_a^{etr^2}$, s_a can be calculated using previously derived expressions after NR algorithm converges and update logarithmic stretches for a certain time interval. This is repeated for each time increment.

Equation 3.76 possesses singularity when trial eigenvalues are equal to each other, $\lambda_a^{etr} = \lambda_b^{etr}$. Hence, we must apply L'Hospital's rule :

$$\lim_{x\to a}\frac{f(x)}{g(x)} = \lim_{x\to a}\frac{f'(x)}{g'(x)} \quad \text{if} \quad \lim_{x\to a}\frac{f(x)}{g(x)} = \frac{0}{0} \tag{3.78}$$

Hence, by applying the rule, one can obtain

$$\lim_{\lambda_a^{etr} \to \lambda_b^{etr}} \frac{s_a - s_b}{\lambda_a^{etr^2} - \lambda_b^{etr^2}} = \frac{1}{2} \frac{c_{aa} - 2\tau_a}{\lambda_a^{etr^4}}. \tag{3.79}$$

CHAPTER 4

VALIDATION OF THE MODEL AND IDENTIFICATION OF THE MATERIAL PARAMETERS

4.1 Uniaxial and volumetric experiments

To validate the model proposed in the previous section, experiments performed by a research group at University of Maryland were used. In the uniaxial and volumetric compression experiments, a silica filled epoxy molding compound (EMC) specimen was used and it is exposed to constant stress values at various temperatures, which covers all transition ranges of the material (above and below T_g) as stated in [5]. According to test results, EMC shows viscoelastic response in hydrostatic and uniaxial loading conditions. EMC is a thermosetting polymer and mostly used as casing of some semiconductors apart from its usage in other products. Hence, it is important to predict stress-strain behaviour of EMC as a function of time via FEA programs.

In both test types, a cylindrical specimen made up of EMC was used. Cylindrical specimen with a radius of 31.75 mm was cured by applying large pressure through a mechanical plunger. Curing temperature was achieved by arranging temperature of a hot plate connected to the mold, within which specimen was located. After curing temperature was reached, required pressure was applied in uniaxial direction via pneumatic cylinder. Then, the specimen was released from mold for 5-min curing time. Finally, post-mold curing process (same temperature without pressure) was applied to the specimen for 2 hours as stated in [5]. A fiber Bragg grating (FBG) sensor was used to measure the strain as a function of time during loading. The sensor was inserted inside the cylinder through a hole located at the center of the cylinder.

4.1.1 Uniaxial compression test

Uniaxial tests were performed in the same test set-up used in the fabrication process, which is shown in Fig. 4.1. Diameter of the chamber is larger than that of specimen to allow radial deformation without shear stress under compression load. Via pneumatic cylinder, air is compressed so that plunger applies a constant compressive pressure to the specimen. The mold assembly is mounted on high precision hot plate so that required temperature is reached. During deformation, data is collected and transferred from the FBG sensor. Specimen was subjected to 1 MPa constant pressure and it is reached in 1 seconds.

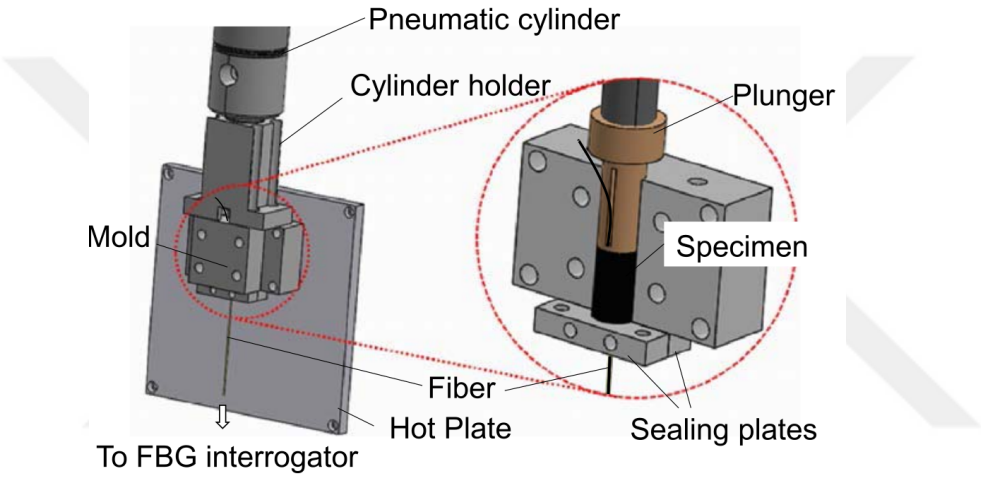

Figure 4.1: Mold assembly for uniaxial compression test [5]

4.1.2 Hydrostatic pressure test

The required pressure to deform the specimen under hydrostatic load is higher than that of uniaxial loading. Thus, a different set-up is used as shown in Fig. 4.2. In this set-up, the specimen is placed in a smaller cylindrical chamber so that the small amount of air (900 mm^3) surrounding the specimen can be compressed in an easier way. Hence, a high constant pressure can be applied. Due to high pressure applied, sealing around the fiber is done by utilizing a deformable sealant so that it applies pressure to prevent leakage. Gas inlet to the chamber is achieved by the usage of

a gas tank and pressure regulator. Pressure is controlled with feedback to the main computer via a transducer that belongs to pressure regulator. Specimen was subjected to 1 MPa constant pressure and it is reached in 1 seconds.

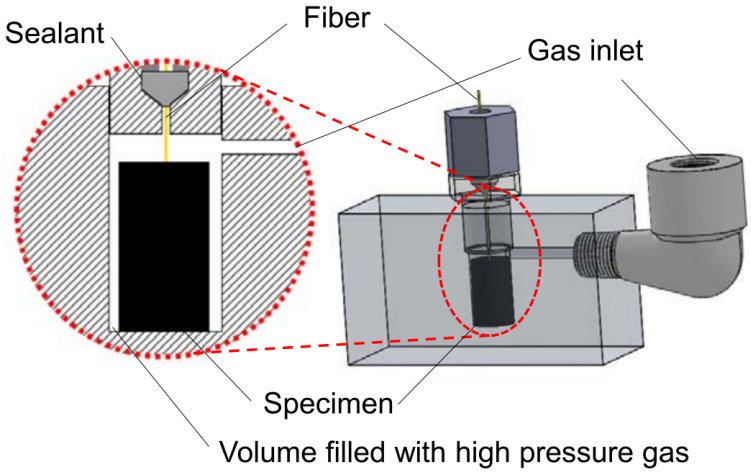

Figure 4.2: Setup for hydrostatic test [5]

4.2 Implementation of the model

To validate the model, same stress conditions should be generated in the finite element model. For this purpose, the model was implemented in FEAP (Finite Element Analysis Program), which is an open source program. A quarter of a complete cube is used by making use of the symmetry about x-y and x-z planes so that internal areas of the complete cube is restricted to move in y and z directions. The unit cube with 1 mm edge length in all three eigenvector directions was meshed with one element so that there is not a displacement gradient throughout the load application area. 1 mm edge length was used so that strain values was easier to interpret since displacements are presented in out.dat file produced by FEAP and they are same as strain values. Besides, the load is divided by an area of 1 mm^2 so that load is equal to the stress. Single element is good enough for this geometry and results are obtained in a more rapid way. Simulations with up to 100 elements were tested to see displacement difference. With more elements, simulation takes too much time and except the corner parts, displacements are close enough to one element case. Corners of the cube de-

flects more while center part of the cube deflects less. This is due to boundary effect. In one element case, all points of the top surface area deflect same amount, which makes easier to interpret data without lack of precision. Two of the cube's internal

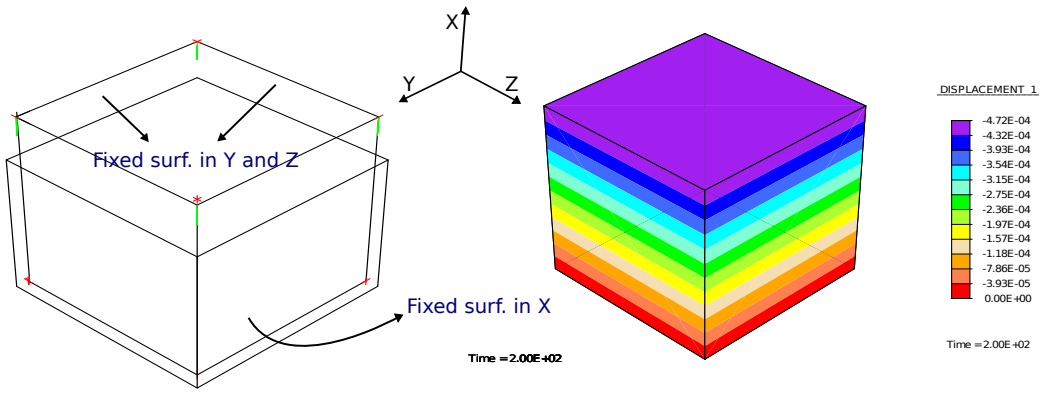

Figure 4.3: Uniaxial deformation of the cube

side surfaces were restricted to deflect in y and z directions ($u_y = 0, u_z = 0$) while the opposite surfaces were free to deflect. In this way, symmetry with respect to x-y and x-z planes was exploited to obtain the same boundary conditions in the experiment. Bottom surface was also restricted to move in x direction ($u_x = 0$). Uniaxial load was applied in negative x direction and it was applied to 4 nodes on the top surface. To apply a total pressure of -1 MPa on the top of the cube with a cross-section area of 1 mm^2, -0.25 N force was applied to each one of four nodes within 1 seconds and then it was kept constant. Thus, the same stress conditions were established as the specimen tested. With deformation, cross-section area of the cube increases in this case and this leads to a decrease in stress as opposed to volumetric test. However, since variation of area was small, a variable load was not applied. In the left part of Fig. 4.3, deformed and undeformed meshes can be observed with a scaling factor of 100.

Same boundary conditions were applied for the hydrostatic analysis. -1 MPa load was applied to all three perpendicular surfaces and they were applied to 4 nodes on the surfaces as -0.25 N. In this case,the cube was forced to deflect in all directions, which decreases its volume as shown in Fig. 4.4. Deformation is shown with a scaling factor of 500 as it is much smaller than reality in this case. Deflection is same for all three directions due to the symmetrical loading and geometry.

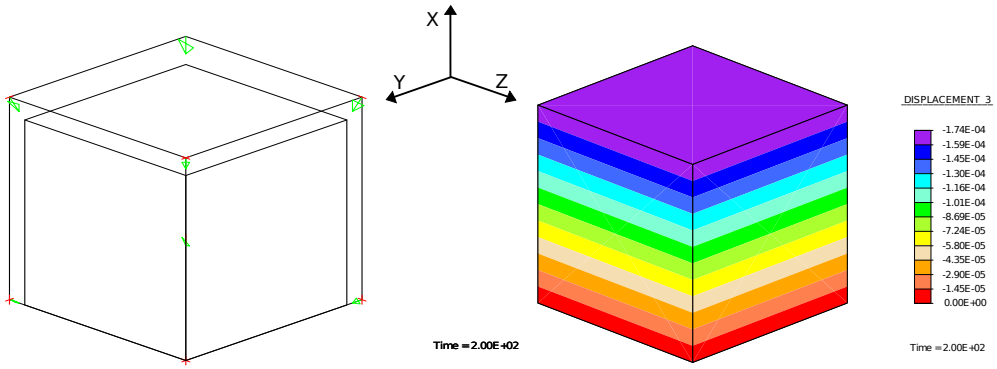

Figure 4.4: Volumetric deformation of the cube

4.3 Sensitivity of the constitutive model to material parameters

In this section, parameters of the model developed in chapter 3 will be investigated and effect of each parameter will be explained relating them to the rheological viscoelastic model in Fig. 2.19. In accordance with this purpose, volumetric and uniaxial creep responses of the silica filled epoxy compound at 145°C are plotted for various values of each parameter and keeping other parameters constant. This temperature is selected since it is close to the glass transition temperature of the material and creep responses of both volumetric and uniaxial tests are distinct. Moreover, the model is also investigated by simulating other viscoelastic behaviours although there are not experimental data for some of these behaviours. Parameters of the epoxy used in cyclic loading with intermediate stress relaxation steps are used for demonstrating effects of creep rate parameter $\dot{\gamma}_0$, power term m and viscous shear modulus μ_v on cyclic loading.

4.3.1 Effect of equilibrium bulk modulus κ^e

Bulk modulus κ^e can be considered as the resistance to the volumetric change. A bigger bulk modulus means that forcing a body to deform by changing its volume is harder compared to the lower values of κ^e since hydrostatic pressure p on the surface of the body reaches to very high values. During deformation of the body, the free energy function (or stored energy) due to volumetric effects increases with determi-

nant of deformation tensor $\det(\boldsymbol{F}) = J$. Equilibrium bulk modulus determines the stiffness of the material at time $t = t_\infty$, at which the material comes to an equilibrium and strain reaches its maximum value ε_∞. Thus, by changing κ^e, stored volumet-

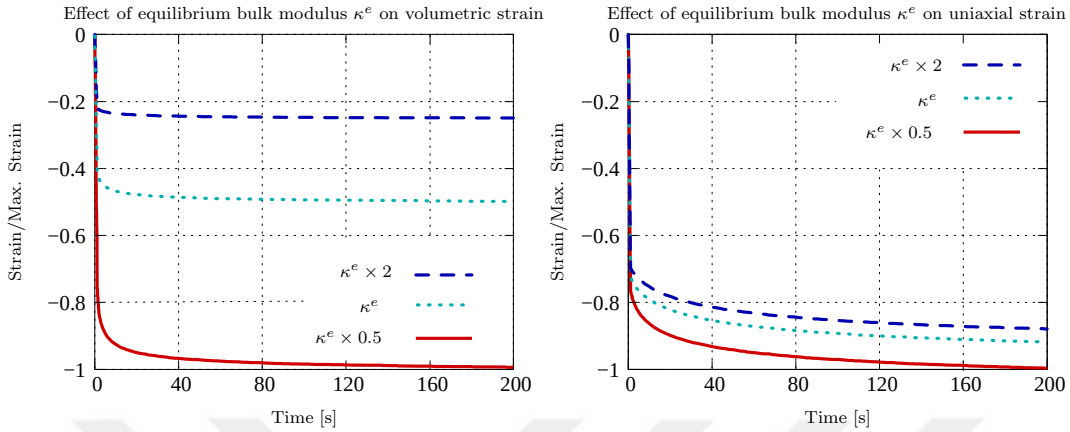

Figure 4.5: Effect of equilibrium bulk modulus κ^e on volumetric (on the left) and uniaxial (on the right) creep at 145°C

ric energy of the material under the hydrostatic pressure can be changed. This can be observed in Fig. 4.5. For higher values of κ^e, equilibrium value of volumetric creep is smaller compared to lower values since the material behaves stiffer to the applied constant load. We can think of this process from the rheological model in Fig. 2.19. Equilibrium branch of the model carries most of the suddenly applied load by stretching in small amounts initially. The rest of the load is carried by the spring (or the dashpot since they are connected in series) of viscous branch since the dashpot is stiff and does not expand much due to its viscosity upon suddenly applied load. In other words, two branches shares the applied load in accordance with their stiffness ratio. As time passed by, the dashpot expands (associated with relaxing chains and related with creep rate formula) by releasing the tip of the viscous spring and consequently reducing the carried load by viscous branch and increasing the carried load by the equilibrium spring. Hence, equilibrium strain value is reached when whole load is carried by equilibrium branch. This time dependent behaviour is observed in Fig. 4.5 between 1-200 seconds. Another important observation from the figure is that difference between initial and equilibrium is smaller for higher values of κ^e. This is because of the fact that the equilibrium spring takes most of the applied load initially

and importance of the dashpot is reduced with less amount of load on it. Thus, it expands in a smaller amount to come to the equilibrium since viscoelastic strain measure $\boldsymbol{b}_e$ on dashpot is already small. Therefore, transition from initial to equilibrium strain value within first 20 seconds is with a smaller strain rate as can be observed from the curvature with very small radius of dotted blue line ($\kappa^e \times 2$) in Fig. 4.5.
In polymers, deforming the body in uniaxial direction (tension or compression) mostly leads to shear deformation (shape dependent or isochoric) rather than volumetric deformation, which makes shear modulus μ a more important parameter in terms of time dependent and equilibrium response. Thus, in many cases under the uniaxial loading, rubber-like materials tend to deform without changing their volume ($\nu = 0.5$) and they are assumed to be incompressible by many researchers. Uniaxial creep also depends on κ^e but not as much as volumetric creep and this can be understood from less dominant above-mentioned behaviours in uniaxial creep response of Fig. 4.5.

4.3.2 Effect of equilibrium shear modulus μ^e

Equilibrium shear modulus μ^e is related with the spring of equilibrium branch and denotes the elastic stiffness of the material. It influences creep behaviour in the same manner with κ^e except that it stores energy due to shape change deformation (isochoric) and stored energy can be considered as a function of total strain measure $\boldsymbol{b}$. In a hydrostatic test, volumetric deformation is only related with bulk modulus. The material is forced to deform by shearing in uniaxial deformation. As a result of this, various values of μ^e make only a difference in uniaxial creep behaviour as illustrated in Fig. 4.6. Creep behaviour shown with dotted red line has less shear modulus value meaning that equilibrium branch carries a lower amount of load. Thus, the viscous branch initially takes significant amount of the applied load compared to higher μ^e values. Initial elastic strain is also higher in magnitude due to lower stiffness of equilibrium branch. Then, as the dashpot relaxes, the change in strain is more distinct and converges to greater (in magnitude) equilibrium strain value with higher rate for low μ^e. Creep rate or $\dot{\boldsymbol{b}}_e$ is higher especially between 1-20th seconds due to dominant elastic stretch in creep rate law. This difference in creep rate reduces as strain gets close to the equilibrium value regardless of value of parameters.

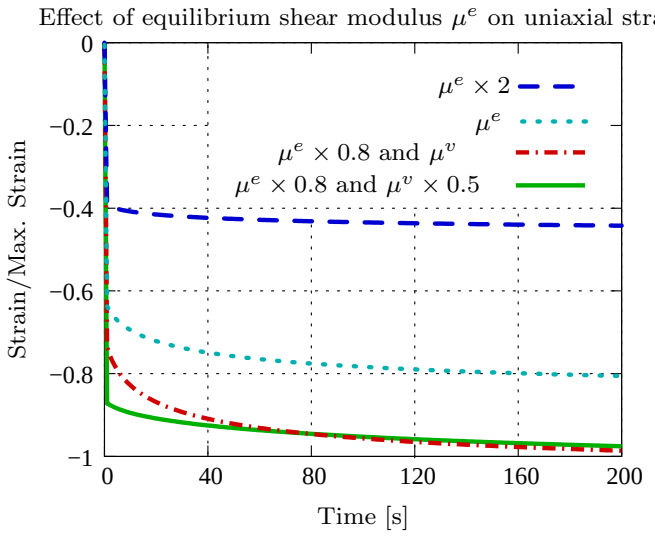

Figure 4.6: Effect of equilibrium shear modulus μ^e on uniaxial creep at 145°C

4.3.3 Effect of viscous shear modulus μ^v

Viscous shear modulus μ^v denotes the stiffness of the spring in the viscous branch of the rheological model. As always, as we increase the value of μ^v, a greater portion of load is carried by the dashpot or the spring initially. Higher values of viscous shear modulus can be selected in order for the viscous branch to carry more load. Thus, the remaining smaller amount of load results in a smaller initial elastic straining (shown in dotted blue line with $\mu^v \times 2$). However, equilibrium load or final strain value must be same regardless of μ^v and this is also shown in the result of Fig. 4.7 via convergence of all lines to the same final strain value. Creep rate $\dot{\gamma}$ is high for greater μ^v values since magnitude of stress carried by the dashpot increases. Also, elastic stretch λ_e initially takes greater portion of total stretch λ leading to greater creep rate at stretched state for all μ^v values. This fact can be observed from the part where creep rate equation derived. Elastic stretch, λ_e takes smaller values at the stretched and relaxed state resulting in a smaller creep rate $\dot{\gamma}$ and consequently smaller rate of elastic part of left Cauchy-Green tensor $\dot{\boldsymbol{b}}_e$ (measure of strain on the viscous spring) around equilibrium point. As elastic strain λ_e on the viscous branch spring is greater, initial change in strain is steeper for $\mu^v \times 2$ compared to other curves. At equilibrium, whole applied load is carried by the equilibrium spring. Differences between all three curves are only how fast they reach equilibrium value and magnitude of initial elastic

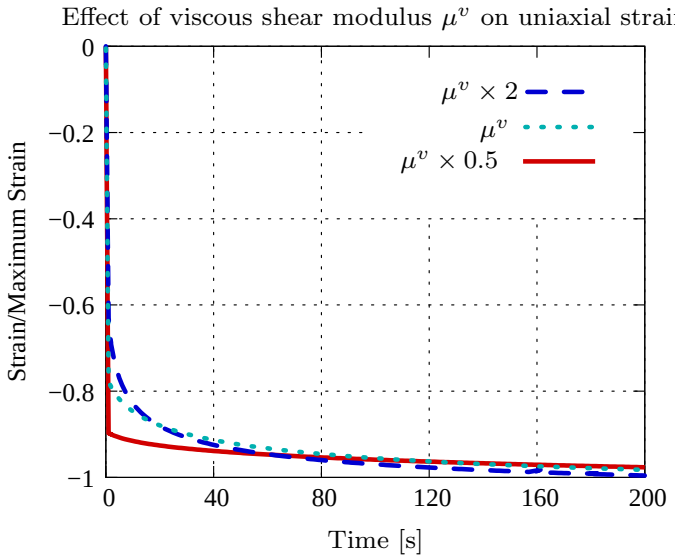

Figure 4.7: Effect of viscous shear modulus μ^v on uniaxial creep at 145°C

strain.

4.3.4 Effect of viscous bulk modulus κ^v

Response of the model to the changes in viscous bulk modulus κ^v is the same with viscous shear modulus except that it generally affects volumetric behaviour and affects uniaxial behaviour in a smaller amount. From rheological model point of view, small values of κ^v transfers all the applied load to the equilibrium branch, which causes the initial total strain to be greater in magnitude as shown in Fig. 4.8. Also, relatively low stress on the dashpot minimise creep rate and strain rate resulting in very long volumetric creep duration as observed from green line($\kappa^v \times 0.2$). An increment in κ^v brings along greater changes in strain in first 20 seconds because of the same reason mentioned for μ^v. After 20 seconds, this is not apparent since elastic stretch, λ_e is close to 1.

Another important observation is that making κ^v very large does not influence creep behaviour significantly. This is probably because of high initial creep rate observed in the dashpot due to significant amount of viscous stress applied to it so that it quickly creeps although initial strain is small. Same reasoning also applies to very large values of viscous shear modulus μ^v.

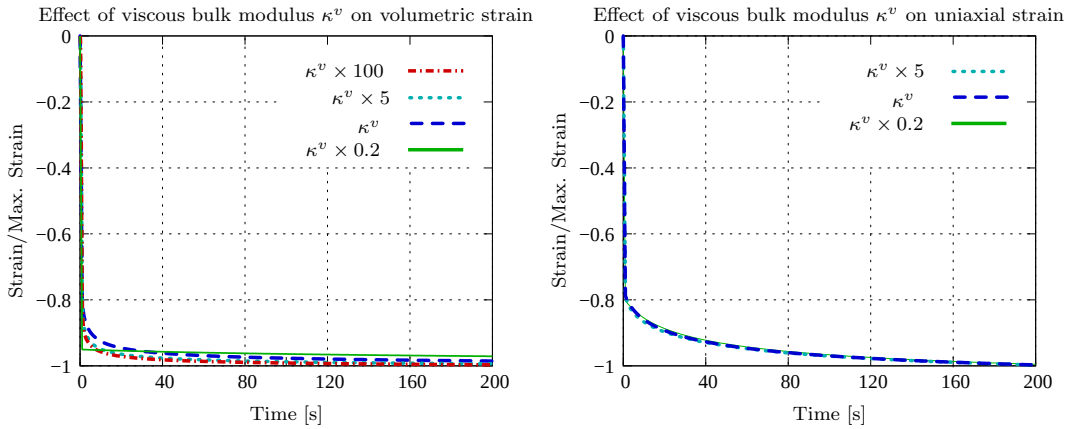

Figure 4.8: Effect of viscous bulk modulus κ^v on volumetric (on the left) and uniaxial (on the right) creep at 145°C

4.3.5 Effect of creep rate parameter $\dot{\gamma}_0$

Creep rate parameter $\dot{\gamma}_0$ directly affects viscosity of the dashpot as shown in Fig. 4.9. Very small values of $\dot{\gamma}_0$ decreases evolution of creep $\dot{\gamma}$ and thereby strain rate (dotted blue line ($\dot{\gamma}_0 \times 0.005$). Thus, one can say that the dashpot has high viscosity for very small values of $\dot{\gamma}_0$ and vice versa. Also, dotted blue curve starts to decline at a lower total strain value because of the stiffer dashpot while there is not a distinct difference in other curves. Slope of strain for dotted blue curve stays nearly constant since evolution of elastic stretch λ_e and stress is small for longer durations in contrast to the other cases.

4.3.6 Effect of power term m

Evolution equation is also dependent on power term m due to the energy or stress dependence term $(\frac{\tau_v}{\hat{\tau}})^m$ added to it. Since τ_v is smaller than 1 MPa, increasing m value decreases creep rate and makes the dashpot very stiff as shown in Fig. 4.10. However, slope of strain is constant for longer durations as previously mentioned. Taking m small cause the dashpot to have low viscosity and the equilibrium spring reaches equilibrium strain at the instant of loading (green line $m \times 0.2$).

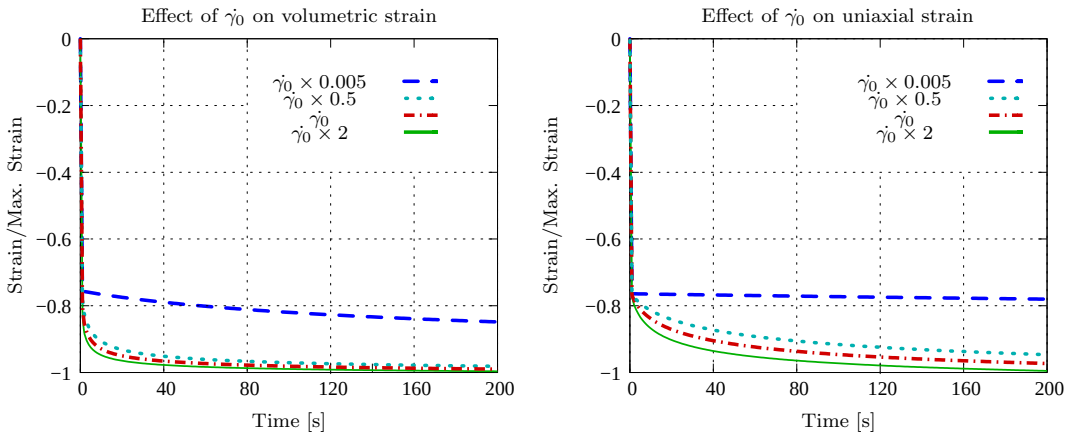

Figure 4.9: Effect of creep rate parameter $\dot{\gamma}_0$ on volumetric (on the left) and uniaxial (on the right) creep at 145°C

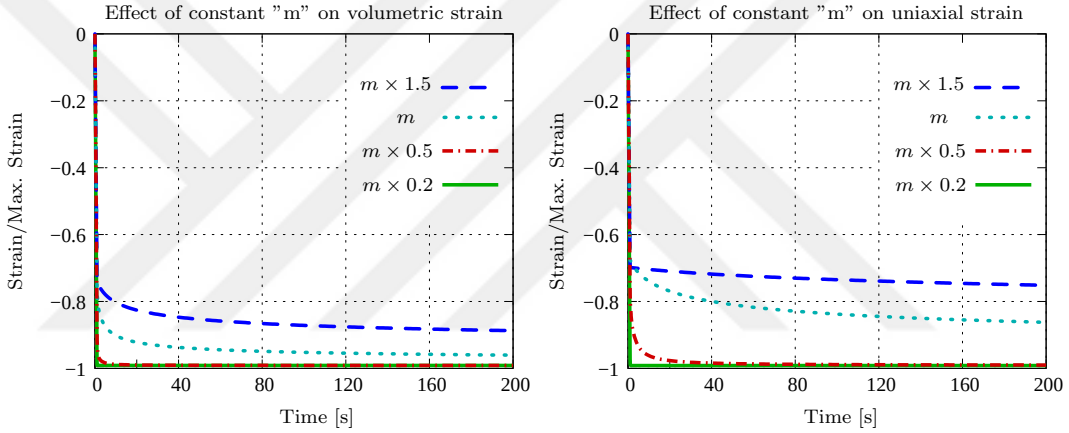

Figure 4.10: Effect of power term m on volumetric (on the left) and uniaxial (on the right) creep at 145°C

4.3.7 Cyclic behaviour

Zig-zag strain input is generally applied to polymeric materials to observe their dissipative nature and behaviour under load that alters direction. In Fig 4.11, area under the stress-strain curve gives the energy dissipated by the material during deformation. Input strain value is varied between -0.01 and 0.01 in 2 cycles and duration is 200 seconds. Stress during loading is higher than unloading. When strain value reaches zero after first half cycle (t = 50 s), there is still negative stress in the material due to relaxation. When the material is loaded in the negative direction, residual stress

is positive. Besides, during the initial part of unloading in the opposite direction (t = 25 s), slope of the curve is steeper since the dashpot resists to shrink and therefore, it directly makes viscous branch more stiffer under compressive load. Then, stress decreases with a smaller constant slope as the dashpot shrinks. Cyclic behaviour of the

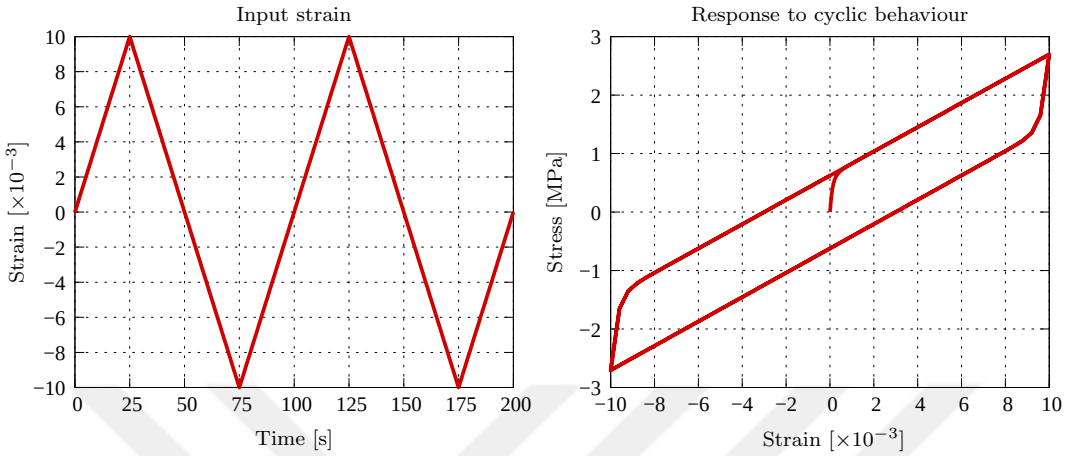

Figure 4.11: Input strain (on the left) and cyclic behaviour (on the right) at 145°C

previously mentioned epoxy compound is examined with various values of important viscous parameters : μ_v, m and $\dot{\gamma}_0$. The effects of parameters are associated with the elements of rheological model and are used to make fitting process easier.

4.3.8 Effect of viscous shear modulus μ_v on cyclic behaviour with intermediate relaxation steps

The first parameter examined is μ_v, which influences amount of initial stress produced in the spring of viscous branch. In progress of time, stress in the spring relaxes due to the elongation of the dashpot reducing consistent tangent moduli. This is observed in Fig. 4.12 as both stress and slope converging to the same values for two different values of μ_v although more energy dissipation occurs when we double μ_v. At a constant strain of 0.01, the model is allowed to relax with a duration of 800 seconds in both loading and unloading. It is observed that 800 seconds is not enough for the model to relax completely as terminal points of loading and unloading does not meet in an equilibrium line. However, we should expect such a line since model is viscoelastic. It is possible for the model to reach this line sooner by increasing

relaxation rate or in other words power term m and creep rate parameter $\dot{\gamma}_0$.

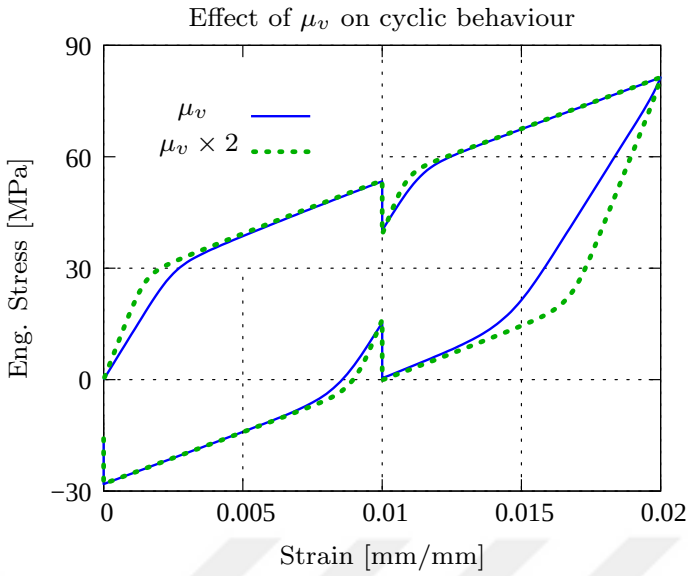

Figure 4.12: Effect of parameter μ_v on cyclic behaviour with intermediate relaxation steps at 150°C

4.3.9 Effect of power term m on cyclic behaviour with intermediate relaxation steps

Power term parameter m enhances relaxation rate especially when high viscous stress exists as m is a power term of viscous stress. In Fig. 4.13, the effect of m on cyclic deformation is shown. Relaxation rate is smaller for $m \times 0.95$, therefore, at the same strain, total stress is higher with higher dissipation.

4.3.10 Effect of creep rate parameter $\dot{\gamma}_0$ on cyclic behaviour with intermediate relaxation steps

Same as m, creep rate parameter $\dot{\gamma}_0$ also affects relaxation rate but in a linear relationship. Besides, it reduces stress in all strain regime same amount while m affects stress at large strain regime in a greater amount.

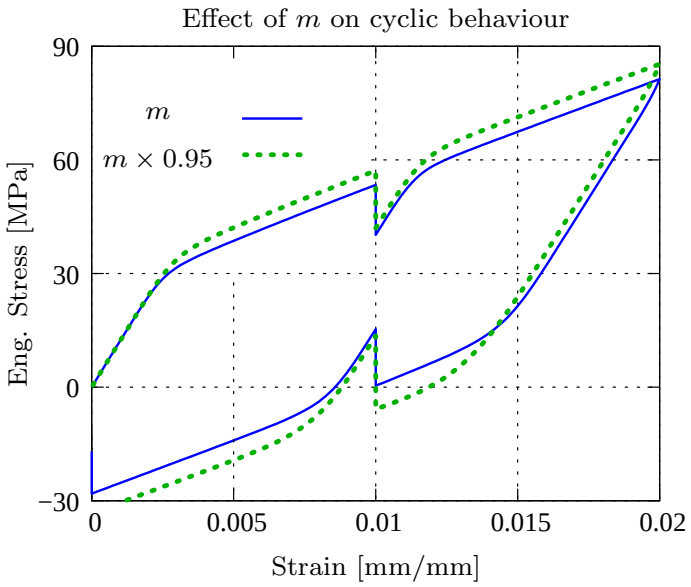

Figure 4.13: Effect of power term m on cyclic behaviour with intermediate relaxation steps at 150°C

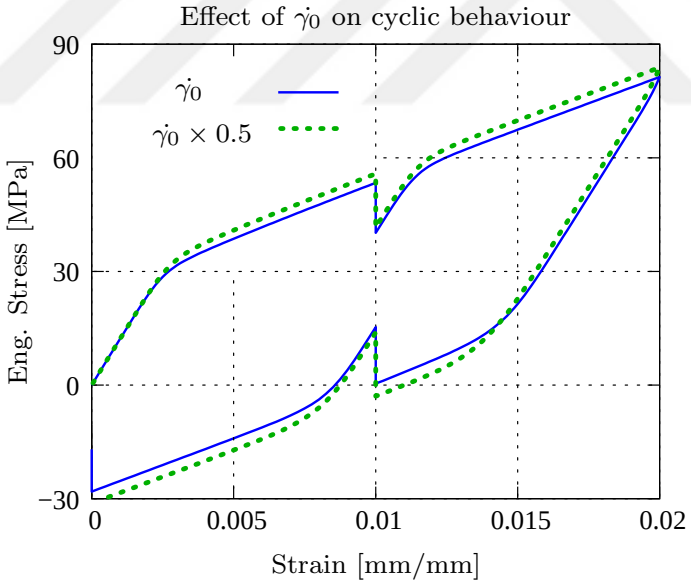

Figure 4.14: Effect of creep rate parameter $\dot{\gamma}_0$ on cyclic behaviour with intermediate relaxation steps at 150°C

4.3.11 Effect of strain rate

Viscoelastic materials are known to have a dependency on strain-rate. Applying load in a very fast way increases resistance shown by the material. In other words, the dashpot in viscous branch becomes stiffer as can be understood from the evolution law of $\boldsymbol{b}_e$. This is shown in Fig. 4.15 with high stress values at the same strain value for faster loadings. Thus, the material has path dependency. Moreover, history of deformation is important for the material.

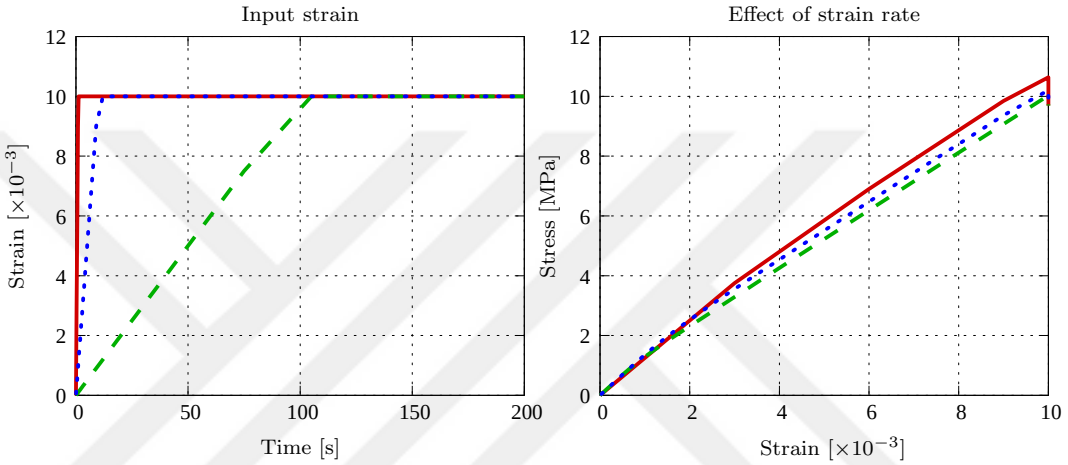

Figure 4.15: Input strain (on the left) and effect of strain rate (on the right) at 145°C

4.3.12 Creep recovery

If the material is loaded up to some constant stress value and then load is removed suddenly, the material does not return to its unloaded state as an elastic material as shown in Fig. 4.16. Instead, elastic part of strain returns to zero rapidly. Then, remaining inelastic strain starts to decline with time and altering rate. During this process, the dashpot returns to its original position as chain segments start to unwind and rotate at junction points. This process may be very slow. Since the material is a thermoset with crosslinks, there is not permanent strain value unlike thermoplastics.

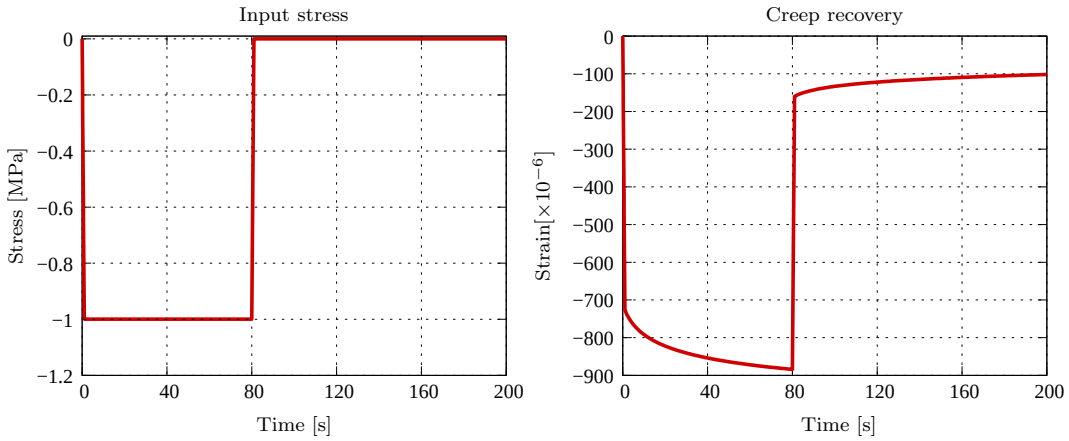

Figure 4.16: Input strain (on the left) and creep recovery (on the right) at 145°C

4.4 Comparison of LVE and NLVE models

In order to observe capability difference between linear and non-linear viscoelastic models, the evolution law of the viscous deformation (creep rate equation) is made linear, which is accomplished by making m equal to 1 and power of the bracket term equal to 0 in the evolution equation 2.50. In Fig. 4.17, the dotted red lines corresponds to the linear viscoelastic simulation response while straight lines corresponds to the non-linear viscoelastic simulation response for both volumetric and uniaxial creep. To observe better with a closer view, creep responses for 40 seconds are also presented. Creep rate is a function of stress amplitude and amount of viscous stretch in the dashpot which are considered in NLVE model. This gives the ability of capturing slope of creep curve (or rate) at each strain-time point in an easier way compared to LVE model. Stress and amount of strain dependence of creep rate can not be taken into consideration in LVE model. Thus, creep response of the conducted tests are better predicted with NLVE model.

4.5 Parameter identification from creep tests

In this section, experimental results mentioned in the previous section are simulated with model by taking the effect of 6 parameters on creep behaviour into consideration. Tests are performed at 18 different temperatures. Around glass transition temperature

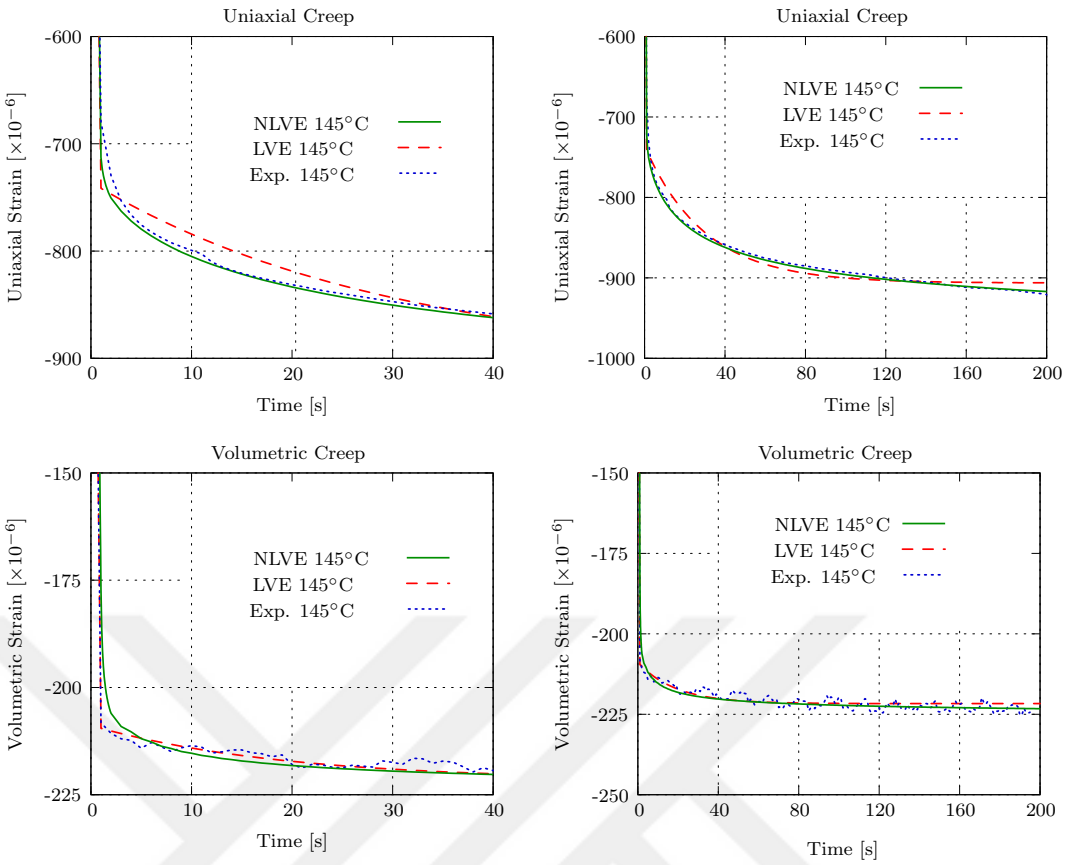

Figure 4.17: Comparison of LVE model and NLVE model for uniaxial creep (on the top), volumetric creep (on the bottom) and for 40 seconds (on the left), 200 seconds (on the right) at 145°C

(130°C), tests are performed for each 5°C temperature difference. Temperatures are between 45°C and 235°C for the performed tests. Only 5 comparison will be given in this chapter and the remaining comparisons are available in appendix A.

Strain values are normalized by dividing the strain by maximum strain reached during 200 seconds since test conductor that supplied data keeps them private. Uniaxial strain values are greater in absolute magnitude than volumetric strain values as expected. This is because of the fact that deforming polymeric material's body in all directions (hydrostatic deformation) is very hard. On the contrary, it is easy to deform by applying the force (isochoric deformation) in one direction. In general, there is 4-5 times of magnitude difference between the creep results of uniaxial and volumetric tests. However, in test results below 110°, uniaxial strain value in magnitude is smaller than volumetric strain value reached at equilibrium and also at initial load-

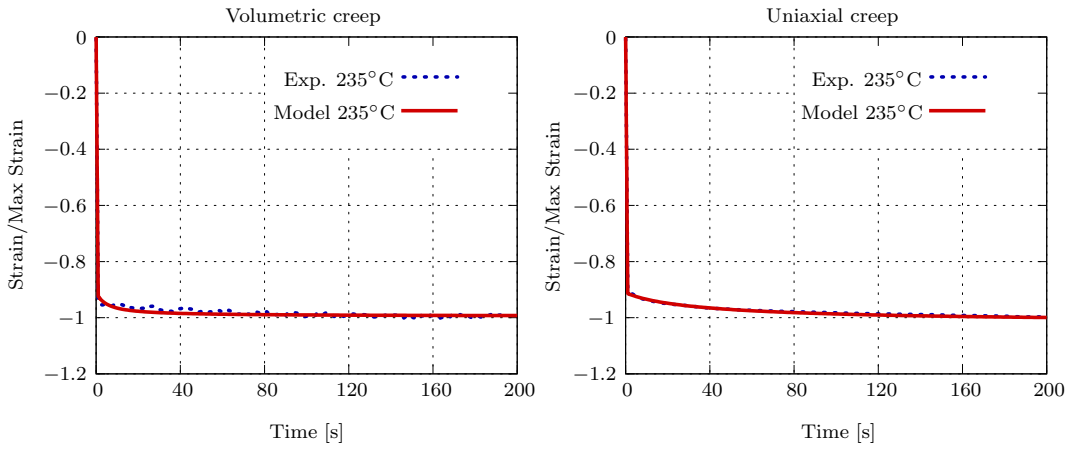

Figure 4.18: Volumetric (on the left) and uniaxial (on the right) creep test at 235°C

ing. Also, change of the uniaxial strain data with 5°C temperature drops are higher in magnitude than it should be at temperatures below 120°. This is not appropriate considering the natural response of epoxy based material. From the tests performed

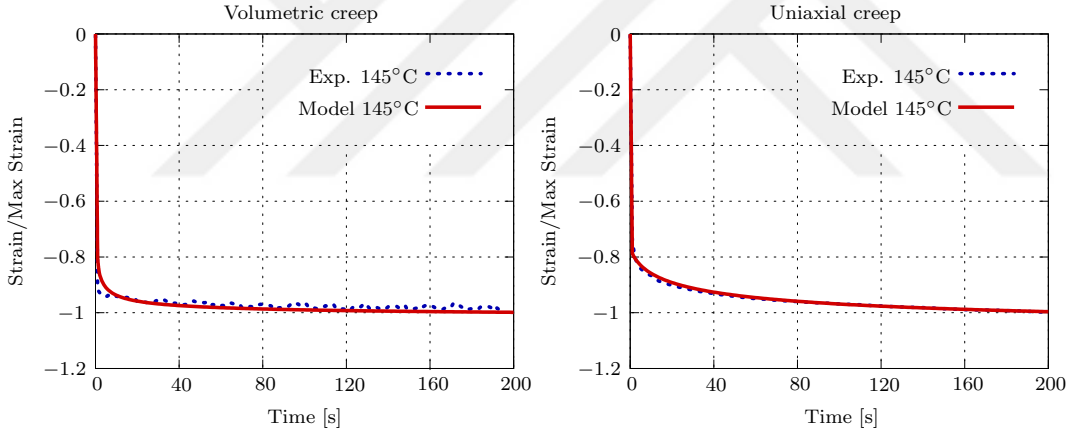

Figure 4.19: Volumetric (on the left) and uniaxial (on the right) creep test at 145°C

at different temperatures in figures 4.18, 4.19, 4.20, 4.21, 4.22, it is observed that viscoelastic time dependent behaviour is more apparent around glass transition temperature (T_g = 130°C) as time dependent behaviour starts at a lower strain/max. strain value and continues up to the normalized value of -1 (equilibrium value). In the range of high temperatures, as mentioned in the second chapter, the curve rapidly declines to a strain close to the equilibrium value and slope of strain curve becomes constant after a rapid transition from vertical part to horizantal part of the curve. On the con-

trary, creep response around T_g still has a negative slope after 200 seconds, which shows that viscoelastic effects are maximum around T_g and have not diminished yet. This is due to the mobility of molecular chains of the material and the significant free volume at high temperatures. At high temperatures, the material is in a rubbery state and free volume is so large that viscoelastic effects occurs instantaneously. However, there is a limit that strain value of the material can reach since epoxy based polymers are thermosets with primary bonds (entanglements and crosslinks).

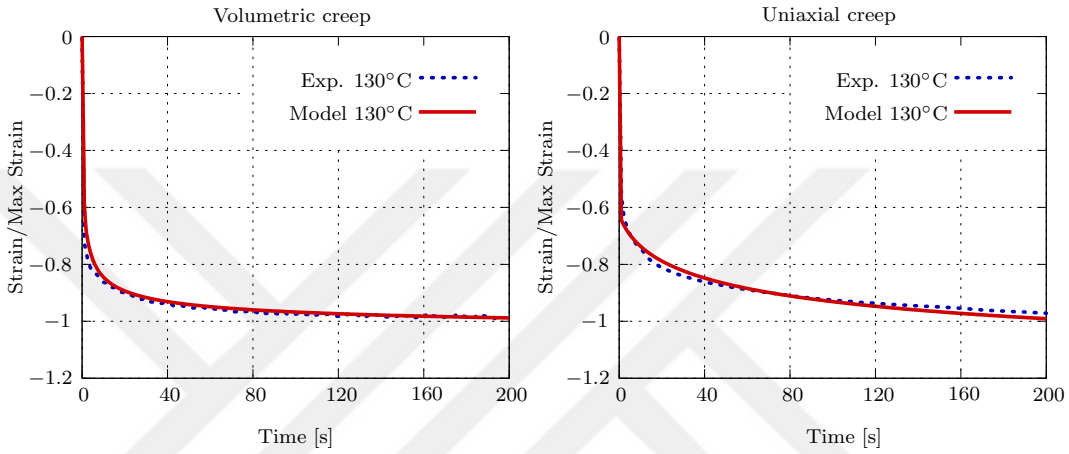

Figure 4.20: Volumetric (on the left) and uniaxial (on the right) creep test at 130°C

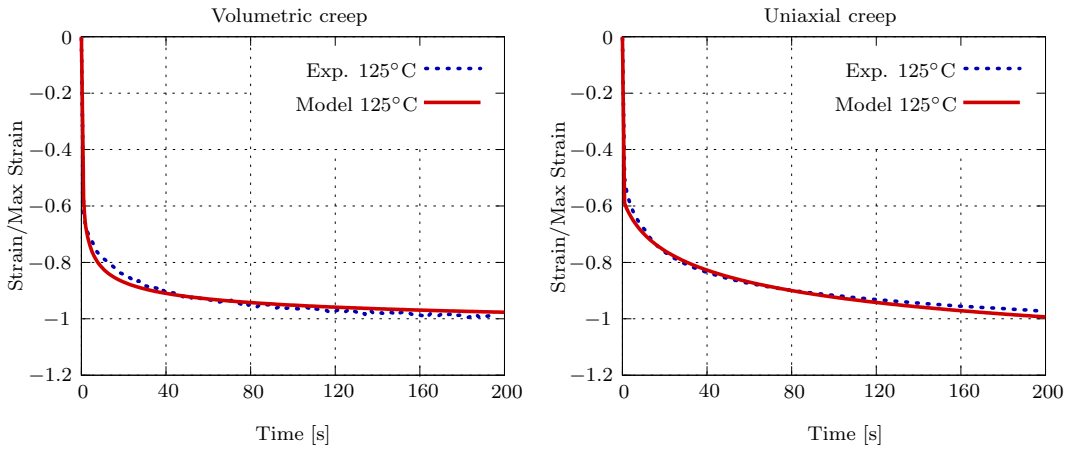

Figure 4.21: Volumetric (on the left) and uniaxial (on the right) creep test at 125°C

Below T_g in Fig. 4.22, the free volume and slope of it (thermal expansion) are rela-

tively smaller. Consequently, viscoelastic effects are little (like a solid) and the material behaves like a glassy solid, of which equilibrium and initial strain values are close to each other.

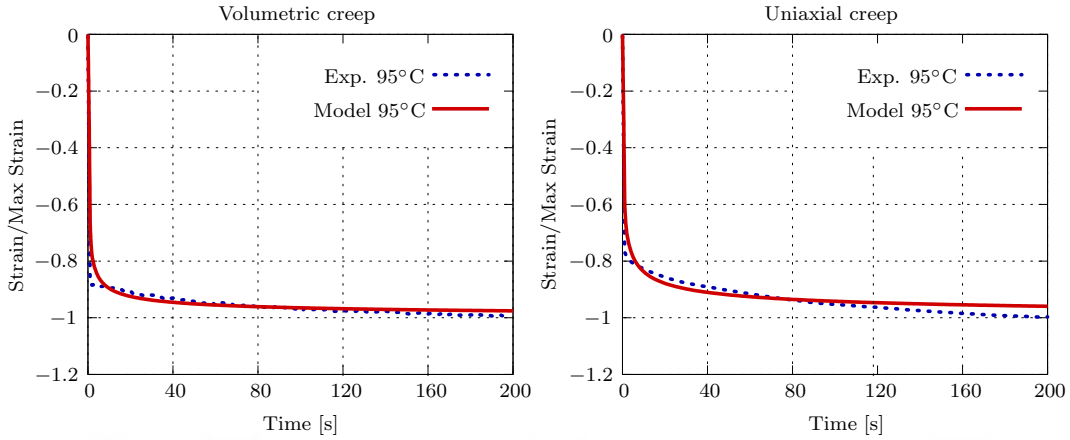

Figure 4.22: Volumetric (on the left) and uniaxial (on the right) creep test at 95°C

Parameters used in fitting for simulation at each temperature are tabulated in table 4.1.

4.6 Variation of material parameters with temperature

Variation of some parameters and ratio of that parameters with temperature are important to understand the response. Thus, in this section, Poisson's ratio, ratio of viscous bulk modulus to equilibrium bulk modulus, ratio of viscous shear modulus to equilibrium shear modulus will be presented as functions of temperature.

4.6.1 Variation of Poisson's ratio over temperature

As observed in Fig. 4.23, initial Poisson's ratio ν_{inst} and equilibrium Poisson's ratio of the characterized material are nearly constant for temperatures above 160°C and they decline rapidly around T_g. This is an expected variation and also common in literature since around T_g there is a sudden drop in all parameters as stated in [41]. Poisson's ratio is obtained from the κ and μ values using the following well-known

Table 4.1: Identified parameters from creep tests at various temperatures

Temperature [°C]	κ^e [MPa]	μ^e [MPa]	κ^v [MPa]	μ^v [MPa]	$\dot{\gamma}_0$	m
45	5100	17600	4200	16000	2.1	3.1
65	4700	16900	4100	15000	2.1	3.4
85	4400	14000	4100	14000	1.1	3.7
95	4200	12600	3900	13000	1.1	3.7
105	3237.5	5630	3600	6000	0.1	3.6
110	2713.02	2620	3300	4500	0.05	3.59
115	2590	1530	3000	2000	0.049	2.5
120	2160.8	784	2200	1100	0.048	2.68
125	1700	547	1900	800	0.75	4.88
130	1550	487	1600	480	0.73	3.98
135	1460	482	1100	400	2.18	4.35
140	1430	414	1000	200	8	4.25
145	1425	352	500	150	20	4
155	1380	272	250	80	15	2.5
175	1360	240	120	54	14.4	2.05
195	1285	215	160	43	12	2.23
215	1200	197	100	37	15	2.2
235	1189	193	96	23.6	15	2.3

elastic relation.

$$\nu = \frac{3\kappa - 2\mu}{2(3\kappa + \mu)} \tag{4.1}$$

It can be also found from the following equation since we know strain values in all directions. The equations give nearly same results.

$$\nu = -\frac{\varepsilon_y}{\varepsilon_x} = -\frac{\varepsilon_z}{\varepsilon_x} \tag{4.2}$$

It is clear that Poisson's ratio takes values close to 0.5 at high temperatures. This indicates that material is close to becoming incompressible at rubbery state, which is in agreement with incompressible assumption of rubbery materials.

Below 110°C, Poisson's ratio becomes smaller than 0.2 and even negative values below 105°C. This is not reasonable obviously. Volumetric strain is greater than uniaxial

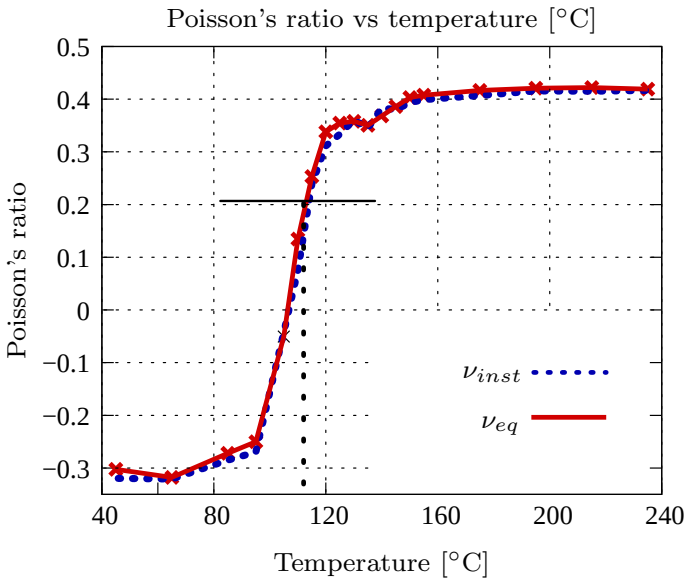

Figure 4.23: Variation of Poisson's ratio over temperature

strain below this temperature. Hence, it is probably due to the unreasonable drop in uniaxial strain below 110°C as previously mentioned. Fitting experimental data is very hard below this temperature since μ^e values must be very large to fit small uniaxial strain. Taking high values of μ keeping other parameters nearly constant leads to negative Poisson's ratio, which is probably an experimental error. This situation also affects fitting quality. However, this might be probably because of the fact that the micro-molecular structure of the epoxy material is very different than rubbery state behaviour at high temperatures. Thus, using a material model developed for rubber-like materials may not be suitable for temperatures below T_g, which motivates us to develop a more suitable one as a future work.

It is also observed that equilibrium Poisson's ratio is a bit greater than instantaneous Poisson's ratio for all temperature values. This is again in agreement with literature [41].

4.6.2 Variation of viscous and elastic parameters E, κ and μ over temperature

Variation of the material parameters is important to understand the complete behaviour. As shown in the left figure of 4.24, ratio of viscous shear/bulk modulus to equilibrium shear/bulk modulus are given with temperature. This figure gives idea

about viscoelastic behaviour. At high temperatures, this ratio is small since the material reaches equilibrium strain quickly and viscous branch's effect is weak compared to equilibrium branch. The r atio is high around glass transition temperature and declines again in glassy state. However, data taken below 110°C is not reliable as stated earlier. It should be also noted that effect of shear modulus is more dominant than bulk modulus.

All three modulus decline with temperature and stay virtually constant above 140°C. Viscous parameters also display same kind of variation although they are not shown in this figure for the sake of simplicity.

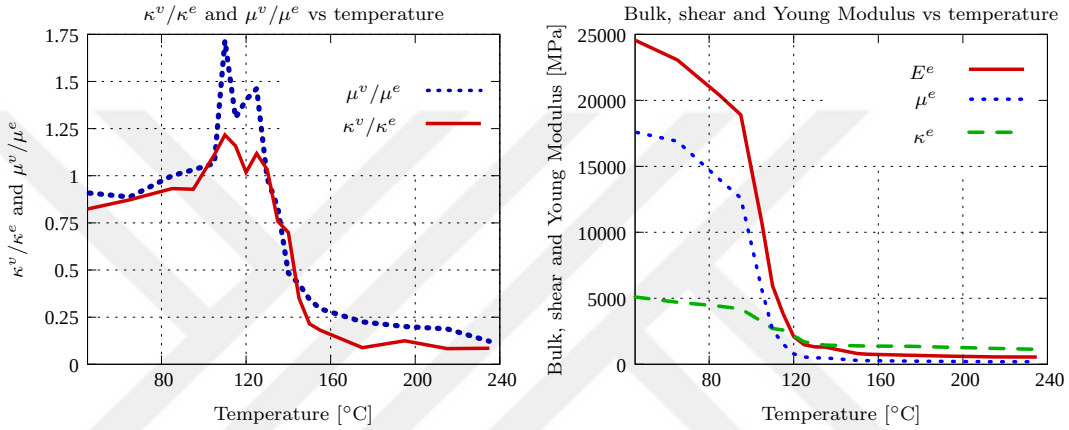

Figure 4.24: Variation of elastic and viscous parameters E, κ and μ over temperature

4.7 Relaxation behaviour of an epoxy compound

This section is devoted to relaxation behaviour of a different epoxy compound subjected to cyclic loading with intermediate relaxation steps. This epoxy compound is different than the one mentioned in the previous section and its tests are used to show stress relaxation and cyclic loading-unloading capability of the model. In this manner, using FEAP, material is loaded upto relatively low strain value (0.004) and it is allowed to relax for a certain amount of time. Tests were repeated at 4 different temperatures : 75°C, 100°C, 125°C, 150°C. The results are shown in figures 4.25, 4.26, 4.27 and 4.28. Besides, the parameters used for fitting are given in table 4.2.

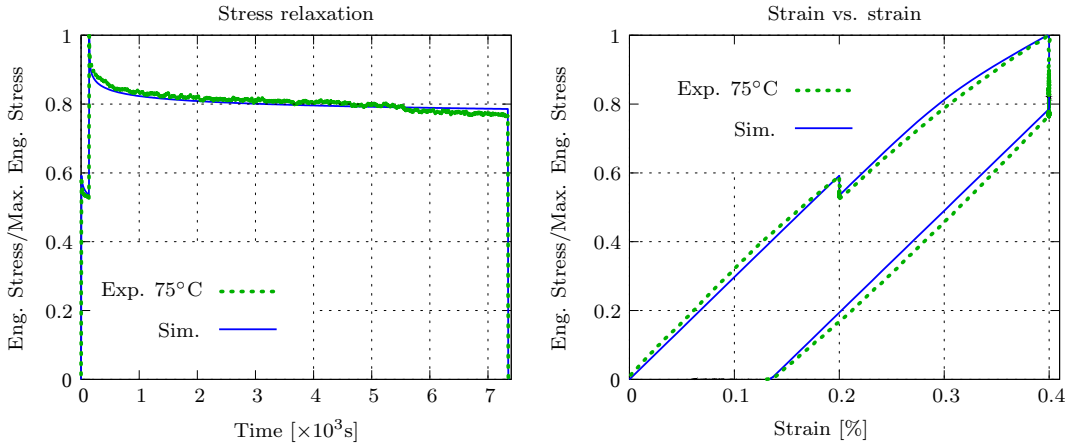

Figure 4.25: Stress relaxation (on the left) and stress vs. strain (on the right) for cyclic behaviour with intermediate relaxation steps at 75°C

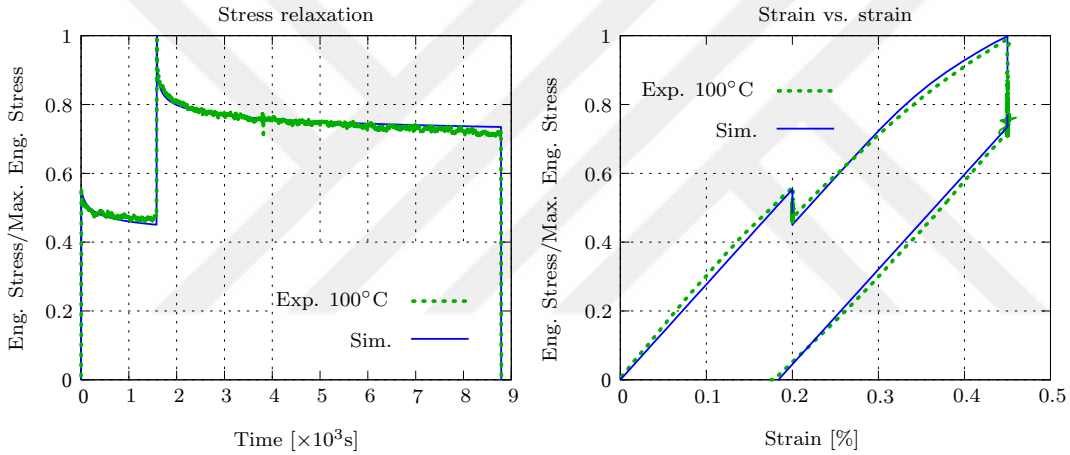

Figure 4.26: Stress relaxation (on the left) and stress vs. strain (on the right) for cyclic behaviour with intermediate relaxation steps at 100°C

If a constant strain value is applied to the material in uniaxial direction, an initial stress value is obtained. Then, chain segments start to rotate and unwind. As a result, same level of strain value is maintained by less stress level. From rheological model point of view, whole initial strain value is in the spring of the viscous branch and it is equal to total strain value or strain value of the equilibrium branch. With time, the dashpot takes a fraction of this strain reducing the stress in the viscous branch. This process is dependent on the evolution law and the parameters included in the equation. It is possible for the dashpot to elongate in a slower way and become stiffer

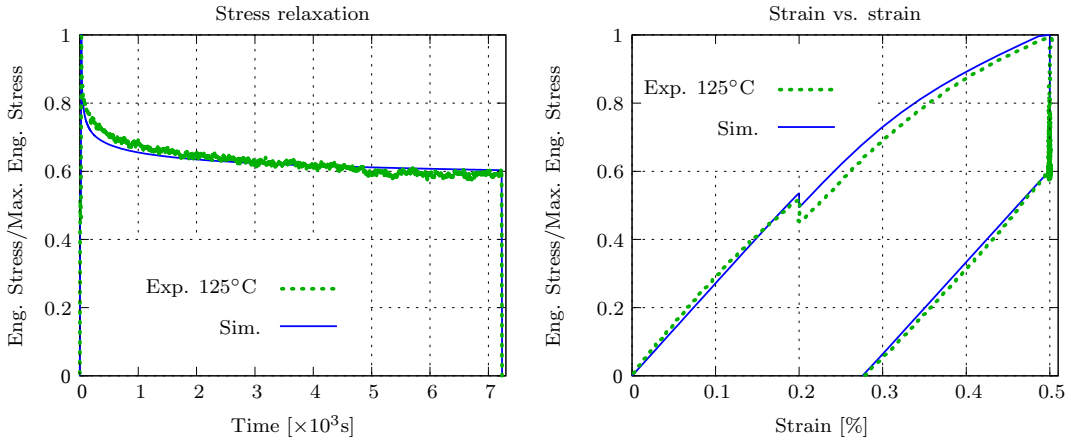

Figure 4.27: Stress relaxation (on the left) and stress vs. strain (on the right) for cyclic behaviour with intermediate relaxation steps at 125°C

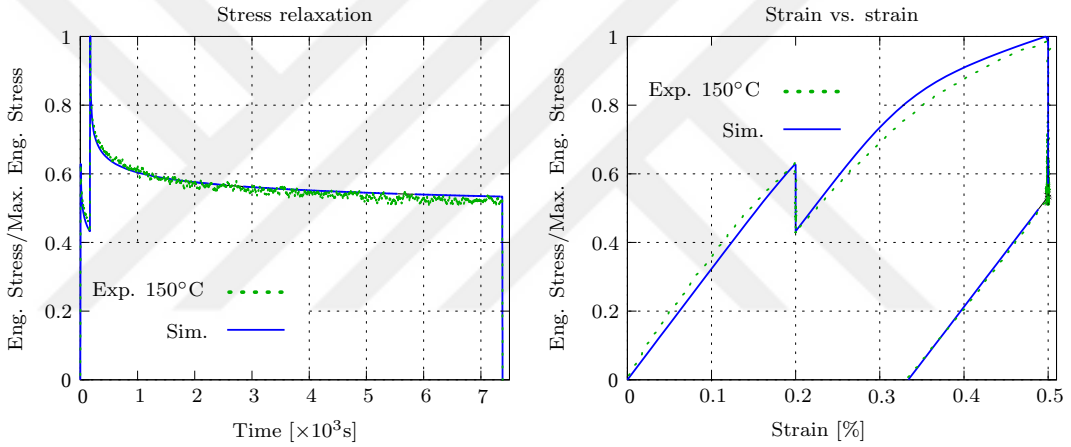

Figure 4.28: Stress relaxation (on the left) and stress vs. strain (on the right) for cyclic behaviour with intermediate relaxation steps at 150°C

for long durations by making creep rate parameter $\dot{\gamma}_0$ and power term m smaller in the evolution equation. However, m is more efficient in higher stress values since it is power term of viscous stress while $\dot{\gamma}_0$ is efficient for all strain regime and affects linearly the relaxation rate. Hence, total stress decreases to maintain the same strain value. Stress relaxation tests are common to see how stress varies with time.

The results of the simulations are in well agreement with experiments for both stress-time and stress-strain curves. It is observed from the figures and the variation of viscous and equilibrium parameters that the viscous behaviour is more dominant

Table 4.2: Identified parameters from cyclic tension tests at various temperatures

Temperature [°C]	κ^e [MPa]	μ^e [MPa]	κ^v [MPa]	μ^v [MPa]	$\dot{\gamma_0}$	m
75	4000	3200	4600	2600	3.3×10^{-13}	10.5
100	3700	2400	4700	3000	1.2×10^{-13}	10.3
125	2500	1900	5100	3100	9×10^{-8}	5.9
150	2000	1100	6000	3800	3×10^{-10}	7.15

at temperatures 125°C and 150°C while stiffness of material is higher at 75°C and 100°C, which is a similar result to that of the other epoxy compound used in the creep tests. Furthermore, related with area under the stress-strain curves, dissipation increases with temperature and residual strain at zero stress is the highest at the 150°C test temperature while maximum stress reached is lowest at that temperature. Lastly, the non-linear regime in stress-strain curve is reached earlier and more pronounced at higher temperatures. This non-linear shape is obtained with higher values of the viscous parameters and the parameters of evolution equation.

CHAPTER 5

CONCLUSION AND FUTURE WORK

5.1 Conclusion

In this study, a new model is presented to predict viscoelastic behaviour of a certain epoxy-based material (although it can be applied to any viscoelastic material). The EMC material was tested under uniaxial compression and hydrostatic loading conditions for various temperatures that cover below and above of glass transition temperature T_g. In this manner, being different than previous models which do not take volumetric time-dependent behaviour into consideration, two different free energy functions of the same form but with the corresponding elastic and viscous κ and μ parameters for equilibrium and viscous branches were used without needing to split them into isochoric and volumetric parts. Model could successfully fit results of volumetric and uniaxial compression tests in the rubbery range and around glass transition range (T_g = 130°C). However, when the results below 110°C were tried to be fitted, although fitting quality was not poor, there were unreasonable increment in equilibrium and viscous shear modulus values with fitting results being worse than the ones around and above T_g. As a result, one can end up with the idea that epoxy-based material changes its molecular structure below glass transition temperature. This makes the proposed free energy function (which is based on 8-chain model used predominantly for rubber-like materials) unreasonable since EMC takes a glassy-solid state with less mobile chain segments in a much more compact form. Therefore, we need a new free energy function below 110°C to capture behaviour with coherent parameters.

Moreover, a new evolution equation developed by Dal and Kaliske [2] for creep rate was used for updating elastic part of rate of left Cauchy-Green tensor. This evolu-

tion equation includes square of elastic stretch and differs from the one proposed by Bergström and Boyce [15].

In chapter 1, general constitutive models of viscoelasticity and a literature survey of epoxy-based materials are given. Similarly, polymeric materials, their well-known behaviours such as creep, relaxation, strain-rate and temperature dependence are explained with relations to their molecular bonding structure in chapter 2. One dimensional rheological models with spring and dashpot are also given to demonstrate the importance of each element in terms of predicting real material's time dependent behaviour and how the parameters of these elements change prediction characteristics of the model. Besides, evolution of creep and free energy function are also given in this chapter. Both of these constitutive equations are explained with their relations to molecular chain stretch. In chapter 3, one dimensional rheological model is extended to three dimensional case with associated deformation tensors as tensorial counterparts of strain values. Deformation tensors, Kirchhoff stresses and consistent tangent moduli are decoupled into elastic and viscoelastic parts to represent equilibrium and viscous branches in rheological model. A residual equation consisting of elastic stretch is formed and solved with NR-iteration algorithm. Algorithm implemented in FEAP is based on the derived equations of chapter 3. In chapter 4, the numerical results are compared with experimental results performed at various temperatures. To demonstrate effects of each parameter, a parametric study is also performed. Lastly, simulation results are given for linear evolution law along with its comparison with non-linear one.

5.2 Future works

As a future work, the proposed model should be improved in order to simulate response below 110°C with a different free energy function and evolution law as material's micro-structure probably changes in a considerable manner. Besides, new tests such as relaxation tests, cyclic deformation and tests with intermediate periods at certain stresses or strains should be performed to characterize material in a more appropriate way. In this manner, viscoplastic response and any other material behaviours can be taken into consideration. Moreover, more inclusive models can be

formed by accounting these behaviours if needed. Since behaviour of the material at various temperatures is wanted to be predicted, evolution equation of creep rate can be reformed to make it dependent on temperature. In this case, there is no need to fit experimental results for each temperature as only one parameter set can be used to predict behaviour at each temperature range. Lastly, the current model can be tried with three dimensional loading and complex geometry cases.

REFERENCES

[1] H. Dal, *Approaches to the modeling of inelasticity and failure of rubberlike materials: theory and nummerics*. PhD thesis, Techn. Univ., Inst. für Statik und Dynamik der Tragwerke, 2012.

[2] H. Dal and M. Kaliske, "Bergström–boyce model for nonlinear finite rubber viscoelasticity: theoretical aspects and algorithmic treatment for the fe method," *Computational Mechanics*, vol. 44, no. 6, pp. 809–823, 2009.

[3] P. Haupt, "On the mathematical modelling of material behavior in continuum mechanics," *Acta Mechanica*, vol. 100, no. 3-4, pp. 129–154, 1993.

[4] H. F. Brinson and L. C. Brinson, "Polymer engineering science and viscoelasticity," *New York: Springer*, vol. 66, p. 79, 2008.

[5] H. S. Lee, Y. Sun, C. Kim, and B. Han, "Characterization of linear viscoelastic behavior of epoxy molding compound subjected to uniaxial compression and hydrostatic pressure," *IEEE Transactions on Components, Packaging and Manufacturing Technology*, vol. 8, no. 8, pp. 1363–1372, 2018.

[6] S. Govindjee and J. C. Simo, "Mullins' effect and the strain amplitude dependence of the storage modulus," *International journal of solids and structures*, vol. 29, no. 14-15, pp. 1737–1751, 1992.

[7] G. A. Holzapfel and J. C. Simo, "A new viscoelastic constitutive model for continuous media at finite thermomechanical changes," vol. 33, pp. 3019–3034, 1996.

[8] A. Lion, "A constitutive model for carbon black filled rubber. experimental investigations and mathematical representations," vol. 8, pp. 153–169, 1996.

[9] M. Kaliske and A. Rothert, "Formulation and implementation of three–dimensional viscoelasticity at small and finite strains," vol. 19, pp. 228–239, 1997.

[10] M. S. Green and A. V. Tobolsky, "A new approach to the theory of relaxing polymeric media," vol. 14, pp. 80–92, 1946.

[11] A. Lion, "On the large deformation behaviour of reinforced rubber at different temperatures," *Journal of the Mechanics and Physics of Solids*, vol. 45, no. 11-12, pp. 1805–1834, 1997.

[12] J. Lubliner, "A model of rubber viscoelasticity," vol. 12, pp. 93–99, 1985.

[13] S. Reese and S. Govindjee, "A theory of finite viscoelasticity and numerical aspects," vol. 35, pp. 3455–3482, 1998.

[14] S. Reese, "A micromechanically motivated material model for the thermo–viscoelastic material behaviour of rubber–like polymers," vol. 19, pp. 909–940, 2003.

[15] J. Bergström and M. Boyce, "Constitutive modeling of the large strain time-dependent behavior of elastomers," *Journal of the Mechanics and Physics of Solids*, vol. 46, no. 5, pp. 931–954, 1998.

[16] P. Haupt and K. Sedlan, "Viscoplasticity of elastomeric materials: Experimental facts and constitutive modelling," vol. 71, pp. 89–109, 2001.

[17] C. Miehe and J. Keck, "Superimposed finite elastic–viscoelastic–plastoelastic stress response with damage in filled rubbery polymers. experiments, modelling and algorithmic implementation," *Journal of the Mechanics and Physics of Solids*, vol. 48, no. 2, pp. 323–365, 2000.

[18] L. R. G. Treloar, *The physics of rubber elasticity*. Oxford University Press, USA, 1975.

[19] A. G. James, A. Green, and G. Simpson, "Strain energy functions of rubber. i. characterization of gum vulcanizates," *Journal of Applied Polymer Science*, vol. 19, no. 7, pp. 2033–2058, 1975.

[20] E. M. Arruda and M. C. Boyce, "A three–dimensional constitutive model for the large stretch behavior of rubber elastic materials," *Journal of the Mechanics and Physics of Solids*, vol. 41, pp. 389–412, 1993.

[21] L. Anand, "A constitutive model for compressible elastomeric solids," *Computational Mechanics*, vol. 18, no. 5, pp. 339–355, 1996.

[22] M. Mooney, "A theory of large elastic deformation," *Journal of applied physics*, vol. 11, no. 9, pp. 582–592, 1940.

[23] P. J. Blatz and W. L. Ko, "Application of finite elastic theory to the deformation of rubbery materials," *Transactions of the Society of Rheology*, vol. 6, no. 1, pp. 223–252, 1962.

[24] C. Miehe, S. Göktepe, and F. Lulei, "A micro–macro approach to rubber–like materials. Part I: The non–affine micro–sphere model of rubber elasticity," vol. 52, pp. 2617–2660, 2004.

[25] C. Miehe and S. Göktepe, "A micro–macro approach to rubber–like materials. Part II: The micro–sphere model of finite rubber viscoelasticity," vol. 53, pp. 2231–2258, 2005.

[26] G. Marrucci, "Dynamics of entanglements: A nonlinear model consistent with the cox–merz rule," vol. 62, pp. 279–289, 1996.

[27] M. Kaliske and G. Heinrich, "An extended tube-model for rubber elasticity: statistical-mechanical theory and finite element implementation," *Rubber Chemistry and Technology*, vol. 72, no. 4, pp. 602–632, 1999.

[28] B. Näser, M. Kaliske, and H. Dal, "Fracture mechanical behaviour of viscoelastic materials," *PAMM*, vol. 7, 12 2007.

[29] A. Johnson, C. Quigley, and C. Freese, "A viscohyperelastic finite element model for rubber," *Computer Methods in Applied Mechanics and Engineering*, vol. 127, no. 1-4, pp. 163–180, 1995.

[30] P. E. Rouse, "A theory of the linear viscoelastic properties of dilute solutions of colling polymers," vol. 21, pp. 1272–1280, 1953.

[31] B. H. Zimm, "Dynamics of polymer molecules in dilute solution: Viscoelasticity, flow birefringence and dielectric loss," vol. 24, pp. 269–278, 1956.

[32] M. Doi and S. F. Edwards, *The Theory of Polymer Dynamics*. Clarendon Press, Oxford, 1986.

[33] F. Tanaka and S. F. Edwards, "Viscoelastic properties of physically crosslinked networks. I: Non–linear stationary viscoelasticity," vol. 43, pp. 247–271, 1992.

[34] F. Tanaka and S. F. Edwards, "Viscoelastic properties of physically crosslinked networks. II: Dynamic mechanical moduli," vol. 43, pp. 289–309, 1992.

[35] F. Ellyin and Z. Xia, "Nonlinear viscoelastic constitutive model for thermoset polymers," *Journal of Engineering Materials and Technology*, vol. 128, no. 4, pp. 579–585, 2006.

[36] R. Schapery, "Nonlinear viscoelastic solids," *International Journal of Solids and Structures*, vol. 37, no. 1-2, pp. 359–366, 2000.

[37] X. Shen, Z. Xia, and F. Ellyin, "Cyclic deformation behavior of an epoxy polymer. part i: experimental investigation," *Polymer Engineering & Science*, vol. 44, no. 12, pp. 2240–2246, 2004.

[38] Y. Hu, Z. Xia, and F. Ellyin, "Deformation behavior of an epoxy resin subject to multiaxial loadings. part i: Experimental investigations," *Polymer Engineering & Science*, vol. 43, no. 3, pp. 721–733, 2003.

[39] Z. Xia, X. Shen, and F. Ellyin, "Cyclic deformation behavior of an epoxy polymer. part ii: Predictions of viscoelastic constitutive models," *Polymer Engineering & Science*, vol. 45, no. 1, pp. 103–113, 2005.

[40] Y. Hu, F. Ellyin, and Z. Xia, "An experimental investigation of normal and shear stress interaction of an epoxy resin and model predictions," *Polymer Engineering & Science*, vol. 41, no. 11, pp. 2047–2060, 2001.

[41] S. Pandini and A. Pegoretti, "Time, temperature, and strain effects on viscoelastic poisson's ratio of epoxy resins," *Polymer Engineering & Science*, vol. 48, no. 7, pp. 1434–1441, 2008.

[42] Z. Xia, X. Shen, and F. Ellyin, "An assessment of nonlinearly viscoelastic constitutive models for cyclic loading: the effect of a general loading/unloading rule," *Mechanics of Time-Dependent Materials*, vol. 9, no. 4, pp. 79–98, 2005.

[43] P. Gromala, B. Muthuraman, B. Öztürk, K. Jansen, and L. Ernst, "Material characterization and nonlinear viscoelastic modelling of epoxy based thermosets for

automotive application," in *Thermal, Mechanical and Multi-Physics Simulation and Experiments in Microelectronics and Microsystems (EuroSimE), 2015 16th International Conference on*, pp. 1–7, IEEE, 2015.

[44] P. J. Gromala, A. Prisacaru, M. Jeronimo, H.-S. Lee, Y. Sun, and B. Han, "Non-linear viscoelastic modeling of epoxy based molding compound for large deformations encountered in power modules," in *Electronic Components and Technology Conference (ECTC), 2017 IEEE 67th*, pp. 834–840, IEEE, 2017.

[45] Y. Hong, D. Papathanassiou, and P. Gromala, "Implementation of non-linear viscoelasticity for epoxy based thermoset polymers," in *Electronic Packaging Technology (ICEPT), 2015 16th International Conference on*, pp. 555–560, IEEE, 2015.

[46] J.-S. Pap, M. Kästner, S. Müller, and I. Jansen, "Experimental characterization and simulation of the mechanical behavior of an epoxy adhesive," *Procedia Materials Science*, vol. 2, pp. 234–242, 2013.

[47] M. Kästner, M. Obst, J. Brummund, K. Thielsch, and V. Ulbricht, "Inelastic material behavior of polymers–experimental characterization, formulation and implementation of a material model," *Mechanics of Materials*, vol. 52, pp. 40–57, 2012.

[48] S. Müller, M. Kästner, J. Brummund, and V. Ulbricht, "A nonlinear fractional viscoelastic material model for polymers," *Computational Materials Science*, vol. 50, no. 10, pp. 2938–2949, 2011.

[49] C. E. Ryther, "The effect of elevated temperature on the inelastic deformation behavior of pmr-15 solid polymer," tech. rep., AIR FORCE INST OF TECH WRIGHT-PATTERSON AFB OH SCHOOL OF ENGINEERING AND ..., 2012.

[50] L. Bardella, "A phenomenological constitutive law for the nonlinear viscoelastic behaviour of epoxy resins in the glassy state," *European Journal of Mechanics-A/Solids*, vol. 20, no. 6, pp. 907–924, 2001.

[51] H. M. James and E. Guth, "Theory of the elastic properties of rubber," *The Journal of Chemical Physics*, vol. 11, no. 10, pp. 455–481, 1943.

[52] A. Cohen, “A Padé approximant to the inverse langevin function,” vol. 30, pp. 270–273, 1991.

APPENDIX A

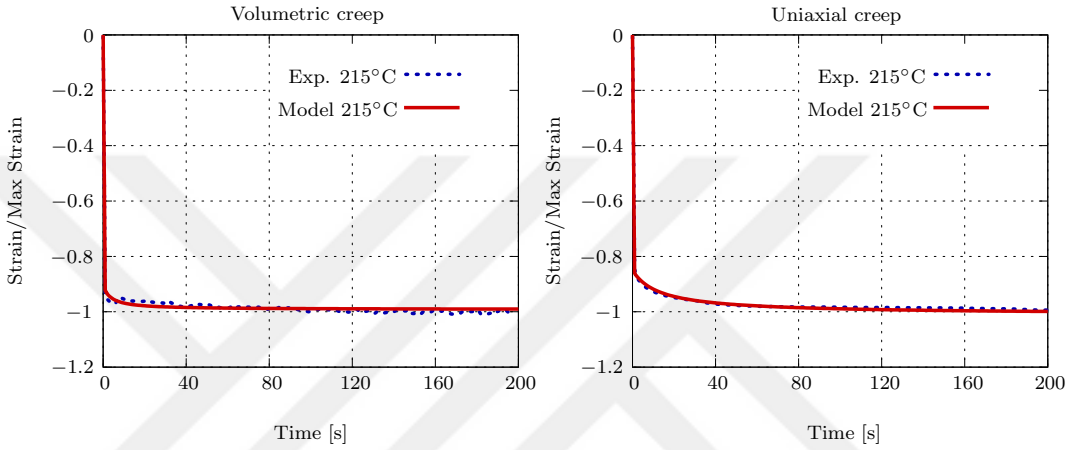

Figure A.1: Volumetric (on the left) and uniaxial (on the right) creep test at 215°C

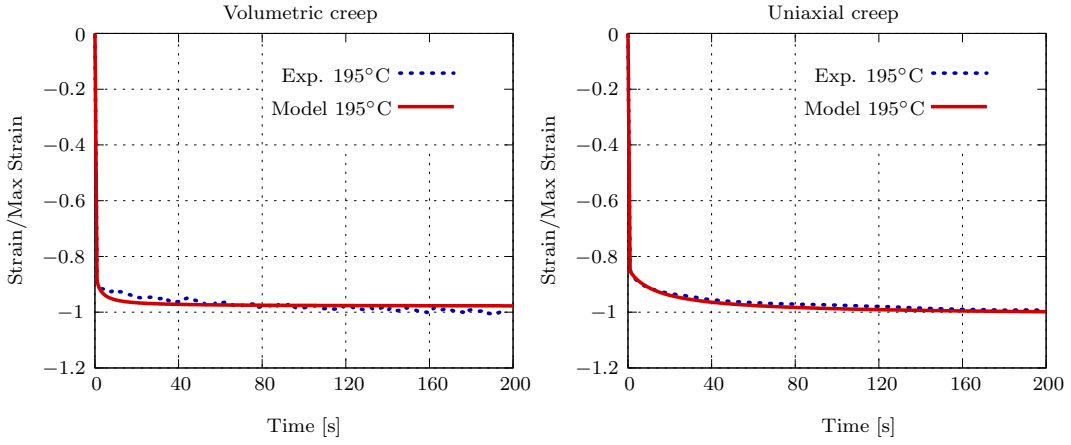

Figure A.2: Volumetric (on the left) and uniaxial (on the right) creep test at 195°C

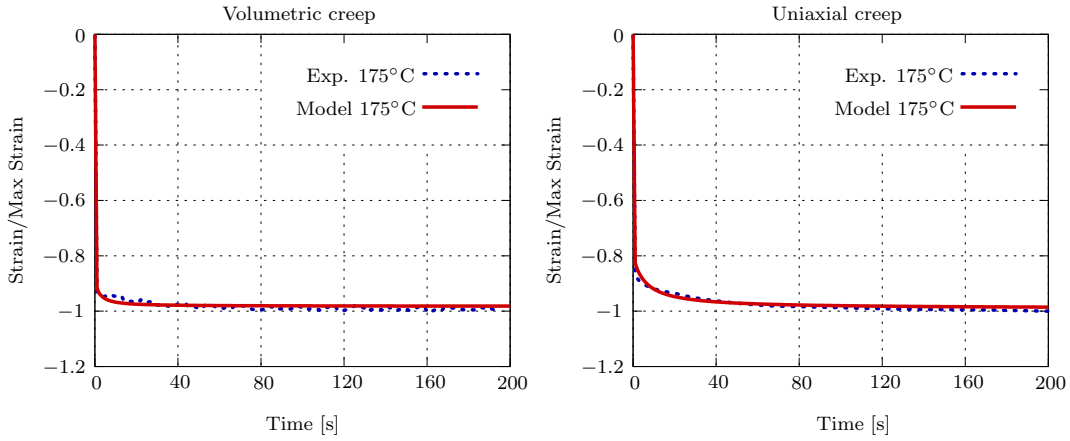

Figure A.3: Volumetric (on the left) and uniaxial (on the right) creep test at 175°C

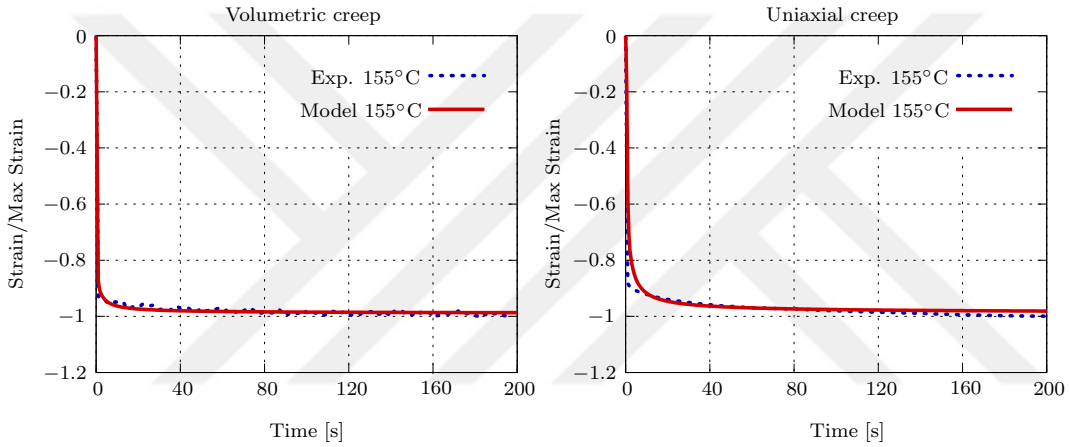

Figure A.4: Volumetric (on the left) and uniaxial (on the right) creep test at 155°C

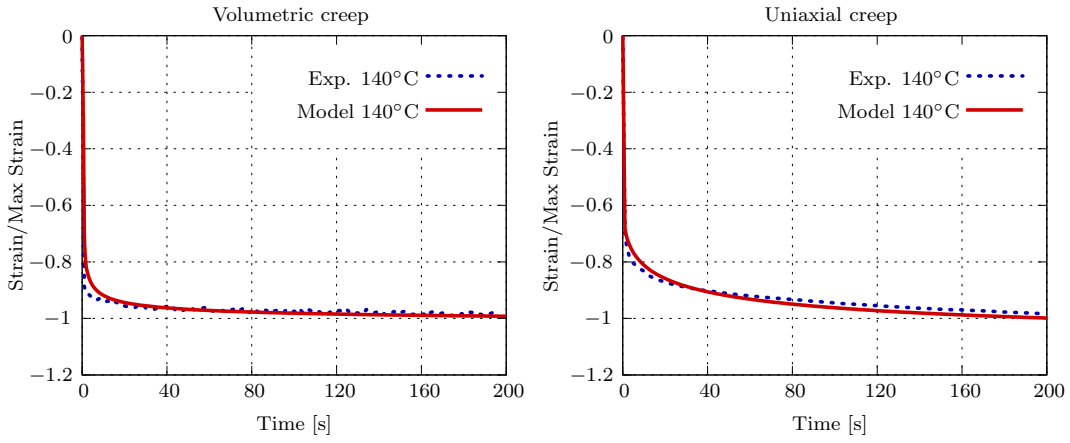

Figure A.5: Volumetric (on the left) and uniaxial (on the right) creep test at 140°C

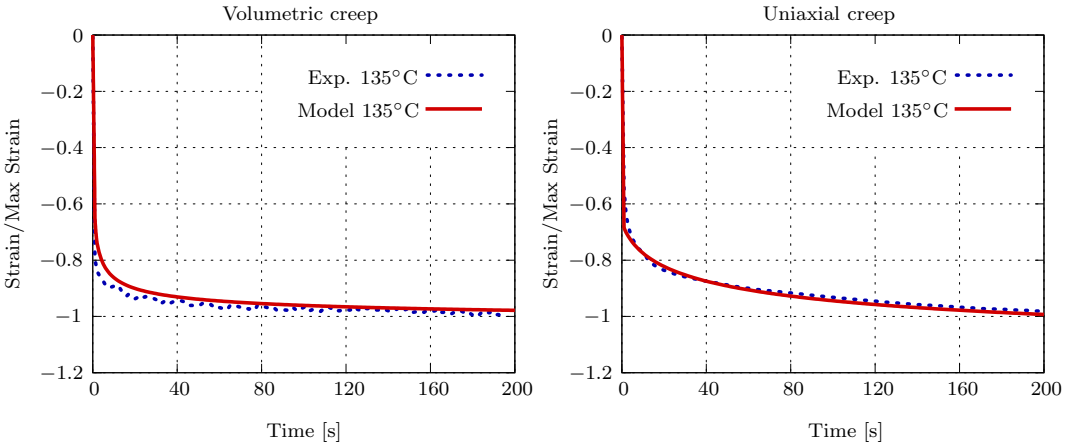

Figure A.6: Volumetric (on the left) and uniaxial (on the right) creep test at 135°C

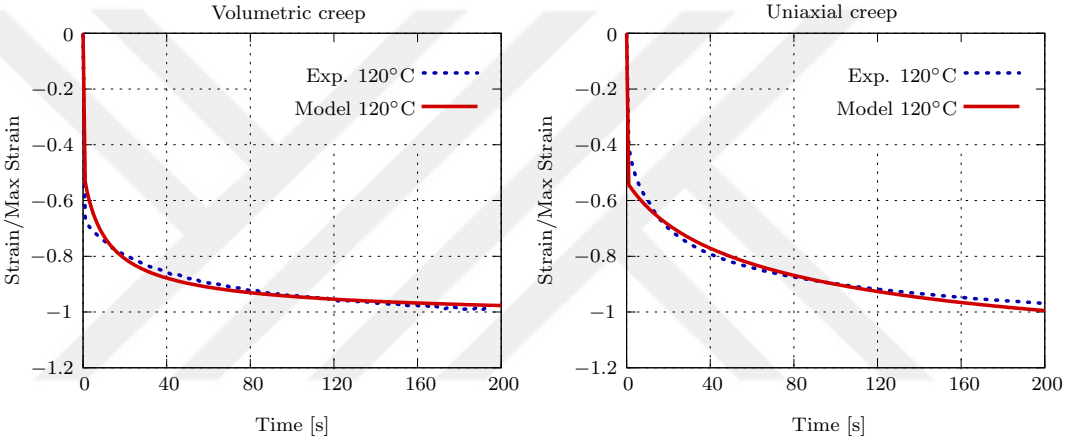

Figure A.7: Volumetric (on the left) and uniaxial (on the right) creep test at 120°C

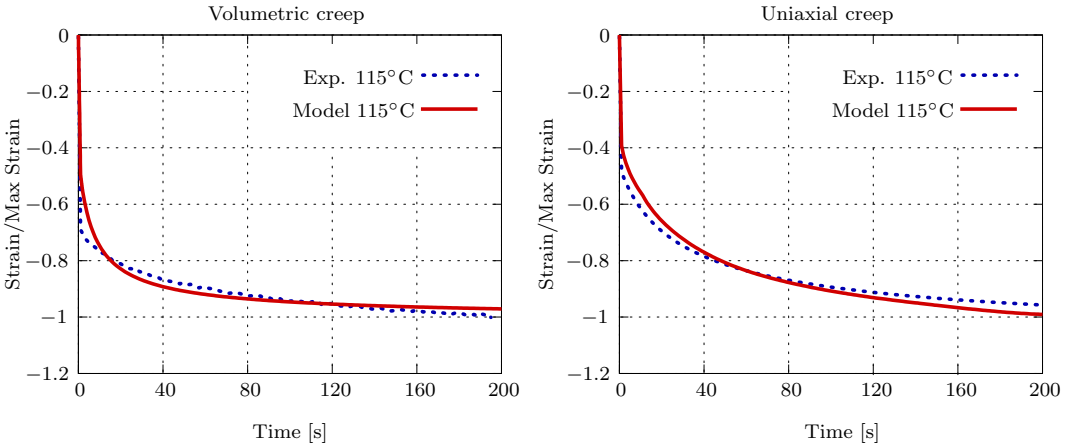

Figure A.8: Volumetric (on the left) and uniaxial (on the right) creep test at 115°C

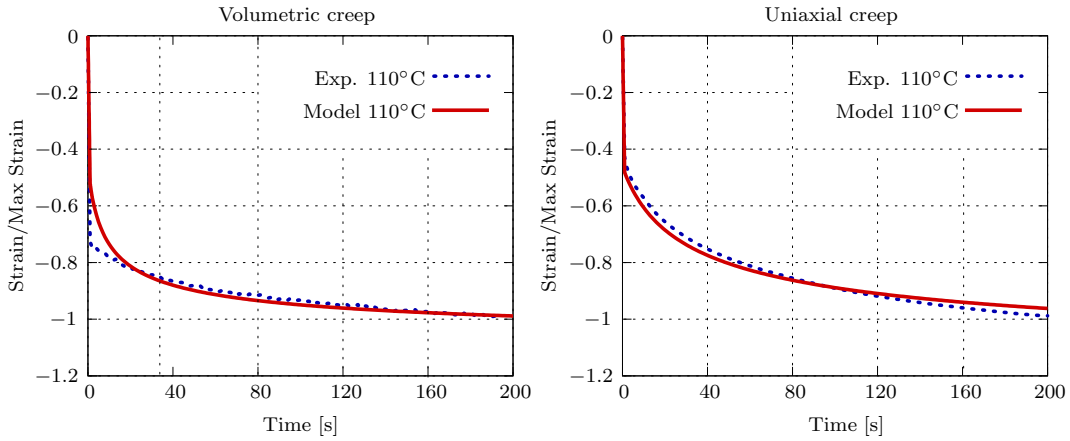

Figure A.9: Volumetric (on the left) and uniaxial (on the right) creep test at 110°C

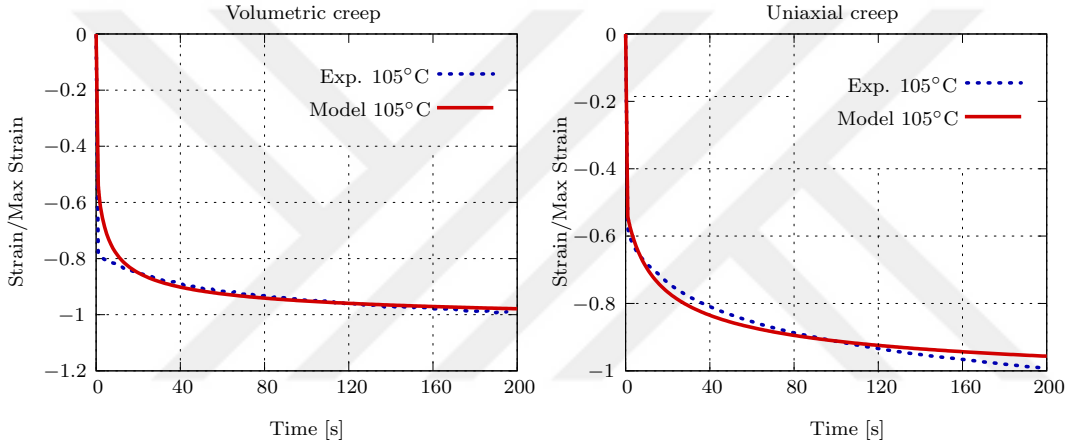

Figure A.10: Volumetric (on the left) and uniaxial (on the right) creep test at 105°C

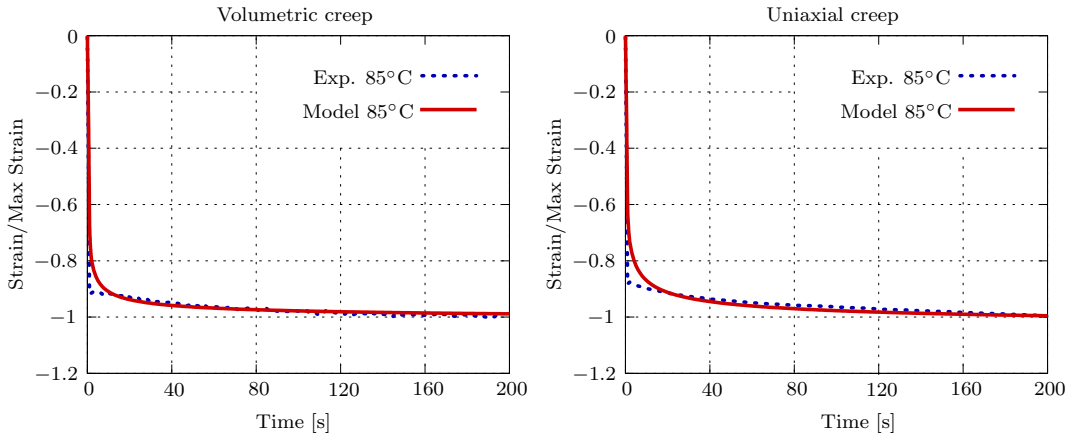

Figure A.11: Volumetric (on the left) and uniaxial (on the right) creep test at 85°C

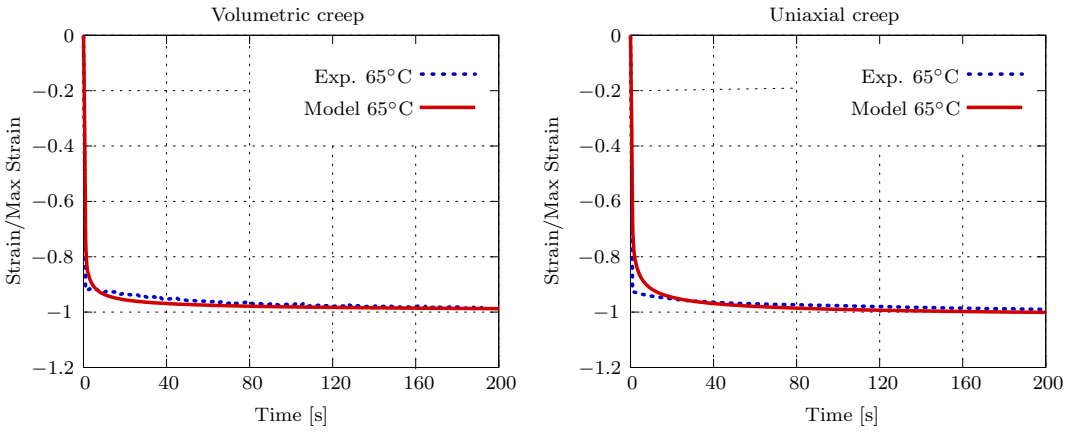

Figure A.12: Volumetric (on the left) and uniaxial (on the right) creep test at 65°C

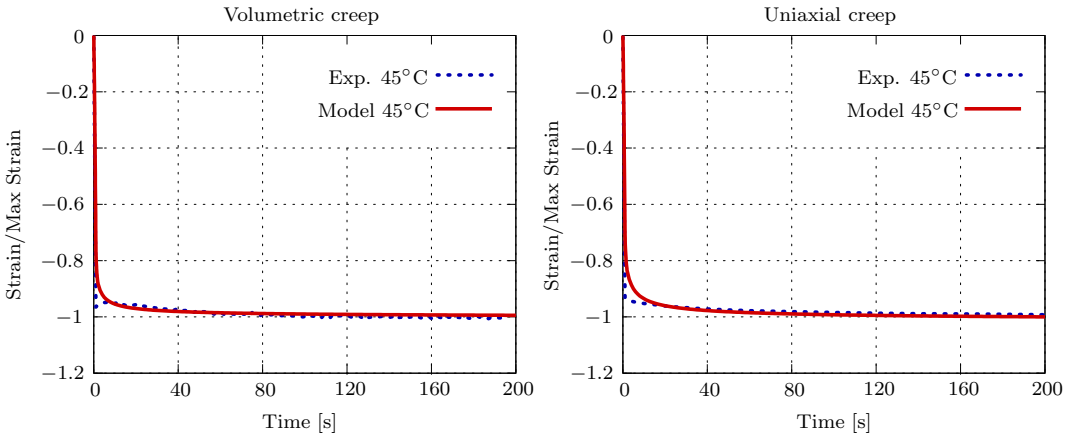

Figure A.13: Volumetric (on the left) and uniaxial (on the right) creep test at 45°C